Records of atmospheric mercury deposition and post-depositional mobility in peat permafrost archives from central and northern Yukon, Canada

by

Sasiri Bandara

A thesis submitted in partial fulfillment of the requirements for the degree of

Master of Science

Department of Earth and Atmospheric Sciences

University of Alberta

Abstract

Environmental archives provide a feasible means for studying the biogeochemical cycling of heavy metals including mercury (Hg). Although many temperate peat bogs have been successfully used to reconstruct natural and anthropogenic atmospheric Hg deposition fluxes, northern circumpolar permafrost peatlands are largely understudied in similar research. Consequently, substantial gaps remain in our understanding of past atmospheric Hg deposition fluxes and present peatland Hg inventories from northern environments. This thesis presents a critical investigation of using peat permafrost archives for quantifying natural and anthropogenic atmospheric Hg deposition fluxes. The first objective of this research was to develop an effective protocol for collecting and processing peat permafrost samples for inorganic geochemical analyses. Refined techniques were established for accurately measuring bulk density and homogenizing well-preserved fibrous peat. This method was then used to reconstruct historic atmospheric Hg deposition from a permafrost peat plateau near Dawson, Yukon, with the aim of resolving a deposition peak corresponding to extensive Klondike gold mining during the late 19th and early 20th centuries. The results revealed an unexpectedly early increase in anthropogenic Hg deposition, which was ultimately interpreted to result from post-depositional Hg mobility within the seasonally thawed active layer. This discovery implies that peat permafrost archives may not provide reliable high-resolution records of atmospheric Hg deposition. However, a subsequent study involving seven Holocene (10,000-year old) peat plateaus from central and northern Yukon reveal that millennial-scale atmospherically deposited Hg concentrations and fluxes were consistently low; ~20.7 ± 9.8 $ng \cdot g^{-1}$ and ~0.51 ± 0.39 $\mu g \cdot m^{-2} \cdot y^{-1}$, respectively. These results were used to demonstrate how peat permafrost Hg inventories could be estimated at the local scale. Provided additional empirical data from sites spanning the northern circumpolar region, future studies may use the same approach to estimate cryosol Hg stocks at regional to global scales and assess the potential vulnerability of Hg release from thawing permafrost with continued climate warming.

Preface

This thesis represents collaborative efforts of several scientists as reflected by the authorship of chapters in preparation for publication. Studies were designed by myself and my thesis supervisors, Drs. Duane Froese and Vincent St. Louis. I was responsible for planning and executing field excursions, collecting samples in the field, conducting laboratory analyses, compiling results, and writing thesis chapters/manuscripts, which were subsequently edited and improved by my coauthors.

Chapter 3 is a manuscript in preparation for Environmental Science and Technology as: Bandara, S., Froese, D. G., St. Louis, V. L., Cooke, C. A., Calmels, F. Post-depositional mercury mobility in active layers of peat permafrost from central Yukon: implications for reconstructing historic mercury deposition fluxes using permafrost archives.

Chapter 4 is a manuscript in preparation for Environmental Science and Technology as: Bandara, S., Froese, D. G., St. Louis, V. L., Cooke, C. A. 10,000 years of atmospherically deposited mercury in peat permafrost archives from central and northern Yukon, Canada.

Acknowledgements

First and foremost, I would like to thank my thesis supervisors, Drs. Duane Froese and Vincent St. Louis, for giving me the freedom to develop original ideas and for encouraging me to strive for excellence through a good dose of constructive criticism. Dr. Froese fostered my early interests in northern environments by supervising my senior undergraduate honors thesis and by involving me in other exciting research projects. I owe a great debt of gratitude for the academic, professional, and personal learning opportunities, and for the excellent mentorship, Dr. Froese has provided over the years.

I would also like to acknowledge the numerous funding agencies that made this research possible. Financial support was provided to me by The W. Garfield Weston Foundation, EnviroNorth, the Northern Scientific Training Program, the Geological Society of America, and the University of Alberta. NSERC Discovery grants awarded to my supervisors and Polar Continental Shelf Program funding awarded to Dr. Trevor Porter also supported this research.

So many people have contributed to this thesis in one way or another. I owe a special thanks to Dr. Colin Cooke for welcoming my ideas with enthusiasm and for providing helpful advice both as a collaborator and thesis committee member. I am also grateful for the input and involvement of Drs. Fabrice Calmels and Trevor Porter. Thanks to Lauren Davies, Matthew Mahony, and Joel Pumple for nurturing my transition from undergraduate to graduate studies. Thanks also to Casey Buchanan, Kasia Stanizewska, Joe Young, Hector Martinez, Gerard Otiniano, Sydney Clackett, and Jonny Vandewint for helping with fieldwork. Thanks to Mark Labbe and Crystal Dodge for technical assistance. Thanks, Emily Moffat, for being genuinely interested in my research and for providing feedback to improve my manuscripts. Thanks also to the other teachers, colleagues, and friends who have contributed to my studies and left a lasting impression on me both professionally and personally. This thesis is a testament to everyone who has been involved.

Lastly, my greatest thank you is to my family. My parents have encouraged me to pursue my passions from a young age. I would not be where I am today without the constant motivation and life lessons from my parents. Thank you also to my brother, Leo, and sister-in-law, Sunethra, for providing advice unconditionally and for inspiring me to achieve my most important goals. Most of all, thank you, Ebberly MacLagan, for your lively spirit, love, and support. As I reflect on this milestone, I look forward to exciting future adventures with you.

Table of Contents

List of Tables

List of Figures

Chapter 1: Mercury in the environment

Introduction

Heavy metals are persistent environmental contaminants that cannot be degraded nor destroyed (Duruibe et al., 2007). These dense elements include lead (Pb), cadmium (Cd), chromium (Cr), arsenic (As), and mercury (Hg), all of which occur naturally in the lithosphere. While some heavy metals are biologically important in trace amounts, many interfere with regular metabolic processes and have harmful effects on wildlife and humans. The biotoxicity of heavy metal contaminants highlights the need for improved scientific understanding of their reservoirs and transport pathways.

In recent decades, biologists and environmental scientists have been especially concerned with Hg, which is released to the atmosphere, biosphere, and hydrosphere through a variety of natural and anthropogenic processes (Givelet et al., 2003; Engstrom et al., 2014). Volcanism, soil erosion, degassing from hydrothermal systems, and marine emissions are the most dominant natural sources of Hg (Schroeder & Munthe, 1998). Anthropogenic sources include coal-fired energy production, precious metal extraction, and waste incineration (Mason et al., 1994; Driscoll et al., 2013). Both natural and anthropogenic Hg emissions are primarily in the form of gaseous elemental Hg (GEM; Hg^0) (Givelet et al., 2003; Enrico et al., 2016), which is hemispherically dispersed due to its long atmospheric residence time of 6 to 12 months (Driscoll et al., 2013). Although reactive gaseous mercury (RGM) and particulate-bound Hg are deposited locally or regionally, GEM is typically carried to remote circumpolar regions via atmospheric transport pathways (Ebinghaus et al., 2002; Durnford et al., 2010; Driscoll et al., 2013). Ecosystem inputs are largely in the form of inorganic Hg(II); however, Hg(II) may be subsequently converted to methylmercury (MeHg) under anoxic conditions (Jensen & Jernelöv, 1969) by sulfate and iron-

reducing bacteria (Compeau & Bartha, 1985; Kerin et al., 2006). Methylmercury is a developmental neurotoxin that bioaccumulates in organisms such as fish and biomagnifies in food chains. The harmful, and sometimes fatal, effects of MeHg have been recognized since the 1956 Hg poisoning event in Minamata, Japan (Poulain & Barkay, 2013).

Whole-ecosystem studies, such as the Mercury Experiment to Assess Atmospheric Loading in Canada and the United States (METAALICUS), have shown that the amount of MeHg produced in a given ecosystem is approximately proportional to atmospheric inputs of Hg(II) (Harris et al., 2007; Swain et al., 2007). This finding, along with insight into severe human health problems resulting from dietary exposure to MeHg, prompted national and international efforts aimed at reducing anthropogenic Hg emissions (Engstrom et al., 2014). The prevailing view is that there has been an approximately threefold increase in atmospheric Hg deposition since pre-industrial times (before AD 1850; Lindberg et al., 2007), even in regions with little or no Hg emission sources such as the Arctic and subarctic (Givelet et al., 2004).

Mercury in the Arctic and subarctic

Mercury loading is elevated in high-latitude environments and has increased over time (AMAP, 2002). According to Wheatley and Wheatley (2000), MeHg contamination is rising among indigenous peoples of northern Canada whose traditional diets include fish and piscivorous species. Various hypotheses have been proposed to explain the observed increase in Hg contamination within the Arctic and subarctic. The “cold condensation” hypothesis suggests a latitudinal Hg gradient (Mackay et al., 1995) due to preferential mobilization of Hg from warm and dry equatorial settings to cool and wet polar regions. This process has also been recognized in other volatile organic compounds such as chlorinated pesticides and polychlorobiphenyls (Wania et al., 1993). Furthermore, a 4,000-year record of atmospheric Hg deposition from a peat core in

northwestern Spain suggests that cold climate phases promote net Hg accumulation in peat bogs (Martınez-Cortizas et al., 1999). Arctic landscapes may also experience enhanced Hg deposition through mercury depletion events (MDEs; Figure 1.1), which occur each spring during polar sunrise (Schroeder et al., 1998). During MDEs, GEM undergoes photochemical oxidation by reactive halogens in the atmosphere (Givelet et al., 2004b) and is converted to RGM, which is then deposited on snow and ice. Some of this Hg may be subsequently re-emitted to the atmosphere through photoreduction (Poulain et al., 2004; Kirk et al., 2006; Brooks et al., 2008).

Figure 1.1 illustrates the cycling of Hg through arctic marine and terrestrial ecosystems. It is hypothesized that continued global climate warming and polar amplification will influence many aspects of this cycle. Reduction in sea-ice extent, earlier onset of snowmelt, delayed onset of snowfall, and increased mean annual temperatures may enhance the efficiency of Hg transport pathways to polar regions. This may also explain the observed Hg enrichment unique to arctic environmental archives despite a decrease in global Hg emissions over recent decades (Cooke et al., 2012). The "algal mercury scavenging hypothesis" suggests that warming temperatures promote Hg sequestration in arctic lake sediments through sorption to organic matter derived from enhanced aquatic productivity (Outridge et al., 2007; Stern et al., 2009). Moreover, it is believed that increased transport of photooxidants and production of reactive halogens in the high latitudes also contribute to the rise in Hg concentrations among arctic biota (Givelet et al., 2004).

Changes in atmospheric Hg deposition, including the aforementioned anthropogenic increase following the Industrial Revolution (ca. AD 1850), are recorded by natural archives. Ice and sediment cores allow for the reconstruction of natural Hg accumulation rates (or fluxes; $\mu g \cdot m^{-2} \cdot y^{-1}$) over extended timescales, whereas tree-rings and high-accumulation peatlands document

more recent changes. When used in conjunction, these different archives provide a comprehensive account of both natural and anthropogenic Hg accumulation rates over time.

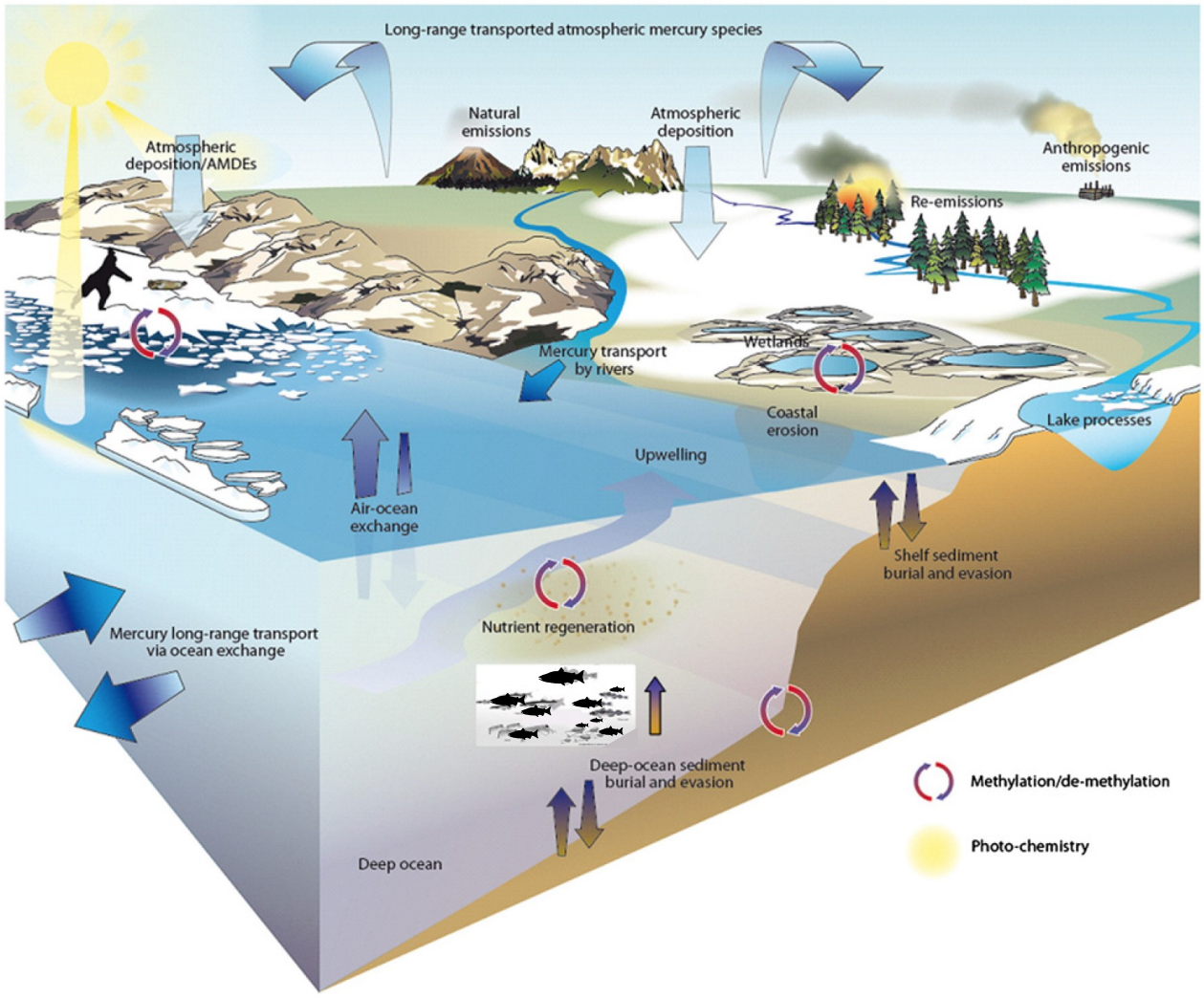

Figure 1.1 Diagram showing the cycling of Hg through arctic marine and terrestrial ecosystems (modified from Stern et al., 2012).

Archives of mercury deposition rates

Lake sediments

Once buried beneath the uppermost active zones, lake sediments are essentially unaffected by bioturbation and redox processes (Biester et al., 2007). Lake sediment Hg is commonly bound within insoluble organo-Hg-sulfides and metacinnabar (HgS), which largely inhibits cross-sediment Hg diffusion (Biester et al., 2007). As Biester et al. (2007) summarize, the stability of inorganic Hg profiles in lake sediments is evidenced by (a) the preservation of Hg peaks in separate cores collected over multiple years from the same lake (Lockhart et al., 2000), (b) the correlation of Hg trends among multiple lakes (Swain et al., 1992), (c) the absence of Hg redistribution in experimental incubations (Fitzgerald et al., 1998), and (d) the strong solid-phase partitioning of Hg from pore-waters in lake sediment cores (Fitzgerald et al., 1998).

An increasing number of studies continue to use lake sediments as archives of Hg pollution in the Arctic and subarctic (Lockhart et al., 1995; Hermanson et al., 1998). However, because lake sediments integrate both direct atmospheric deposition and runoff-derived loadings from adjacent catchment soils, it may be difficult to distinguish changes in rates of atmospheric deposition from basin-specific runoff influences. Lake sediment Hg records may be further complicated by chemical diagenesis associated with sulphate reduction at the sediment-water interface, sediment focusing prior to burial (Norton et al., 1987; Norton et al., 1990), and decreased metal retention within sediments due to lake acidification (Dillon et al., 1986).

Glacial firn and ice

Although glacial firn and ice from Greenland have been used to reconstruct atmospheric deposition of some trace metals including Pb (Boutron et al., 1998), comparable Hg records from such archives are uncommon. Schuster et al. (2002) and Beal et al. (2015) present the only

comprehensive reconstructions of atmospheric Hg deposition from glacial ice cores in North America. Meltwater processes and photoreduction influence the chemistry of snow and ice, which may dampen or otherwise complicate the Hg record (Brimblecombe et al., 1985; Lalonde et al., 2000). According to Givelet (2004), background metal concentrations in ice cores may be so low (sub-pg·g^{-1}) that studies based on these records are challenged by analytical detection limits and potential contamination during sample processing. Additionally, the limited geographic distribution of perennially frozen snow and ice restricts reconstructions based on such archives to alpine and circumpolar settings (Givelet, 2004).

Tree-rings

Tree-rings have been effective archives for reconstructing temporal variability in atmospheric pollutants (Watmough, 1999; Bindler et al., 2004) and for mapping pollution from aerosols such as Pb (Tommasini et al., 2000). However, few studies document comprehensive Hg records in tree-rings. This may be due to uncertainties regarding the mechanisms by which trees acquire Hg.

A recent study by Wright et al. (2014) suggests that dendrochemistry may effectively reveal watershed-scale differences in atmospheric Hg as well as long-term regional and global trends. The widespread distribution of certain tree species across many ecological and geophysical gradients also strengthens the validity of using tree-ring records to quantify changes in atmospheric Hg concentrations over time (Bindler et al., 2004). Nonetheless, Hg concentrations derived through dendrochemistry are influenced by proximity to point sources of Hg, species-specific and age-dependent partitioning (Wright et al., 2014), and various local environmental parameters controlling tree growth such as mean annual temperature, precipitation, and relative humidity.

Peat bogs

Because Hg binds strongly to organic matter (Xia et al., 1999), peat has the capacity to intercept and retain Hg over millennial timescales (Bindler, 2003; Martınez-Cortizas et al., 1999). Although some minerotrophic (or groundwater-fed) peatlands provide reliable records of atmospheric Hg deposition (Roos-Barraclough & Shotyk, 2003; Shotyk et al., 2003), most studies concerning atmospheric Hg deposition come from ombrotrophic peatlands that receive moisture and nutrient inputs exclusively from the atmosphere (Clymo, 1987). Changing rates of wet and dry Hg deposition may be preserved in peat cores from ombrotrophic bogs. These archives can therefore contain thousands of years of Hg deposition as exemplified by the 14,500-year record from the Jura Mountains of Switzerland studied by Roos-Barraclough et al. (2002b).

Most peatland reconstructions of atmospheric Hg deposition originate from the temperate zone of Europe and northeast North America, while only a few studies (Shotyk et al., 2003; Givelet et al., 2004; Outridge & Sanei, 2010) present comprehensive long-term results from high-latitude peat deposits. Additional studies examining arctic and subarctic ombrotrophic peatlands, particularly those underlain by syngenetic permafrost, will improve our understanding of long-term atmospheric Hg deposition. Such peat permafrost deposits are well-preserved and minimally influenced by organic matter decomposition and humification as demonstrated by Outridge and Sanei (2010).

Hg, permafrost, and regional climate change

Permafrost, which consists of ground that has remained at or below 0°C for two or more consecutive years, underlies much of the terrestrial arctic as well as some arctic submarine environments (AMAP/CAFF/IASC, 2005). According to recent climate models, the global permafrost region is expected to undergo a reduction in areal extent of 52 ± 23% by the year 2100

(Schaefer et al., 2014). Widespread permafrost degradation may mobilize significant stocks of organic carbon (OC) and OC-bound heavy metals, such as Hg, to adjacent aquatic environments (MacDonald et al., 2005), including thermokarst ponds, which rapidly produce MeHg (St. Louis et al., 2005). The addition of dissolved organic carbon and nutrients to thermokarst ponds and lakes, combined with stronger thermal stratification of these water bodies, may cause anoxia and thereby amplify microbial methylation of inorganic Hg (Stern et al., 2012). This link between Hg biogeochemistry and the carbon cycle in northern environments poses a potential threat to ecosystem health, particularly with projected climate warming and permafrost thaw.

A variety of environmental proxies including hydrogen and oxygen isotope ratios in ice cores have been used to reconstruct Holocene climate change in the northern high-latitudes. According to Kaufman et al. (2004), northwestern Canada was subject to the "Holocene Thermal Maximum" (HTM) between ca. 11,000 and 8,000 years before present. This period of warm climate was initiated by an orbital precession-driven insolation peak, but was followed by climate cooling during the middle Holocene, and subsequent warming during the late Holocene (Ritchie et al., 1983; Lauriol et al., 2009). Cryostratigraphy and paleogeography reveal the influence of such climate change on regional permafrost (Burn, 1997); however, concentrations and fluxes of heavy metal compounds such as OM-bound Hg in regional permafrost deposits is poorly constrained over the same timescales. Studies aimed at quantifying millennial-scale Hg budgets using natural archives, especially well-preserved syngenetic peat permafrost, may improve our understanding of climate-permafrost-Hg relations and aid in assessing the susceptibility of Hg release from future permafrost thaw.

Thesis objectives and organization

Careful collection and processing methods must be followed to accurately quantify stocks and fluxes of contaminants in permafrost. Several key publications suggest analytical protocols for conducting geochemical investigations of temperate peat bogs (Roos-Barraclough et al., 2002; Givelet et al., 2004; Le Roux & De Vleeschouwer, 2010), but an effective methodology for peat permafrost is not described in the literature. A major concern with inorganic geochemical studies of peat and sediment archives is the possibility of physical compression and cross-contamination during core collection and handling (Givelet et al., 2004). Moreover, elemental loss by volatilization during sample drying and homogenization is also recognized as a potential source of error (Ross-Barraclough et al., 2002). Methodological issues may hinder inter-comparisons of geochemical results from these types of archives (Le Roux & De Vleeschouwer, 2010). It is therefore important to establish suitable and replicable techniques for collecting, processing, and analyzing cores to ensure that final concentration and flux data are not merely artefacts of the methodologies used. This data quality assurance is a crucial prerequisite for making reliable interpretations and conclusions.

Chapter 2 of this thesis presents a technical communication on field and laboratory methods involved in quantifying Hg concentrations and fluxes in northern circumpolar permafrost archives. Site selection and core collection, transport, storage, and handling are among the topics discussed. A particular emphasis is placed on subsampling strategies, density calculations, and subsample homogenization. The chapter concludes with quality assurance and quality control results that highlight the effectiveness of the proposed protocol.

The protocol established in Chapter 2 is implemented in Chapter 3 to investigate historic Hg deposition with the aim of resolving an anthropogenic signal corresponding to extensive gold

mining in the Klondike. The results from this study reveal an apparent issue in using permafrost archives for detailed reconstructions of atmospheric Hg deposition rates. Pore-water/ice oxygen isotopes ($\delta^{18}O$) suggest that Hg may be susceptible to post-depositional mobility within the active layer. This implies that caution must be exercised when using shallow permafrost archives for similar studies.

Chapter 4 presents quantified Hg concentrations and millennial-scale fluxes from several syngenetic peat permafrost archives in central and northern Yukon. These results offer new information on how much atmospherically deposited Hg is stored in typical peat permafrost deposits and the rates at which such stocks accumulated throughout the Holocene (last 10,000 years). This data regarding pre-industrial natural Hg sequestration in peat permafrost provides a reliable baseline for (a) assessing the significance of anthropogenic Hg accumulation rates since industrialization, and (b) future evaluations concerning the potential vulnerability of Hg release from permafrost degradation in northern circumpolar regions. Chapter 5 discusses key conclusions from the thesis and proposes directions for future research.

References

AMAP. (2002). Arctic pollution 2002 Arctic Monitoring and Assessment Program (AMAP). Oslo, Norway. 112 pp.

AMAP/CAFF/IASC. (2005). Arctic climate impact assessment. Cambridge, UK. Cambridge University Press. 1042 pp.

Beal, S. A., Osterberg, E. C., Zdanowicz, C. M., & Fisher, D. A. (2015). Ice core perspective on mercury pollution during the past 600 years. *Environmental science & technology*, *49*(13), 7641-7647.

Biester, H., Bindler, R., Martinez-Cortizas, A., & Engstrom, D. R. (2007). Modeling the past atmospheric deposition of mercury using natural archives. *Environmental science & technology*, *41*(14), 4851-4860.

Bindler, R. (2003). Estimating the natural background atmospheric deposition rate of mercury utilizing ombrotrophic bogs in southern Sweden. *Environmental science & technology*, *37*(1), 40-46.

Bindler, R., Renberg, I., Klaminder, J., & Emteryd, O. (2004). Tree rings as Pb pollution archives? A comparison of 206 Pb/207 Pb isotope ratios in pine and other environmental media. *Science of the Total Environment*, *319*(1), 173-183.

Boutron, C. F., Vandal, G. M., Fitzgerald, W. F., & Ferrari, C. P. (1998). A forty-year record of mercury in central Greenland snow. *Geophysical Research Letters*, *25*(17), 3315-3318.

Brimblecombe, P., Tranter, M., Abrahams, P. W., Blackwood, I., Davies, T. D., & Vincent, C. E. (1985). Relocation and preferential elution of acidic solute through the snowpack of a small, remote, high-altitude Scottish catchment. *Annals of Glaciology*, *7*, 141-147.

Brooks, S., Arimoto, R., Lindberg, S., & Southworth, G. (2008). Antarctic polar plateau snow surface conversion of deposited oxidized mercury to gaseous elemental mercury with fractional long-term burial. *Atmospheric Environment*, *42*(12), 2877-2884.

Burn, C. R. (1997). Cryostratigraphy, paleogeography, and climate change during the early Holocene warm interval, western Arctic coast, Canada. *Canadian Journal of Earth Sciences*, *34*(7), 912-925.

Clymo, R. S. (1987). The ecology of peatlands. *Science Progress (Oxford)*, *71*, 593-614.

Compeau, G. C., & Bartha, R. (1985). Sulfate-reducing bacteria: principal methylators of mercury in anoxic estuarine sediment. *Applied and environmental microbiology*, *50*(2), 498-502.

Cooke, C. A., Wolfe, A. P., Michelutti, N., Balcom, P. H., & Briner, J. P. (2012). A Holocene perspective on algal mercury scavenging to sediments of an arctic lake. *Environmental science & technology*, *46*(13), 7135-7141.

Dillon, P. J., Scholer, P. J., & Evans, H. E. (1986). 210Pb fluxes in acidified lakes. In *Sediments and Water Interactions* (pp. 491-499). Springer New York.

Driscoll, C. T., Mason, R. P., Chan, H. M., Jacob, D. J., & Pirrone, N. (2013). Mercury as a global pollutant: sources, pathways, and effects. *Environmental science & technology*, *47*(10), 4967-4983.

Durnford, D., Dastoor, A., Figueras-Nieto, D., & Ryjkov, A. (2010). Long range transport of mercury to the Arctic and across Canada. *Atmospheric Chemistry and Physics*, *10*(13), 6063-6086.

Duruibe, J. O., Ogwuegbu, M. O. C., & Egwurugwu, J. N. (2007). Heavy metal pollution and human biotoxic effects. *International Journal of Physical Sciences*, *2*(5), 112-118.

Ebinghaus, R., Kock, H. H., Temme, C., Einax, J. W., Löwe, A. G., Richter, A., ... & Schroeder, W. H. (2002). Antarctic springtime depletion of atmospheric mercury. *Environmental science & technology*, *36*(6), 1238-1244.

Engstrom, D. R., Fitzgerald, W. F., Cooke, C. A., Lamborg, C. H., Drevnick, P. E., Swain, E. B., ... & Balcom, P. H. (2014). Atmospheric Hg emissions from preindustrial gold and silver extraction in the Americas: A reevaluation from lake-sediment archives. *Environmental science & technology*, *48*(12), 6533-6543.

Enrico, M., Le Roux, G., Marusczak, N., Heimbürger, L. E., Claustres, A., Fu, X., ... & Sonke, J. E. (2016). Atmospheric mercury transfer to peat bogs dominated by gaseous elemental mercury dry deposition. *Environmental science & technology*, *50*(5), 2405-2412.

Fitzgerald, W. F., Engstrom, D. R., Mason, R. P., & Nater, E. A. (1998). The case for atmospheric mercury contamination in remote areas. *Environmental Science & Technology*, *32*(1), 1-7.

Givelet, N. (2004). Long-term Records of Atmospheric Deposition of Mercury in Peat Cores from Arctic, and Comparison with Bogs in the Temperate Zone. *Doctoral dissertation*.

Givelet, N., Le Roux, G., Cheburkin, A., Chen, B., Frank, J., Goodsite, M. E., ... & Rheinberger, S. (2004). Suggested protocol for collecting, handling and preparing peat cores and peat samples for physical, chemical, mineralogical and isotopic analyses. *Journal of Environmental Monitoring*, *6*(5), 481-492.

Givelet, N., Roos-Barraclough, F., & Shotyk, W. (2003). Predominant anthropogenic sources and rates of atmospheric mercury accumulation in southern Ontario recorded by peat cores from three bogs: comparison with natural "background" values (past 8000 years). *Journal of Environmental Monitoring*, *5*(6), 935-949.

Givelet, N., Roos-Barraclough, F., Goodsite, M. E., Cheburkin, A. K., & Shotyk, W. (2004). Atmospheric mercury accumulation rates between 5900 and 800 calibrated years BP in the High Arctic of Canada recorded by peat hummocks. *Environmental science & technology*, *38*(19), 4964-4972.

Harris, R. C., Rudd, J. W., Amyot, M., Babiarz, C. L., Beaty, K. G., Blanchfield, P. J., ... & Heyes, A. (2007). Whole-ecosystem study shows rapid fish-mercury response to changes in mercury deposition. *Proceedings of the National Academy of Sciences*, *104*(42), 16586-16591.

Hermanson, M. H. (1998). Anthropogenic mercury deposition to Arctic lake sediments. *Water, Air, and Soil Pollution*, *101*(1-4), 309-321.

Jensen, S., & Jernelöv, A. (1969). Biological methylation of mercury in aquatic organisms. *Nature*, 233, 753-754.

Kaufman, D. S., Ager, T. A., Anderson, N. J., Anderson, P. M., Andrews, J. T., Bartlein, P. J., ... & Dyke, A. S. (2004). Holocene thermal maximum in the western Arctic (0–180 W). *Quaternary Science Reviews*, *23*(5), 529-560.

Kerin, E. J., Gilmour, C. C., Roden, E., Suzuki, M. T., Coates, J. D., & Mason, R. P. (2006). Mercury methylation by dissimilatory iron-reducing bacteria. *Applied and environmental microbiology*, *72*(12), 7919-7921.

Kirk, J. L., St. Louis, V. L., & Sharp, M. J. (2006). Rapid reduction and reemission of mercury deposited into snowpacks during atmospheric mercury depletion events at Churchill, Manitoba, Canada. *Environmental science & technology*, *40*(24), 7590-7596.

Lalonde, J. D., Poulain, A. J. M., & Amyot, M. (2000). Mercury dynamics in snow. In *Proceedings of the 11th Annual International Conference on Heavy Metals in the Environment.* School of Public Health, University of Michigan, Ann Arbor, MI.

Lauriol, B., Lacelle, D., Labrecque, S., Duguay, C. R., & Telka, A. (2009). Holocene evolution of lakes in the Bluefish Basin, northern Yukon, Canada. *Arctic*, *62*(2), 212-224.

Le Roux, G., & De Vleeschouwer, F. (2010). Preparation of peat samples for inorganic geochemistry used as palaeoenvironmental proxies. *Mires and Peat*, *7*, 1-9.

Lindberg, S., Bullock, R., Ebinghaus, R., Engstrom, D., Feng, X., Fitzgerald, W., ... & Seigneur, C. (2007). A synthesis of progress and uncertainties in attributing the sources of mercury in deposition. *AMBIO: A Journal of the Human Environment*, *36*(1), 19-33.

Lockhart, W. L., MacDonald, R. W., Outridge, P. M., Wilkinson, P., DeLaronde, J. B., & Rudd, J. W. M. (2000). Tests of the fidelity of lake sediment core records of mercury deposition to known histories of mercury contamination. *Science of the Total Environment*, *260*(1), 171-180.

Lockhart, W. L., Wilkinson, P., Billeck, B. N., Hunt, R. V., Wagemann, R., & Brunskill, G. J. (1995). Current and historical inputs of mercury to high-latitude lakes in Canada and to Hudson Bay. *Water, Air, and Soil Pollution*, *80*(1-4), 603-610.

MacDonald, R. W., Harner, T., & Fyfe, J. (2005). Recent climate change in the Arctic and its impact on contaminant pathways and interpretation of temporal trend data. *Science of the total environment*, *342*(1), 5-86.

Mackay, D., Wania, F., & Schroeder, W. H. (1995). Prospects for modeling the behavior and fate of mercury, globally and in aquatic systems. In *Mercury as a Global Pollutant* (pp. 941-950). Springer Netherlands.

Martınez-Cortizas, A., Pontevedra-Pombal, X., Garcıa-Rodeja, E., Novoa-Munoz, J. C., & Shotyk, W. (1999). Mercury in a Spanish peat bog: archive of climate change and atmospheric metal deposition. *Science*, *284*(5416), 939-942.

Mason, R. P., Fitzgerald, W. F., & Morel, F. M. (1994). The biogeochemical cycling of elemental mercury: anthropogenic influences. *Geochimica et Cosmochimica Acta*, *58*(15), 3191-3198.

Norton, S. A., & Kahl, J. S. (1987). A comparison of lake sediments and ombrotrophic peat deposits as long-term monitors of atmospheric pollution. *New Approaches to Monitoring Aquatic Ecosystems*, 40-57.

Norton, S. A., Dillon, P. J., Evans, R. D., Mierle, G., & Kahl, J. S. (1990). The history of atmospheric deposition of Cd, Hg, and Pb in North America: evidence from lake and peat bog sediments. In *Acidic Precipitation* (pp. 73-102). Springer New York.

Outridge, P. M., & Sanei, H. (2010). Does organic matter degradation affect the reconstruction of pre-industrial atmospheric mercury deposition rates from peat cores? - A test of the hypothesis using a permafrost peat deposit in northern Canada. *International Journal of Coal Geology*, *83*(1), 73-81.

Outridge, P. M., Sanei, H., Stern, G. A., Hamilton, P. B., & Goodarzi, F. (2007). Evidence for control of mercury accumulation rates in Canadian High Arctic lake sediments by variations of aquatic primary productivity. *Environmental science & technology*, *41*(15), 5259-5265.

Poulain, A. J., & Barkay, T. (2013). Cracking the mercury methylation code. *Science*, *339*(6125), 1280-1281.

Poulain, A. J., Lalonde, J. D., Amyot, M., Shead, J. A., Raofie, F., & Ariya, P. A. (2004). Redox transformations of mercury in an Arctic snowpack at springtime. *Atmospheric Environment*, *38*(39), 6763-6774.

Ritchie, J. C., Cwynar, L. C., and Spear, R. W., 1983: Evidence from north-west Canada for an early Holocene Milankovitch thermal maximum. *Nature*, 305: 126–128.

Roos-Barraclough, F., & Shotyk, W. (2003). Millennial-scale records of atmospheric mercury deposition obtained from ombrotrophic and minerotrophic peatlands in the Swiss Jura Mountains. *Environmental science & technology*, 37(2), 235-244.

Roos-Barraclough, F., Givelet, N., Martinez-Cortizas, A., Goodsite, M. E., Biester, H., & Shotyk, W. (2002). An analytical protocol for the determination of total mercury concentrations in solid peat samples. *Science of the total environment*, 292(1), 129-139.

Roos-Barraclough, F., Martinez-Cortizas, A., García-Rodeja, E., & Shotyk, W. (2002b). A 14 500-year record of the accumulation of atmospheric mercury in peat: volcanic signals, anthropogenic influences and a correlation to bromine accumulation. *Earth and Planetary Science Letters*, 202(2), 435-451.

Schaefer, K., Lantuit, H., Romanovsky, V.E., Schuur, E.A.G., and Witt, R. (2014). The impact of the permafrost carbon feedback on global climate. *Environmental Research Letters*, 9, 085003, doi: 10.1088/1748-9326/9/8/085003.

Schroeder, W. H., Anlauf, K. G., Barrie, L. A., Lu, J. Y., Steffen, A., Schneeberger, D. R., & Berg, T. (1998). Arctic springtime depletion of mercury. *Nature*, 394(6691), 331-332.

Schroeder, W. H., & Munthe, J. (1998). Atmospheric mercury—an overview. *Atmospheric Environment*, 32(5), 809-822.

Schuster, P. F., Krabbenhoft, D. P., Naftz, D. L., Cecil, L. D., Olson, M. L., Dewild, J. F., ... & Abbott, M. L. (2002). Atmospheric mercury deposition during the last 270 years: a glacial ice core record of natural and anthropogenic sources. *Environmental Science & Technology*, *36*(11), 2303-2310.

Shotyk, W., Goodsite, M. E., Roos-Barraclough, F., Frei, R., Heinemeier, J., Asmund, G., ... & Hansen, T. S. (2003). Anthropogenic contributions to atmospheric Hg, Pb and As accumulation recorded by peat cores from southern Greenland and Denmark dated using the 14 C "bomb pulse curve". *Geochimica et Cosmochimica Acta*, *67*(21), 3991-4011.

Stern, G. A., MacDonald, R. W., Outridge, P. M., Wilson, S., Chetelat, J., Cole, A., ... & Zdanowicz, C. (2012). How does climate change influence arctic mercury?. *Science of the total environment*, *414*, 22-42.

Stern, G. A., Sanei, H., Roach, P., Delaronde, J., & Outridge, P. M. (2009). Historical interrelated variations of mercury and aquatic organic matter in lake sediment cores from a subarctic lake in Yukon, Canada:

further evidence toward the algal-mercury scavenging hypothesis. *Environmental science & technology*, *43*(20), 7684-7690.

St. Louis, V. L., Sharp, M. J., Steffen, A., May, A., Barker, J., Kirk, J. L., ... & Smol, J. P. (2005). Some sources and sinks of monomethyl and inorganic mercury on Ellesmere Island in the Canadian High Arctic. *Environmental science & technology*, *39*(8), 2686-2701.

Swain, E. B., Engstrom, D. R., Brigham, M. E., Henning, T. A., & Brezonik, P. L. (1992). Increasing rates of atmospheric mercury deposition in midcontinental North America. *Science*, *257*(5071), 784-787.

Swain, E. B., Jakus, P. M., Rice, G., Lupi, F., Maxson, P. A., Pacyna, J. M., ... & Veiga, M. M. (2007). Socioeconomic consequences of mercury use and pollution. *Ambio: A Journal of the Human Environment*, *36*(1), 45-61.

Tommasini, S., Davies, G. R., & Elliott, T. (2000). Lead isotope composition of tree rings as bio-geochemical tracers of heavy metal pollution: a reconnaissance study from Firenze, Italy. *Applied Geochemistry*, *15*(7), 891-900.

Wania, F., & Mackay, D. (1993). Global fractionation and cold condensation of low volatility organochlorine compounds in polar regions. *Ambio*, 10-18.

Watmough, S. A. (1999). Monitoring historical changes in soil and atmospheric trace metal levels by dendrochemical analysis. *Environmental pollution*, *106*(3), 391-403.

Wheatley, B., & Wheatley, M. A. (2000). Methylmercury and the health of indigenous peoples: a risk management challenge for physical and social sciences and for public health policy. *Science of the Total Environment*, *259*(1), 23-29.

Wright, G., Woodward, C., Peri, L., Weisberg, P. J., & Gustin, M. S. (2014). Application of tree rings [dendrochemistry] for detecting historical trends in air Hg concentrations across multiple scales. *Biogeochemistry*, *120*(1-3), 149-162.

Xia, K., Skyllberg, U. L., Bleam, W. F., Bloom, P. R., Nater, E. A., & Helmke, P. A. (1999). X-ray absorption spectroscopic evidence for the complexation of Hg (II) by reduced sulfur in soil humic substances. *Environmental science & technology*, *33*(2), 257-261.

Chapter 2: A protocol for collecting and processing permafrost cores for inorganic geochemistry

Introduction

Peat cores from ombrotrophic (rain-fed) bogs have attracted the attention of paleoenvironmental researchers in recent decades. Regional changes in hydrology, climate, and vegetation are well-preserved in these peat records (Xie et al., 2000; Barber et al., 2003; Page et al., 2004; Charman et al., 2006; De Vleeschouwer et al., 2009). These archives are also thought to faithfully document changes in atmospheric chemistry, which makes them ideal for studying past atmospheric deposition of toxic heavy metals including lead (Pb) (Martínez-Cortizas et al., 1997; Kempter et al., 1997; Brännvall et al., 1997; Shotyk et al., 1998; Novák et al., 2003; Klaminder et al., 2003; Monna et al., 2004; Kylander et al., 2010) and mercury (Hg) (Pheiffer-Madsen, 1981; Martinez-Cortizas, 1999; Biester et al., 2002; Roos-Barraclough, Martinez-Cortizas, et al., 2002; Bindler, 2003; Givelet et al., 2003; Roos-Barraclough & Shotyk, 2003; Biester et al., 2007). The effectiveness of using peat to reconstruct atmospheric contaminant deposition is confirmed by agreements in relative accumulation rates (fluxes) between different bogs and between peat and other natural archives (Bindler et al., 2004). This utility of ombrotrophic peat applies to studies of anthropogenic contaminant deposition since the Industrial Revolution (ca. AD 1850) and studies of pre-industrial background fluxes resulting from natural processes.

While the advantage of using peat cores to quantify atmospheric deposition of heavy metals is clear, the lack of a universally accepted analytical protocol may hinder interpretations and inter-comparisons of heavy metal fluxes derived by different laboratories and research groups (Givelet et al., 2004). Recognizing that some fluctuations in geochemical profiles from peat archives may be artefacts of the analytical procedures used (Le Roux & De Vleeschouwer, 2010) has resulted in

three fundamental papers (Roos-Barraclough et al., 2002; Givelet et al., 2004; Le Roux & De Vleeschouwer, 2010) outlining methods in processing peat samples for inorganic geochemistry. However, these recommended protocols deal solely with peat from low-latitude bogs. A detailed methodology for handling peat permafrost cores from northern circumpolar and alpine environments is not described in the literature.

Syngenetic peat permafrost from ombrotrophic bogs may contain well-preserved records of atmospheric heavy metal deposition (Outridge & Sanei, 2010). These archives, some of which have accumulated for thousands of years, are not as susceptible to alteration by peat decomposition and organic matter humification as their low-latitude peat bog counterparts. Syngenetic peat permafrost archives also contain meteoric waters in their pore-ice, which may be analyzed for oxygen and hydrogen isotope ratios ($\delta^{18}O$ and $\delta^{2}H$) to obtain additional paleoclimatic information (Bandara et al., 2017). Here, we recognize the strengths of peat permafrost archives and present a comprehensive protocol for successfully using them in paleoenvironmental and ecotoxicological research. We discuss methodologies already in place for handling peat cores from temperate bogs and propose refinements that should be applied when dealing with well-preserved peat permafrost. Emphasis is placed on subsampling, homogenizing, and accurately calculating densities of fibrous peat. The proposed protocol is intended to provide a strong foundation for future studies concerning inorganic geochemistry in permafrost cores.

Proposed protocol

Site selection

Appropriate site selection and efficient coring techniques are integral to successful geochemical studies based on peat archives. Depending on specific research objectives, the field strategy should consider (a) peatland topography and thickness, (b) botanical composition and

abundance of mineral matter, (c) active layer and permafrost condition, (d) degree of peat decomposition, (e) rate of peat accumulation, and (f) proximity to human activities and potentially important geologic processes (Givelet et al., 2004). Some of these criteria can be assessed through remote sensing. For instance, optical remote sensing and digital elevation models (DEMs) may help identify ombrotrophic peat sites with stable (or undisturbed) permafrost as indicated by extensive ice-wedge networks and an absence of thermokarst features (Bandara et al., 2017). Similarly, Normalized Difference Vegetation Index (NDVI), which is a measure of "greenness" in photosynthetically active vegetation, may be used to prospect for a suitable chronosequence of sites (Bandara et al., 2017; Jones et al., 2012) for long-term reconstructions of atmospheric heavy metal deposition. These remote sensing-based evaluations may be validated through the use of previously published soil databases and by ground truthing prior to or during field work.

Ombrotrophic peatlands are favorable archives for studies of atmospheric deposition because they receive inputs exclusively from the atmosphere. The optimal location for coring within an ombrotrophic peatland is a raised dome, as it typically contains the most accurate account of atmospheric deposition with the greatest temporal resolution. Although lateral and upward migration of dissolved ions from weathering of underlying bedrock may influence geochemical profiles in temperate bogs (Shotyk & Steinmann, 1994), such effects are typically diminished where there is permafrost.

In the absence of ombrotrophic bogs, minerotrophic peat deposits may serve as viable archives of atmospheric heavy metal deposition although they receive inputs from the atmosphere and by groundwater inflow and surface water runoff. Some constituents may be provided exclusively by the atmosphere as documented in several studies that successfully reconstruct atmospheric deposition of Pb and Hg using minerotrophic peat (Shotyk, 2002; Shotyk et al., 2003;

Roos-Barraclough & Shotyk, 2003). However, geochemical results from such archives must be interpreted carefully given that some metals may be derived from bedrock weathering.

Field planning

Ideally, permafrost coring should commence in winter or early spring prior to the onset of seasonal thaw of the active layer. This would allow for cleanly drilling and extracting a frozen monolith that is not altered by compaction or expansion. Eliminating physical alteration of near-surface peat is critical for detailed investigations aimed at quantifying recent atmospheric deposition of contaminants due to human activities. Vertical compaction of the peat profile increases peat density, decreases apparent accumulation rates, and thus obscures changes in concentrations and fluxes of atmospherically deposited constituents. Effects of core compaction on age-depth relations are discussed in detail elsewhere (Givelet et al., 2004).

Core collection

A motorized corer designed specifically for collecting frozen peat is described in the literature (Nørnberg et al., 2004). However, a portable earth-drill (Figure 2.1A) equipped with a heavy-duty diamond-edged core barrel provides a more reliable method for smoothly cutting through ice-rich permafrost (Calmels et al., 2005) and is therefore recommended. This latter approach permits for recovering unaltered permafrost cores of 10 cm diameter to a maximum depth of ~7 m, which is beyond the basal depth of many arctic and subarctic peatlands. Cores collected though this method should be cleaned using stainless steel blades, then carefully described, photographed, wrapped in pre-labelled polyethylene core bags, and stored in coolers with ice-packs immediately following extraction. A chest freezer intermittently powered by a portable generator provides a feasible means of keeping cores frozen during transport to a more permanent storage facility.

Core subsampling

Permafrost core processing begins with systematic discarding of potentially contaminated outside edges. Core segments are then cut in half lengthwise using a rock saw equipped with a 35-cm diameter diamond cutting wheel (Figure 2.1B). This process produces a flat surface, which may be scraped clean with stainless steel blades for imaging and making detailed observations (Figure 2.1C). Cryostratigraphic descriptions are recommended and should follow conventional classification systems such as those presented in Murton and French (1994) and French and Schur (2010).

One half of each core is typically archived for future work and replication studies, while the remaining half is processed according to the procedure outlined in Figure 2.2. Cores should be subsampled in a walk-in freezer set at about -5 °C to prevent thaw. A compact table saw with a 15-cm diameter diamond cutting wheel and an adjustable guide allows for precise subsampling at 1-cm intervals. This is essential for maximizing the signal to noise ratio of geochemical profiles (Givelet et al., 2004), especially in uppermost layers that are expected to contain anthropogenic records.

Dating and age-depth models

Establishing accurate chronologies is critical for paleoenvironmental and ecotoxicological research involving peat archives. Because organic material is exceptionally well-preserved in peat permafrost, pre- and post-bomb radiocarbon (^{14}C) dating are effective chronological techniques. Terrestrial plant macrofossils, and ideally sphagnum (*Sphagnum spp.)* capitula, should be cleaned by standard acid-base-acid (ABA) pre-treatment and submitted to a suitable laboratory for Accelerator Mass Spectrometry (AMS) ^{14}C dating. During macrofossil selection, care should be taken to avoid roots that penetrate older peat layers and imply erroneously young ^{14}C ages for a

depth in question (Weiss et al., 2002). Issues of old carbon contamination are less likely to occur in peat permafrost archives compared to temperate bogs, which may be more hydrologically connected. In addition to pre- and post-bomb ^{14}C dating, peat permafrost sequences can also be dated using other short-lived radioisotopes (e.g., ^{210}Pb, ^{137}Cs, and ^{241}Am) and tephrochronology (Oldfield et al., 1979; Appleby et al., 1988; Swindles et al., 2010). All of these methods may be successfully combined using the *P_Sequence* function of OxCal (Bronk Ramsey, 2009) to produce a reliable age-depth model that accounts for uncertainties and assumptions inherent to each dating technique (Froese et al., 2016). Strong chronological constraints and high-resolution age-depth models are prerequisites for deriving accurate geochemical fluxes in peat permafrost archives.

Cuboid method for density calculation

Precisely quantifying bulk density (BD) is also important for reconstructing accumulation rates of atmospherically deposited constituents. Several conventional techniques of calculating peat BD are described in the literature (Riley, 1989; Day et al., 1979). A manual stainless steel press has also been used to extract frozen peat plugs of known volume, which may be subsequently weighed to calculate BD (Nørnberg et al., 2004). However, when applied to ice-rich peat permafrost, these methods are challenged by uncertainties in precision and issues of peat compaction, expansion, and loss due to thaw. In light of these potential handling problems, we present a new technique (referred to as the "cuboid method") that is easily replicated and yields accurate BD measurements in peat permafrost archives.

The cuboid method (Figure 2.3) begins with core subsampling in a walk-in freezer as described above and summarized in Figure 2.2. After a cuboid aliquot has been cut, it is lightly sanded using 80-grit sandpaper to have flat, rectangular faces. A digital caliper (±0.01 mm) and a digital analytical balance (±0.0001 g) are used to determine physical dimensions and mass,

respectively. The cuboid is subsequently dried in an oven for 24 hours at 80 °C and reweighed. Peat bulk densities are calculated as the fraction of final (dry) mass to initial (wet) volume. Peat from cuboid aliquots are discarded following density calculations as they may have been contaminated during handling and drying. The accuracy of density measurements may be improved by (1) avoiding obvious heterogeneities, such as wood fragments and roots, during subsampling, (2) maximizing physical dimensions of cuboids to sufficiently represent a depth of interest, and (3) avoiding any peat that may have been compressed or decompressed during core recovery and handling.

The analytical uncertainty of density measurements made through the cuboid method may be calculated using individual uncertainties of cuboid dimensions and masses. If a digital caliper with an uncertainty of ±0.01 mm and a digital analytical balance with an uncertainty of ±0.0001 g are used, then the final uncertainty in density will be approximately ±0.0003 $g \cdot cm^{-3}$ for an average peat sample with a true bulk density of 0.1 $g \cdot cm^{-3}$. In this case, the total analytical uncertainty in density is approximately 0.4%. Given that peat mass and volume can vary disproportionately, the total uncertainty in density calculations may vary within and among different peat deposits.

Pore-water/ice geochemistry and isotope analyses

Pore-water geochemistry can reveal useful information about bogs, including the trophic status of different peat layers within a single profile (Shotyk & Steinmann, 1994). Electrical conductivity, pH, major and trace element cations and anions, and dissolved organic carbon are among the commonly measured metrics of pore-waters. However, in syngenetic peat permafrost, oxygen and hydrogen isotope ratios ($\delta^{18}O$ and $\delta^{2}H$) from pore-water/ice may also be quantified to assess biophysical conditions at these peatlands and reconstruct peleoclimatic change (Bandara et al., 2017).

As outlined in the subsampling and analysis strategy in Figure 2.2, pore-ice geochemistry is conducted on semi-cylindrical aliquots from depths of interest. These subsamples are stored in pre-labeled, vacuum-sealed polyethylene sample bags and thawed in a cool, dark setting to prevent evaporative enrichment of $\delta^{18}O$ and $\delta^{2}H$. Liquid water is transferred from sample bags to small polyethylene bottles using a padded vice to compress the thawed peat. Geochemical analyses are conducted on these waters immediately for optimal data quality. Pore-waters are filtered through clean 0.2 μm membranes for oxygen and hydrogen isotope analyses on a Picarro L2130-i water isotope analyzer (1σ = 0.1‰ for $\delta^{18}O$ and 0.5‰ for $\delta^{2}H$). After extracting water, the remaining peat material is placed in pre-labeled, sterile 50 mL centrifuge tubes for freeze-drying. Oven drying is not recommended due to potential contamination from the laboratory environment and possible volatilization of certain chemical species even at low heat (Roos-Barraclough, Givelet, et al., 2002; Le Roux & De Vleeschouwer, 2010).

Automated mortar and pestle method for homogenization

Freeze-dried peat samples should be completely homogenized prior to geochemical analyses (e.g., total C, N, Pb, and Hg) to attain reliable measurements. Conventional sediment homogenizing techniques include crushing and mixing by hand in plastic sample bags, manual grinding using a ceramic mortar and pestle, and automated pulverizing with coffee grinders and ball mills. These methods, however, are time consuming and only partially homogenize fibrous peat from well-preserved permafrost archives. Therefore, we propose an alternative technique for homogenizing such samples. In this technique, freeze-dried peat samples are homogenized using a Retsch RM 200 automated agate mortar and pestle as shown in Figure 2.4. Most samples can be pulverized to a fine powder in under 3 minutes without a noticeable increase in temperature. Peat powder from each sample should be carefully poured out of the mortar and all components of the

machine must be rinsed with deionized water and carefully wiped with acetone-soaked paper towels to prevent cross-contamination. A quality control peat permafrost core (QCSB-DH15) was analyzed to assess the precision of total Hg concentration measurements. Results in Table 2.1 reveal that the homogenization method outlined above is highly effective as there are no significant additions or losses of Hg to or from peat samples.

Total Hg analysis

Many non-destructive and destructive methods of measuring various major and trace elements in peat are described in the literature (Givelet et al., 2004). A method for quantifying total Hg concentrations in homogenized peat samples is discussed here. A Milestone Direct Mercury Analyzer (DMA-80) is recommended as it does not require sample pre-treatment or wet chemistry prior to analysis. The instrument has a working range of 0.03 – 1500 $ng \cdot g^{-1}$ (Dual-cell version) or 0.01 – 1500 $ng \cdot g^{-1}$ (Tri-cell version) of Hg per sample and operates using an integrated sequence of thermal decomposition, catalyst conversion, amalgamation, and atomic absorption spectrophotometry as described by US EPA Method 7473 (USEPA, 2007). Peat samples should be analyzed using a program of 60 s drying time, 200 °C drying temperature, 180 s decomposition time, and 750 °C decomposition temperature.

We recommend preparing an appropriate quality control standard for data quality assurance purposes. This internal standard should be handled using the same techniques and stored in the same cool, dark environment as unknown samples. Certified Standard Reference Materials (SRMs), instrument blanks, boat blanks, and duplicates should also be analyzed with unknown samples for quality assurance purposes. Results in Table 2.1 demonstrate the high precision and accuracy of the Dual-cell DMA-80.

Hg flux calculation

Total Hg concentrations quantified using a DMA-80 can be combined with peat accumulation rates and bulk densities to derive Hg flux. Atmospherically deposited Hg flux ($\mu g \cdot m^{-2} \cdot y^{-1}$) from a peat archive is calculated using the following equation:

$$\text{Hg flux} = 10 \cdot [\text{Hg}] \cdot \text{BD} \cdot \text{AR}$$

where [Hg] is the total Hg concentration ($ng \cdot g^{-1}$), BD is the peat bulk density ($g \cdot cm^{-3}$), and AR is the peat accumulation rate ($cm \cdot y^{-1}$). Similar equations are often applied in paleoenvironmental and ecotoxicological studies to derive fluxes of other inorganic geochemical constituents.

References

Appleby, P.G., Nolan, P.J., Oldfield, F., Richardson, N., and Higgitt, S.R. (1988). 210 Pb dating of lake sediments and ombrotrophic peats by gamma essay: *Science*, v. 69, p. 157–177.

Bandara, S., Froese, D.G., Porter, T.J., Calmels, F., and Sanborn, P. (2017). Holocene climate change and thermokarst activity as recorded by stable isotopes in drained thermokarst lake basin permafrost from the Old Crow Flats, Yukon, Canada. *Manuscript in preparation*.

Barber, K.E., Chambers, F.M., and Maddy, D. (2003). Holocene palaeoclimates from peat stratigraphy: Macrofossil proxy climate records from three oceanic raised bogs in England and Ireland: *Quaternary Science Reviews*, v. 22, p. 521–539, doi: 10.1016/S0277-3791(02)00185-3.

Biester, H., Bindler, R., Martinez-Cortizas, A., and Engstrom, D.R. (2007). Modeling the past atmospheric deposition of mercury using natural archives: *Environmental Science and Technology*, v. 41, p. 4851–4860, doi: 10.1021/es0704232.

Biester, H., Kilian, R., Franzen, C., Woda, C., Mangini, A., and Schöler, H.F. (2002). Elevated mercury accumulation in a peat bog of the Magellanic Moorlands, Chile (53°S) - An anthropogenic signal from the Southern Hemisphere: *Earth and Planetary Science Letters*, v. 201, p. 609–620, doi: 10.1016/S0012-821X(02)00734-3.

Bindler, R. (2003). Estimating the natural background atmospheric deposition rate of mercury utilizing ombrotrophic bogs in Southern Sweden: *Environmental Science and Technology*, v. 37, p. 40–46, doi: 10.1021/es020065x.

Bindler, R., Klarqvist, M., Klaminder, J., and Förster, J. (2004). Does within-bog spatial variability of mercury and lead constrain reconstructions of absolute deposition rates from single peat records? The example of Store Mosse, Sweden: *Global Biogeochemical Cycles*, v. 18, doi: 10.1029/2004GB002270.

Brännvall, M.L., Bindler, R., Emteryd, O., Nilsson, M., and Renberg, I. (1997). Stable isotope and concentration records of atmospheric lead pollution in peat and lake sediments in Sweden: *Water, Air, and Soil Pollution*, v. 100, p. 243–252, doi: 10.1023/A:1018360106350.

Bronk Ramsey, C. (2009). Bayesian Analysis of Radiocarbon Dates: *Radiocarbon*, v. 51, p. 337–360, doi: 10.2458/azu_js_rc.v51i1.3494.

Calmels, F., Gagnon, O., and Allard, M. (2005). A portable Earth-drill system for permafrost studies: *Permafrost and Periglacial Processes*, v. 16, p. 311–315, doi: 10.1002/ppp.529.

Charman, D.J., Blundell, A., Chiverrell, R.C., Hendon, D., and Langdon, P.G. (2006). Compilation of non-annually resolved Holocene proxy climate records: Stacked Holocene peatland palaeo-water table reconstructions from northern Britain: *Quaternary Science Reviews*, v. 25, p. 336–350, doi: 10.1016/j.quascirev.2005.05.005.

Day, J.H., Rennie, P.J., Stanek, W., and Raymond, G.P. (1979). Peat Testing Manual: Technical Memorendum: *National Research Council of Canada - Muskeg Subcommittee*.

De Vleeschouwer, F., Piotrowska, N., Sikorski, J., Pawlyta, J., Cheburkin, a., Le Roux, G., Lamentowicz, M., Fagel, N., and Mauquoy, D. (2009). Multiproxy evidence of `Little Ice Age' palaeoenvironmental changes in a peat bog from northern Poland: *The Holocene*, v. 19, p. 625–637, doi: 10.1177/0959683609104027.

French, H., and Shur, Y. (2010). The principles of cryostratigraphy: *Earth-Science Reviews*, v. 101, p. 190–206, doi: 10.1016/j.earscirev.2010.04.002.

Froese, D.G., Davies, L.J., Appleby, P., Bandara, S., van Bellen, S., Magnan, G., Mullan-Boudreau, G., Noernberg, T., Shotyk, W., Staniszewska, K., and Zaccone, C. (2016). High-resolution age modelling of peat bog profiles using pre and postbomb 14C, 210Pb and cryptotephra data from Alberta and Yukon peatlands: *Dating the Anthropocene in Environmental Archives Workshop.*

Givelet, N., Roos-Barraclough, F., and Shotyk, W. (2003). Predominant anthropogenic sources and rates of atmospheric mercury accumulation in southern Ontario recorded by peat cores from three bogs: comparison with natural "background" values (past 8000 years).: J*ournal of environmental monitoring : JEM*, v. 5, p. 935–949, doi: 10.1039/b307140e.

Givelet, N., Le Roux, G., Cheburkin, A., Chen, B., Frank, J., Goodsite, M.E., Kempter, H., Krachler, M., Noernberg, T., Rausch, N., Rheinberger, S., Roos-Barraclough, F., Sapkota, A., Scholz, C., et al. (2004). Suggested protocol for collecting, handling and preparing peat cores and peat samples for physical, chemical, mineralogical and isotopic analyses: *Journal of environmental monitoring : JEM*, v. 6, p. 481–492, doi: 10.1039/b401601g.

Jones, M.C., Grosse, G., Jones, B.M., and Walter Anthony, K. (2012). Peat accumulation in drained thermokarst lake basins in continuous, ice-rich permafrost, northern Seward Peninsula, Alaska: *Journal of Geophysical Research: Biogeosciences*, v. 117, doi: 10.1029/2011JG001766.

Kempter, H., Görres, M., and Frenzel, B. (1997). Ti and Pb Concentrations in rainwater-fed bogs in Europe as indicators of past anthropogenic activities: *Water, Air, and Soil Pollution*, v. 100, p. 367–377, doi: 10.1023/A:1018376509985.

Klaminder, J., Renberg, I., Bindler, R., and Emteryd, O. (2003). Isotopic trends and background fluxes of atmospheric lead in northern Europe: Analyses of three ombrotrophic bogs from south Sweden: *Global Biogeochemical Cycles*, v. 17, doi: 10.1029/2002gb001921.

Kylander, M.E., Klaminder, J., Bindler, R., and Weiss, D.J. (2010). Natural lead isotope variations in the atmosphere: *Earth and Planetary Science Letters*, v. 290, p. 44–53, doi: 10.1016/j.epsl.2009.11.055.

Le Roux, G., and De Vleeschouwer, F. (2010). Preparation of peat samples for inorganic geochemistry used as palaeoenvironmental proxies: *Mires and Peat*, v. 7, p. 1–9.

Martinez-Cortizas, A. (1999). Mercury in a Spanish Peat Bog: Archive of Climate Change and Atmospheric Metal Deposition: *Science*, v. 284, p. 939–942, doi: 10.1126/science.284.5416.939.

Martínez-Cortizas, A., Pontevedra-Pombal, X., Nóvoa Muñoz, J.C., and García-Rodeja, E. (1997). Four thousand years of atmospheric Pb, Cd and Zn deposition recorded by the ombrotrophic peat bog of Penido Vello (Northwestern Spain): *Water, Air, and Soil Pollution*, v. 100, p. 387–403, doi: 10.1023/A:1018312223189.

Monna, F., Petit, C., Gulllaumet, J.P., Jouffroy-Bapicot, I., Blanchot, C., Dominik, J., Losno, R., Richard, H., Lévêque, J., and Chateau, C. (2004). History and Environmental Impact of Mining Activity in Celtic Aeduan Territory Recorded in a Peat Bog (Morvan, France): *Environmental Science and Technology*, v. 38, p. 665–673, doi: 10.1021/es034704v.

Murton, J.B., and French, H.M. (1994). Cryostructures in permafrost, Tuktoyaktuk coastlands, western arctic Canada: *Canadian Journal of Earth Sciences*, v. 31, p. 737–747, doi: 10.1139/e94-067.

Nørnberg, T., Goodsite, M.E., and Shotyk, W. (2004). An improved motorized corer and sample processing system for frozen peat: *Arctic*, v. 57, p. 242–246.

Novák, M., Emmanuel, S., Vile, M.A., Erel, Y., Véron, A., Pačes, T., Wieder, R.K., Vaněček, M., Štěpánová, M., Břízová, E., and Hovorka, J. (2003). Origin of lead in eight central European peat bogs determined from isotope ratios, strengths, and operation times of regional pollution sources: *Environmental Science and Technology*, v. 37, p. 437–445, doi: 10.1021/es0200387.

Oldfield, F., Appleby, P.G., Cambray, R.S., Eakins, J.D., Barber, K.E., Battarbee, R.W., Pearson, G.R., and Williams, J.M. (1979). 210 Pb, 137 Cs and 239 Pu Profiles in Ombrotrophic Peat: *Oikos*, v. 33, p. 40–45.

Outridge, P.M., and Sanei, H. (2010). Does organic matter degradation affect the reconstruction of pre-industrial atmospheric mercury deposition rates from peat cores? - A test of the hypothesis using a permafrost peat deposit in northern Canada: *International Journal of Coal Geology*, v. 83, p. 73–81, doi: 10.1016/j.coal.2010.04.004.

Page, S.E., Wűst, R.A.J., Weiss, D., Rieley, J.O., Shotyk, W., and Limin, S.H. (2004). A record of Late Pleistocene and Holocene carbon accumulation and climate change from an equatorial peat bog (Kalimantan, Indonesia): implications for past, present and future carbon dynamics: *Journal of Quaternary Science*, v. 19, p. 625–635, doi: 10.1002/jqs.884.

Pheiffer-Madsen, P. (1981). Peat bog records of atmospheric mercury deposition.: *Nature*, v. 293, p. 127–130, doi: 10.1038/293127a0.

Riley, J.L. (1989). Laboratory Methods for Testing Peat: Ontario Peatland Inventory Project: *Ontario Ministry of Northern Development and Mines*, v. 145.

Roos-Barraclough, F., and Shotyk, W. (2003). Millennial-scale records of atmospheric mercury deposition obtained from ombrotrophic and minerotrophic peatlands in the Swiss Jura mountains: *Environmental Science and Technology*, v. 37, p. 235–244, doi: 10.1021/es0201496.

Roos-Barraclough, F., Givelet, N., Martinez-Cortizas, A., Goodsite, M.E., Biester, H., and Shotyk, W. (2002). An analytical protocol for the determination of total mercury concentrations in solid peat samples: *Science of the Total Environment*, v. 292, p. 129–139, doi: 10.1016/S0048-9697(02)00035-9.

Roos-Barraclough, F., Martinez-Cortizas, A., García-Rodeja, E., and Shotyk, W. (2002). A 14 500 year record of the accumulation of atmospheric mercury in peat: Volcanic signals, anthropogenic influences and a correlation to bromine accumulation: *Earth and Planetary Science Letter*s, v. 202, p. 435–451, doi: 10.1016/S0012-821X(02)00805-1.

Shotyk, W. (2002). The chronology of anthropogenic, atmospheric Pb deposition recorded by peat cores in three minerogenic peat deposits from Switzerland: *Science of the Total Environment*, v. 292, p. 19–31, doi: 10.1016/S0048-9697(02)00030-X.

Shotyk, W., and Steinmann, P. (1994). Pore-water indicators of rainwater-dominated versus groundwater-dominated peat bog profiles (Jura Mountains, Switzerland): *Chemical Geology*, v. 116, p. 137–146, doi: 10.1016/0009-2541(94)90162-7.

Shotyk, W., Goodsite, M.E., Roos-Barraclough, F., Frei, R., Heinemeier, J., Asmund, G., Lohse, C., and Hansen, T.S. (2003). Anthropogenic contributions to atmospheric Hg, Pb and As accumulation recorded by peat cores from southern Greenland and Denmark dated using the 14C "bomb pulse

curve": *Geochimica et Cosmochimica Acta*, v. 67, p. 3991–4011, doi: 10.1016/S0016-7037(03)00409-5.

Shotyk, W., Weiss, D., Appleby, P.G., Cheburkin, A.K., Frei, R., Kramers, J.D., Reese, S., and Van Der Knaap, W.O. (1998). History of Atmospheric Lead Deposition Since 12,370 14C yr BP from a Peat Bog, Jura Mountains, Switzerland: *Science*, v. 281, p. 1635–1640, doi: 10.1126/science.281.5383.1635.

Swindles, G., Vleeschouwer, F. De, and Plunkett, G. (2010). Dating peat profiles using tephra: stratigraphy, geochemistry and chronology: *Mires and Peat*, v. 7, p. 1–9, http://www.doaj.org/doaj?func=fulltext&aId=896235.

USEPA. (2007). Mercury in solids and solutions by thermal decomposition, amalgamation, and atomic absorption spectrophotometry - method 7473 - total Mercury: SW-846, *Test Methods for Evaluating Solid Waste, Physical/Chemical Methods*, p. 1–17, http://www.epa.gov/osw/hazard/testmethods/sw846/pdfs/7473.pdf.

Weiss, D., Shotyk, W., Rieley, J., Page, S., Gloor, M., Reese, S., and Martinez-Cortizas, A. (2002). The geochemistry of major and selected trace elements in a forested peat bog, Kalimantan, SE Asia, and its implications for past atmospheric dust deposition: *Geochimica et Cosmochimica Acta*, v. 66, p. 2307–2323, doi: 10.1016/S0016-7037(02)00834-7.

Xie, S., Nott, C.J., Avsejs, L.A., Volders, F., Maddy, D., Chambers, F.M., Gledhill, A., Carter, J.F., and Evershed, R.P. (2000). Palaeoclimate records in compound-specific dD values of a lipid biomarker in ombrotrophic peat: *Organic Geochemistry*, v. 31, p. 1053–1057, doi: 10.1016/S0146-6380(00)00116-9.

Figures and Tables

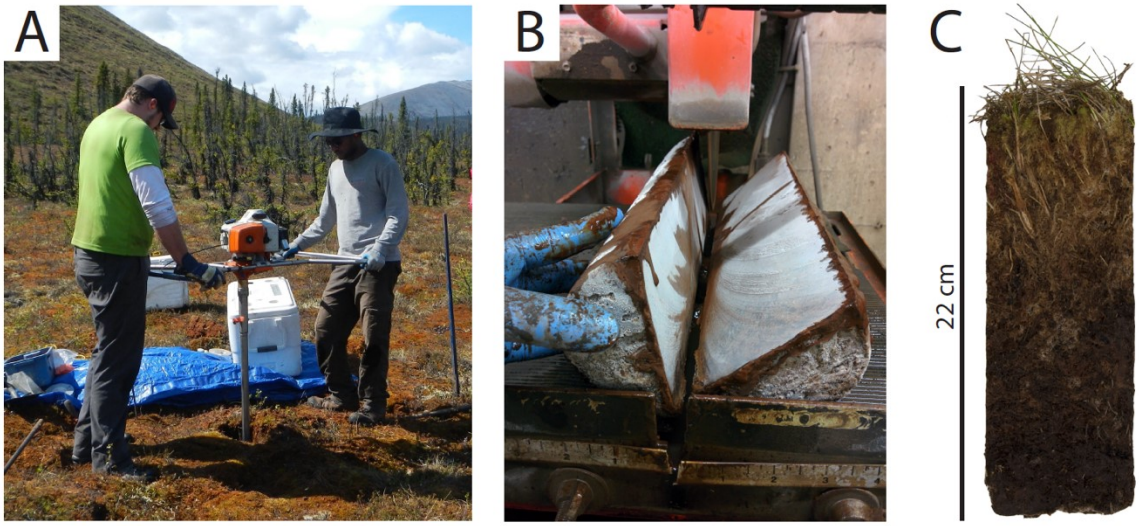

Figure 2.1 (A) Recovering peat permafrost cores using a portable earth-drill equipped with a heavy-duty diamond-edged core barrel (Calmels et al., 2005), (B) splitting a peat permafrost core in half using a rock saw with a 35 cm diameter diamond cutting wheel, (C) cross-sectional image of a 22 cm long near-surface peat core which was cut using the saw in panel B.

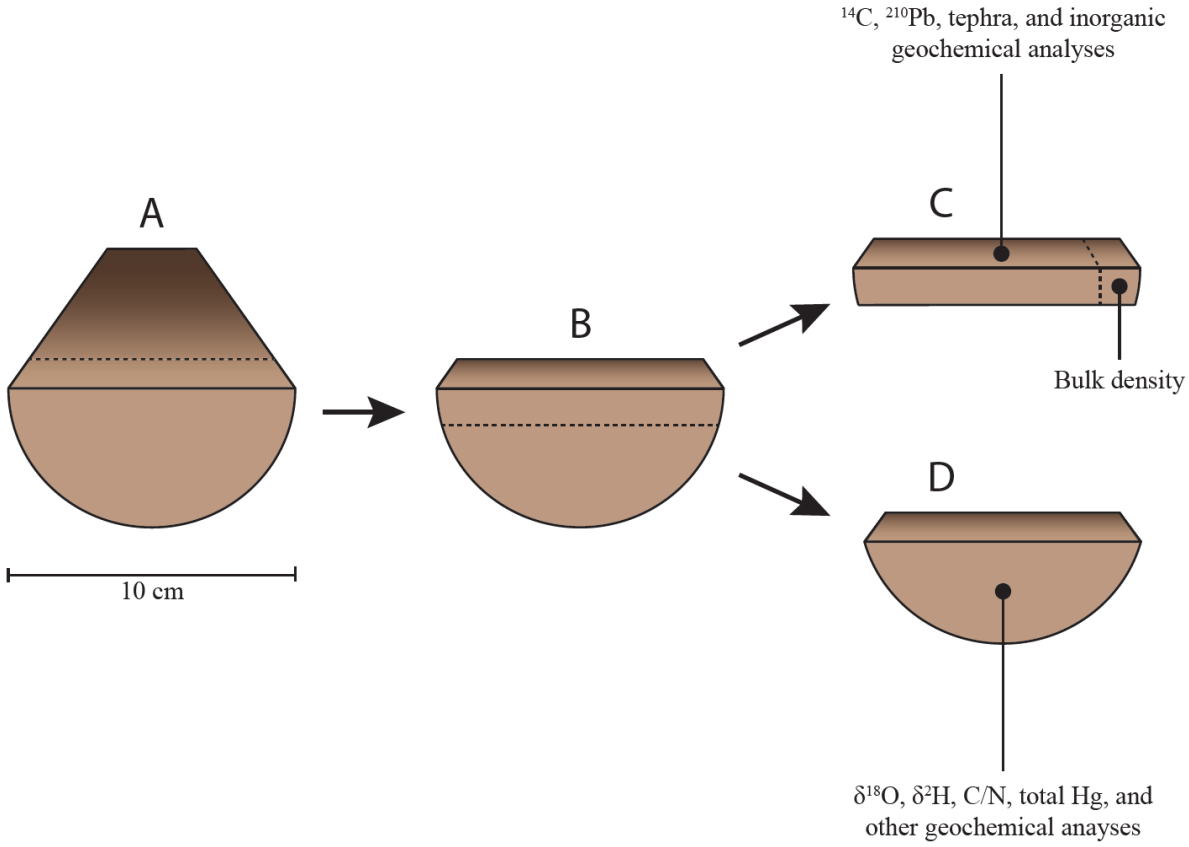

Figure 2.2 Flow chart outlining proposed procedure for processing fibrous peat permafrost samples. (A) Split core segments are subsampled at 1-cm intervals using a compact table saw, (B) subsamples are further subdivided, (C) one aliquot is used for constraining chronology and calculating bulk density, and (D) remaining aliquot is used for geochemical analyses, including pore-water/ice stable isotopes and total Hg.

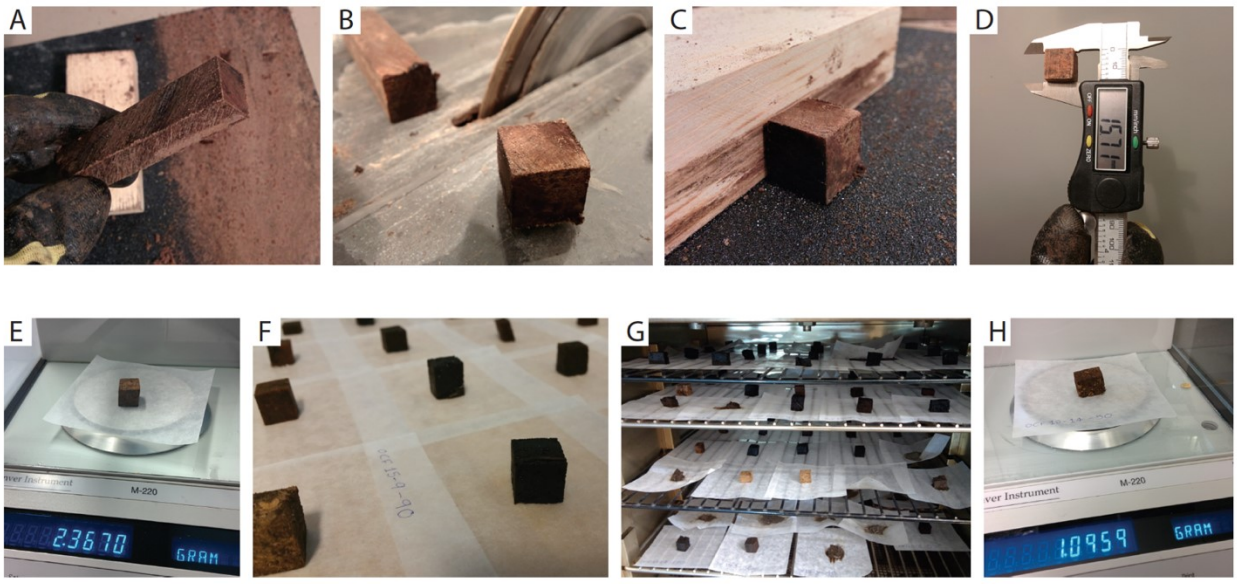

Figure 2.3 Cuboid method for density calculation. (A) Original peat permafrost samples sanded to be rectangular prisms, (B) cuboid aliquot cut using compact table saw with 15 cm diameter diamond cutting wheel, (C) cuboid sanded using 80-grit sandpaper to have flat, rectangular faces, (D) digital caliper (± 0.01 mm) used to measure physical dimensions of cuboid for volume calculation, (E) digital analytical balance (± 0.0001 g) used to measure wet weight, (F) cuboids thawed at room temperature, (G) cuboids completely dried in oven at 80 °C for 24 hours, and (H) dry weight measured using digital analytical balance. Bulk (dry) density of a given sample was quantified by dividing the dry mass of the sample by its initial (wet) volume. Cuboids were cut in a walk-in freezer at -5 °C to prevent thaw. Subsamples taken for density calculation were excluded from geochemical analyses to prevent potential issues from added or lost constituents during sanding and oven drying.

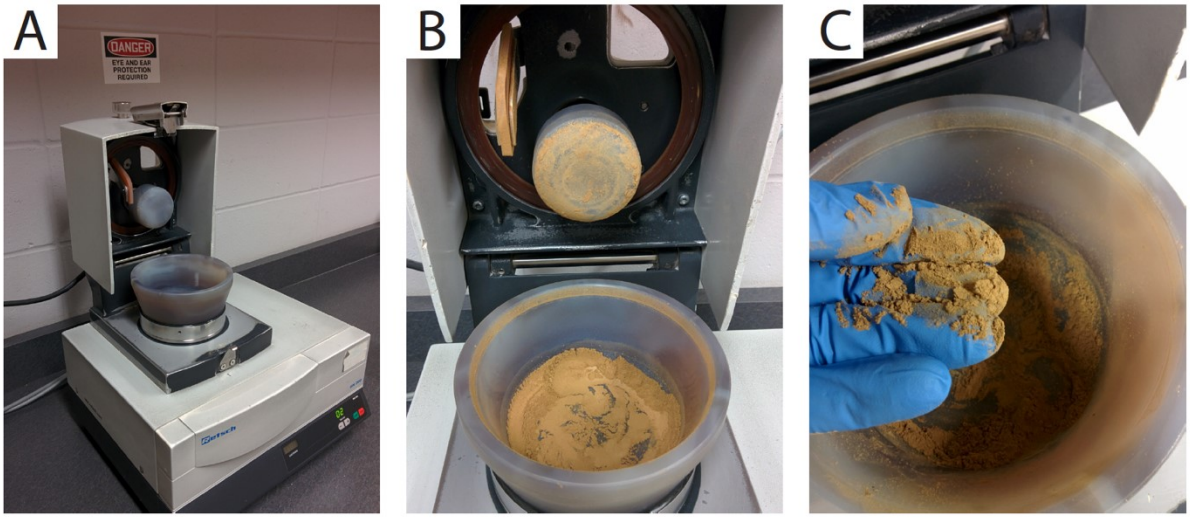

Figure 2.4 Proposed method for homogenizing freeze-dried peat samples. (A) A Retsch RM 200 automated agate mortar and pestle is recommended for homogenizing peat samples, (B) fibrous peat pulverized after 2 minutes of operation, and (C) completely homogenized peat powder after an additional minute of grinding. Peat powder should be carefully poured into a 50-mL centrifuge tube. All components of the automated agate mortar and pestle should be meticulously rinsed with water and wiped using paper towel soaked in acetone to prevent cross-contamination.

Table 2.1 Accuracy and precision of instrument blanks, nickel boat blanks, unknown sample duplicates, a quality control standard (QCSB-DH15), and a certified standard reference material (MESS-3 marine sediment; certified value: 91 ± 9 $\mu g \cdot kg^{-1}$). Measurements were made using a Dual-cell Milestone DMA-80 with the following program settings: 60 s drying time, 200 °C drying temperature, 180 s decomposition time, and 750 °C decomposition temperature.

	Hg Concentration ($ng \cdot g^{-1}$)				Relative standard deviation (%)
	Min	Max	Mean	Standard deviation	
Instrument blank (n=6)	0.0324	0.0623	0.0475	0.0124	26.11
Boat blank total (n=6)	0.0357	0.0656	0.0461	0.0110	23.86
QCSB-DH15 (n=12)	13.1074	14.1946	13.7100	0.3203	2.336
MESS-3 (n=12)	81.8014	89.3468	85.7717	2.0427	2.382

***Duplicate average % difference (*n=11*): 1.54%**

Chapter 3: Post-depositional mercury mobility in active layers of peat permafrost from central Yukon: implications for reconstructing historic mercury deposition fluxes using permafrost archives

ABSTRACT

Ombrotrophic peat archives in regions underlain by permafrost are thought to provide reliable records of atmospheric mercury (Hg) deposition.[1–3] Here, we analyze permafrost core segments from a rapidly aggrading raised peat plateau in central Yukon in an effort to reconstruct natural and anthropogenic Hg deposition fluxes during the last 400 years. Our results reveal a close correlation between Hg concentrations and pore-water/ice $\delta^{18}O$. Permafrost pore-ice acquires meteoric water isotopes over centennial to millennial timescales, but active layer pore-waters are mobilized and fractionated by evaporation and freezing over annual timescales. We suggest that atmospherically deposited Hg is also subject to mobilization within the active layer through chemo-physical interactions involving complexing and solubilizing agents in DOM-rich pore-waters. This new insight on post-depositional Hg mobility within the active layer, highlighted by the correlation between Hg concentrations and pore-water/ice $\delta^{18}O$, suggests that caution must be exercised when interpreting peat permafrost as high-resolution archives of historic Hg deposition.

INTRODUCTION

Mercury (Hg) is a global contaminant that is cycled through the earth system by a variety of natural and anthropogenic processes.[1,4,5] Volcanism, degassing from hydrothermal systems, wildfires, soil erosion, and marine emissions are thought to be the most dominant natural sources of Hg to the atmosphere.[6] Anthropogenic sources, such as coal-fired energy production, precious-metal extraction, and waste incineration, have produced the majority (70-80%) of global Hg emissions since the onset of the Industrial Revolution (ca. AD 1850).[7–9] Approximately 95% of atmospheric Hg is in the form of reduced gaseous elemental mercury (GEM; Hg^0),[6,10] which may be hemispherically dispersed due to its long atmospheric residence time of 0.5-2 years.[6] GEM can also become oxidized to Hg^{2+} and deposited on land, freshwater, or the ocean surface by wet or dry deposition.[11] Oxidized species such as gaseous oxidized mercury (GOM; Hg^{2+}) and particulate-bound mercury (Hg_p) account for less than 5% of global atmospheric Hg, but may be proportionately more abundant near sources of emissions where they are typically deposited.[6,10] Importantly, Hg^{2+} may be converted to methylmercury (MeHg) under anoxic conditions[12] in wetlands, sediments, and lake bottom waters by microorganisms such as sulfate- and iron-reducing bacteria.[13,14] Methylmercury, which bioaccumulates in living organisms and biomagnifies through food chains, is a neurotoxin whose debilitating effects have been globally recognized since the deadly Hg poisoning event of 1956 in Minamata, Japan.[15] Whole-ecosystem studies, such as the Mercury Experiment to Assess Atmospheric Loading in Canada and the United States (METAALICUS), have demonstrated that the production of MeHg within an aquatic system is approximately proportional to atmospheric Hg inputs.[16,17] This finding and other information regarding the potency of MeHg have prompted international initiatives, such as the Minamata

Convention (http://www.mercuryconvention.org/), aimed at better understanding the global Hg biogeochemical cycle and protecting human health and the environment from Hg pollution.

To effectively assess the impact of anthropogenic Hg emissions, naturally occurring (or background) concentrations and fluxes must first be quantified.[18] Widely utilized archives of pre-industrial and modern atmospheric Hg deposition include soils,[19] firn and ice,[20,21] lake sediments,[8,22] and peat deposits.[1–3] There are inherent challenges to using each of these archives; however, it has been suggested that minerotrophic[23,24] and ombrotrophic[25–29] peatlands are viable for reconstructing atmospheric Hg deposition over decadal to millennial timescales.[30,31] Due to restricted groundwater inflow and minimal organic matter humification in comparison to their warm-climate counterparts, northern peat bogs and raised permafrost peatlands are thought to contain excellent Hg deposition records.[32]

Here, we analyze permafrost core segments from a rapidly aggrading peat plateau near Dawson, Yukon, Canada, to reconstruct Hg deposition fluxes during the last 400 years. We place an emphasis on the past 150 years when anthropogenic emissions have been known to increase, locally due in part to extensive gold mining in the Klondike. The discrepancy between our record and widely accepted accounts of global atmospheric Hg deposition is explored through the use of pore-water/ice oxygen isotope ($\delta^{18}O$) measurements. The correlation between pore-water/ice $\delta^{18}O$ and corresponding Hg concentrations provides new insight into post-depositional Hg mobility which may challenge the robustness of northern peat archives that have long been considered faithful recorders of atmospheric Hg deposition.

MATERIALS AND METHODS

Study site

The KH32 (informal name) peat plateau is located adjacent to the Klondike Highway, approximately 32 km east of Dawson, Yukon, Canada (Figure 3.1). The study site lies within the Klondike Plateau Ecoregion which was largely unglaciated and contains surface deposits composed of colluvium, alluvium, and glacial outwash terraces covered by silts and peat.[33] Bedrock in this region belongs to the Yukon-Tanana Terrane and is dominated by a suite of metasedimentary and igneous rocks from former volcanic island arc and continental shelf depositional environments.[33,34] Due to the presence of ice-rich peat permafrost, the coring location (64°02'18.3"N 138°50'23.2"W; 404 masl) is raised relative to its surroundings and is therefore characterized by nutrient-poor, ombrotrophic conditions. Surface vegetation at KH32 consists of black spruce (*Picea mariana*), white spruce (*Picea glauca*), dwarf birch (*Betula nana*), Labrador tea (*Rhododendron tomentosum*), kinnikinnick (*Arctostaphylos uva-ursi*), cloudberry (*Rubus chamaemorus*), reindeer lichen (*Cladonia rangifernia*), and sphagnum moss (*Sphagnum spp.*). Local mean annual temperature is -4.1 °C and mean annual precipitation is 324 mm.[35] Channeled by the Klondike River valley, prevailing winds at KH32 are predominantly from the west/southwest and north/northeast during both summer and winter.[36]

Core collection and dating

A 129-cm active layer/shallow peat permafrost core was recovered from KH32 using a portable gas-powered earth-drill equipped with a 40 cm long, 10 cm diameter, core barrel as described in Calmels et al. (2005).[37] The core was collected on May 25, 2016. Thaw depth at the time of collection was 24 cm below the ground. Core segments (~25 cm long on average) were individually sealed in clean polyethylene bags and kept frozen during transport to the University

of Alberta. Terrestrial plant macrofossils subsampled from the core were chemically pretreated following a standard acid-base-acid (ABA) protocol and submitted for Accelerator Mass Spectrometry (AMS) ^{14}C dating at the André E. Lalonde AMS Laboratory at the University of Ottawa (Table A1.1). Radiocarbon dates were calibrated using OxCal v4.2,[38] and the IntCal13[39] and Bomb13NH1[40] calibration curves were used accordingly. Freeze-dried, homogenized aliquots of peat were submitted for ^{210}Pb dating (CRS model[41] corroborated by ^{137}Cs and ^{226}Ra) at Flett Research Ltd. in Winnipeg, Manitoba, Canada (Table A1.1).

Sample processing and analysis

Core segments were cut in half lengthwise using a diamond-bladed rock saw. Split core segments were cleaned using stainless steel razor blades, then imaged and characterized (Table A1.2) based on the cryostratigraphic classification scheme of Murton and French (1994).[42] Subsamples were taken at 2-cm intervals along the entire 129 cm length of the core. Working in a cold-room at -5 °C to prevent thaw, a cuboid aliquot was cut from each subsample for calculating (dry) bulk density (BD; Figure A1.1). Loss on ignition (LOI) was measured as described in the supporting information (Appendix 1). Pore-waters were extracted using a felt-padded benchtop vise and subsequently analyzed for oxygen stable isotope ratios using a Picarro L2130-i water isotope analyzer (σ = 0.1‰ for $\delta^{18}O$). Frozen peat subsamples from each depth were freeze-dried, homogenized using a Retsch RM 200 automated agate mortar and pestle (Figure A1.2), and analyzed for total Hg concentration (THg; all forms of Hg) using a Dual-cell Milestone DMA-80 (US EPA Method 7473)[43] at the University of Alberta Biogeochemical Analytical Service Laboratory. Accuracy and precision of instrument blanks, boat blanks, duplicates, quality controls, and the certified standard reference material (MESS-3 [marine sediment, certified value: 91 ± 9 $ng \cdot g^{-1}$]) associated with DMA-80 measurements are presented in Table A1.3.

RESULTS AND DISCUSSION

Core stratigraphy and chronology

The *P_Sequence* function on OxCal v4.2,[38] was used in conjunction with ^{14}C and ^{210}Pb results to produce a composite Bayesian age-depth model which best represents peat accumulation rates at KH32 (Figure A1.3). The age-depth model reveals that peat accumulation rates have averaged ~0.3 $cm \cdot y^{-1}$ during the last 400 years (Figure A1.4B). Increased accumulation rates of up to ~1.4 $cm \cdot y^{-1}$ in the uppermost 6 cm of the profile represent low-density contemporary growing-layer sphagnum moss that has not yet been subject to decomposition and subsequent compaction. The ^{210}Pb activity profile of the study core reveals an irregular, but approximately exponential, decrease as a function of depth (Figure 3.2E) and therefore provides useful chronological information. The significance of unexpected ^{210}Pb peaks at depths of 56 and 78 cm is discussed below. Compiled geochemical results organized by depth and modelled age are presented in Table A1.4.

Hg concentrations and fluxes

Total Hg concentrations in our peat core range from 18 to 140 $ng \cdot g^{-1}$ during the last 400 years (Figure 3.2A). Concentrations remain relatively low (~22 $ng \cdot g^{-1}$) until ca. AD 1670, but exhibit an overall increase thereafter. Atmospherically deposited Hg fluxes, expressed in $\mu g \cdot m^{-2} \cdot y^{-1}$, were calculated using the following equation:

$$\text{Hg flux} = 10 \cdot [\text{Hg}] \cdot \text{BD} \cdot \text{AR}$$

where [Hg] is the Hg concentration in $ng \cdot g^{-1}$ (Figure 3.2A), BD is the peat bulk density in $g \cdot cm^{-3}$ (Figure A1.4A), and AR is the peat accumulation rate in $cm \cdot y^{-1}$ (Figure A1.4B). Hg fluxes range between ~1 and 206 $\mu g \cdot m^{-2} \cdot y^{-1}$ (Figure 3.2B). Given that AR remains largely unchanged at

approximately 0.3 $cm \cdot y^{-1}$ for much of the record, BD and [Hg] are the main controls on Hg deposition flux.

The anomalously high Hg fluxes at a depth of ~6 cm (ca. AD 2007) are likely artefacts of rapid sphagnum growth and a lack of compaction within, and immediately underlying, the growing layer. Overall, our Hg concentration and flux profiles differ from previously published records. Relatively low levels of wet and dry atmospheric Hg deposition are expected until the onset of the Industrial Revolution (ca. AD 1850), following which anthropogenic sources of Hg become more locally and globally significant.[31,44–46] The hypothesized Hg signal from Klondike gold mining is not apparent in the reconstructed record. Instead, the increase in Hg concentrations observed in our core begins much earlier than we would expect from human activities. This implies that changes in atmospheric Hg deposition rates are not the only factors influencing the distribution of Hg in our peat archive.

Pore-water/ice $\delta^{18}O$ and its correlation with Hg concentration

The $\delta^{18}O$ measurements from pore-water/ice in the study core provide insight into potential chemo-physical processes affecting the Hg record. Precise $\delta^{18}O$ measurements are commonly obtained from ice-cores[47,48] and syngenetic permafrost archives[49,50] for reconstructing paleoclimatic and paleoenvironmental conditions in light of hydroclimatic fractionation mechanisms.[51,52] Arctic and subarctic syngenetic permafrost typically contains pore-ice that is isotopically characteristic of late-summer/autumn precipitation because this water percolates to the base of the active layer (i.e. top of permafrost) prior to the onset of freeze-up in winter.[49,50] With the exception of $\delta^{18}O$ enrichment at the base of the episodically thawed transition zone[53] (~80 cm depth) due to meteoric water contributions from an exceptionally warm summer, syngenetic peat permafrost in our core (58-129 cm depth) contains relatively stable $\delta^{18}O$ values

averaging -21.4‰ (Figure 3.3). These results are within range of the expected isotopic signature for late-summer/autumn precipitation (approximately -21‰) near Dawson, Yukon.[54–58]

In contrast to the underlying permafrost, pore-waters within the active layer of our core contain more complex $\delta^{18}O$ signatures. Bottom-up freezing at the base of the active layer (~56 cm depth) during the onset of winter induces freezing fractionation[59] whereby heavier isotopes of oxygen (^{18}O) are preferentially drawn downwards to the freezing front. This process has resulted in $\delta^{18}O$ enrichment from 50-60 cm and a consequent $\delta^{18}O$ depletion between 40-50 cm (Figure 3.3). Pore-ice $\delta^{18}O$ values from 20-30 cm resemble unaltered meteoric waters from the autumn of 2015. Conversely, pore-waters in overlying peats show enrichment due to evaporation following seasonal thaw of the active layer, which had penetrated to a depth of ~24 cm at the time of core collection in late May, 2016.

The pore-water/ice $\delta^{18}O$ profile is positively correlated with total Hg concentration (R^2 = 0.4; Figure A1.5) suggesting that common processes are affecting both variables. This correlation also implies that anthropogenic Hg deposited on the KH32 peat plateau has been mobile with meteoric waters in the active layer. More specifically, vertical migration of pore-waters may have transported atmospherically deposited Hg through the active layer thereby altering any record of historic deposition that would otherwise be preserved. We discuss this possibility in more detail below.

Active layer Hg mobility

According to our age-depth model (Figure A1.3), the AD 1850 ground surface is now at a depth of 50 cm. If the AD 1850 active layer was about the same thickness (~56 cm) as it is today, then when anthropogenic Hg emissions to the atmosphere began to increase globally (AD 1850), the base of the active layer at our site reached peat that dates to ca. AD 1670 (Figure 3.4). Early

anthropogenic Hg emissions sequestered by, or deposited onto, the peat plateau during the mid-19th century was subject to cycling within the active layer. Thus, there has been a downward displacement of anthropogenic Hg pollution beginning around ca. AD 1850. This also explains the absence of a hypothesized increase in Hg concentrations from extensive gold mining in the Klondike between ca. AD 1896 and 1920.[60–62] During this interval Hg was widely used on riffles of sluice boxes to amalgamate gold before being vaporized by heat during the refining process.[63,64]

Our results indicate an increase in Hg concentrations since ca. AD 1670 (i.e., at the base of AD 1850 active layer; Figure 3.4). At first glance, this may appear to mark the onset of anthropogenic Hg pollution given that natural background levels of Hg are low and stable before this time. However, attributing this rise in Hg concentration to a concurrent rise in anthropogenic Hg pollution is problematic because global atmospheric Hg emissions did not increase significantly until industrialization (ca. AD 1850).[31,44–46] The increase in Hg concentration since AD 1670 is more likely due to late 19th and early 20th century Hg pollution migrating vertically downward through the active layer to the top of permafrost, where it has since become immobilized (Figure 3.4). The correlation between Hg concentration peaks and pore-water/ice $\delta^{18}O$ enrichments therefore result from active layer Hg mobility rather than changes in atmospheric Hg deposition rates.

Biogeochemical factors controlling the mobility of heavy metals in mineral soils and peat have been intensively studied.[65–67] In the case of Hg in rain-fed bogs, the dominant form of initial Hg sequestration is via foliar uptake of GEM dry deposition (~80%).[68,69] However, this Hg can be transferred to pore-waters and deeper peat via litterfall and plant senescence. Wet deposition of Hg accounts for about 20% of initial atmospheric deposition in peat bogs.[68,69] This Hg is typically available to move with peat pore-waters immediately following deposition. We hypothesize that

the correlation between pore-water $\delta^{18}O$ and Hg concentration in our core reflects a common mechanism – the vertical transport of both water and Hg within active layer pore-waters. This may be partly due to increasing Hg partitioning in the aqueous phase as active layer peat degrades, to some degree, before becoming frozen-in by aggrading permafrost. This freezing process, which we term "cryosequestration", facilitates the conversion of pore-water-Hg from the base of the active layer to pore-ice-Hg at the top of permafrost. Hence, cryosequestration results in the long-term storage of atmospherically deposited Hg in the absence of permafrost thaw (Figure 3.4).

Mechanisms of Hg mobility within the active layer

Post-depositional Hg mobility is primarily controlled by adsorption and complexation reactions involving OH^-, Cl^-, and other organic anion ligands in solution.[70–74] The high affinity of Hg^{2+} to anionic ligands in pore-waters allows for effective post-depositional movement because resulting compounds, including $HgCl_2$ and $Hg(OH)_2$, are highly soluble, and therefore mobile, at the chloride and pH ranges of typical peat bogs.[70,75,76] Humic substances and fulvic acids found in bog waters between pH 3 and 6 are also strong complexing and solubilizing agents which contribute to Hg mobilization.[76–80] Pore-waters that were filtered through 0.2 μm nylon membranes for $\delta^{18}O$ analyses in this study had pH values ranging from 4.25 to 5.5 (Figure A1.6). These waters also exhibited yellow/brown colouration (Figure A1.6), indicating the presence of dissolved organic matter (DOM)[81,82] and organic host molecules for facilitating Hg mobility within pore-waters.[70,76,79,83] This notion is reinforced by the generally elevated LOI values (Figure 3.2D) which suggest a lack of clay minerals and therefore minimal immobilization of Hg through the formation of insoluble organo-mineral complexes.[79] Considered collectively, there is good evidence that the vertical migration of DOM-rich bog waters can also mobilize Hg.

In our peat core, hydrologic connectivity and post-depositional metal mobility is further supported by ^{210}Pb results (Figure 3.2E). Similar to Hg, Pb also commonly occurs as a divalent cation with potential for mobility within DOM-rich bog waters.[11,84–86] It is therefore not surprising to see a positive correlation between Hg concentration and Pb activity (Figure 3.2A and E). Both constituents exhibit anomalous peaks at ~56 cm and ~78 cm corresponding to the bases of the active layer and transition zone respectively. One caveat of post-depositional Pb mobility is that ^{210}Pb may be an imperfect chronometer which overestimates accumulation rates at shallow depths.[87,88] However, our composite Bayesian age-model (Figure A1.3) incorporates AMS ^{14}C dates from terrestrial plant macrofossils, including post-bomb dates at shallow depths, which collectively provide additional chronological information for this study.

Implications of post-depositional metal mobility

The usefulness of ombrotrophic peat archives for reconstructing atmospheric deposition of Hg, and possibly other heavy metals, depends on whether the degree of post-depositional mobility is small enough to preserve changes in atmospheric deposition rates.[66,76,89] In this study, we document evidence for post-depositional Hg mobility in a permafrost peat plateau near Dawson, Yukon, using pore-water/ice δ^{18}O measurements. Mobility inferred from the correlation between Hg concentration and δ^{18}O is further supported by ^{210}Pb distribution, which shows a similar pattern albeit at a lower resolution because fewer samples were analyzed for ^{210}Pb. Given the strong affinity of Hg^{2+} to anionic ligands in DOM-rich pore-waters, and the subsequent migration of resulting compounds within the active layer, we suggest that peat permafrost archives may not contain straightforward records of atmospheric Hg deposition as previously hypothesized. Geochemical characterization of pore-waters, including δ^{18}O measurements, are recommended as suitable screening methods for post-depositional Hg mobility in future investigations using peat

permafrost archives for historic atmospheric deposition reconstructions. Furthermore, experimentally applied isotope tracers may aid in not only identifying post-depositional mobility, but also quantifying rates at which subsurface Hg migration occurs. For instance, Branfireun et al. (2005)[90] demonstrated rapid vertical and horizontal migration of Hg using ^{202}Hg isotope tracing. The same technique could be used at KH32 to test the hypothesis that any experimentally applied ^{202}Hg will migrate downwards from the peat surface to the base of the active layer within one complete thaw cycle. Future research may also investigate post-depositional partitioning of Hg and test for potential correlations between total Hg concentration and chromophoric DOM as quantified by absorbance spectroscopy.

ASSOCIATED CONTENT

Supporting Information (Appendix 1)

Bulk density measurement method (Figure A1.1), peat homogenization method (Figure A1.2), composite Bayesian age-depth model (Figure A1.3), bulk density and peat accumulation rate (Figure A1.4), correlation between pore-water/ice $\delta^{18}O$ and total Hg concentration (Figure A1.5), pore-water pH and colouration due to DOM (Figure A1.6), AMS ^{14}C data and CRS ^{210}Pb data (Table A1.1), cryostratigraphic classification of cores (Table A1.2), DMA-80 data quality (Table A1.3), compiled geochemical results organized by depth and modelled age (Table A1.4), and LOI method (Appendix 1).

ACKNOWLEDGMENTS

Funding for this research was provided by The W. Garfield Weston Foundation, EnviroNorth, the Geological Society of America, and NSERC. Special thanks to Joseph Young, Casey Buchanan, and Alireza Saidi-Mehrabad for assistance with core collection; Mark Labbe and Crystal Dodge for technical support with sample processing; and Dr. Daniel Alessi, Sarah Shakil, and Emily Moffat for insight and expertise that greatly improved the manuscript.

FIGURES AND TABLES

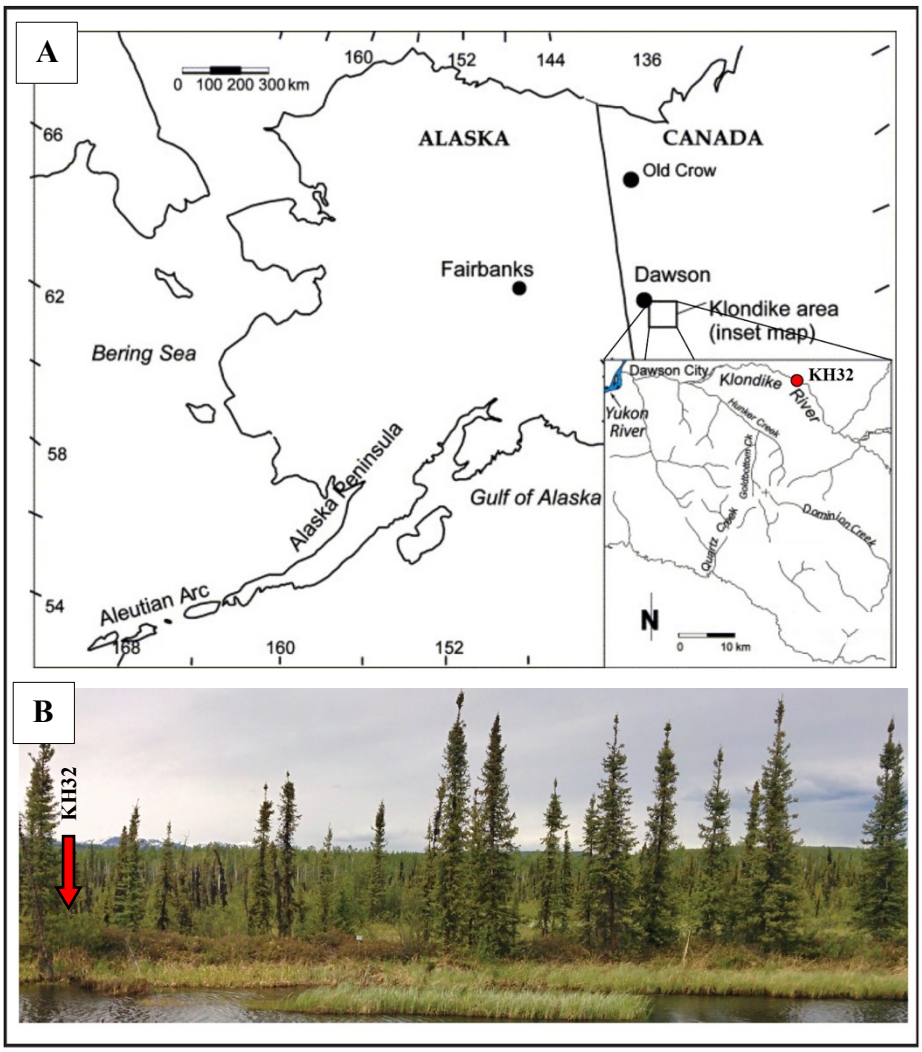

Figure 3.1 (A) Map showing study site with reference to Dawson, Yukon (modified from Froese et al., 2002)[91] and (B) image of peat plateau, KH32, from which the study core was collected.

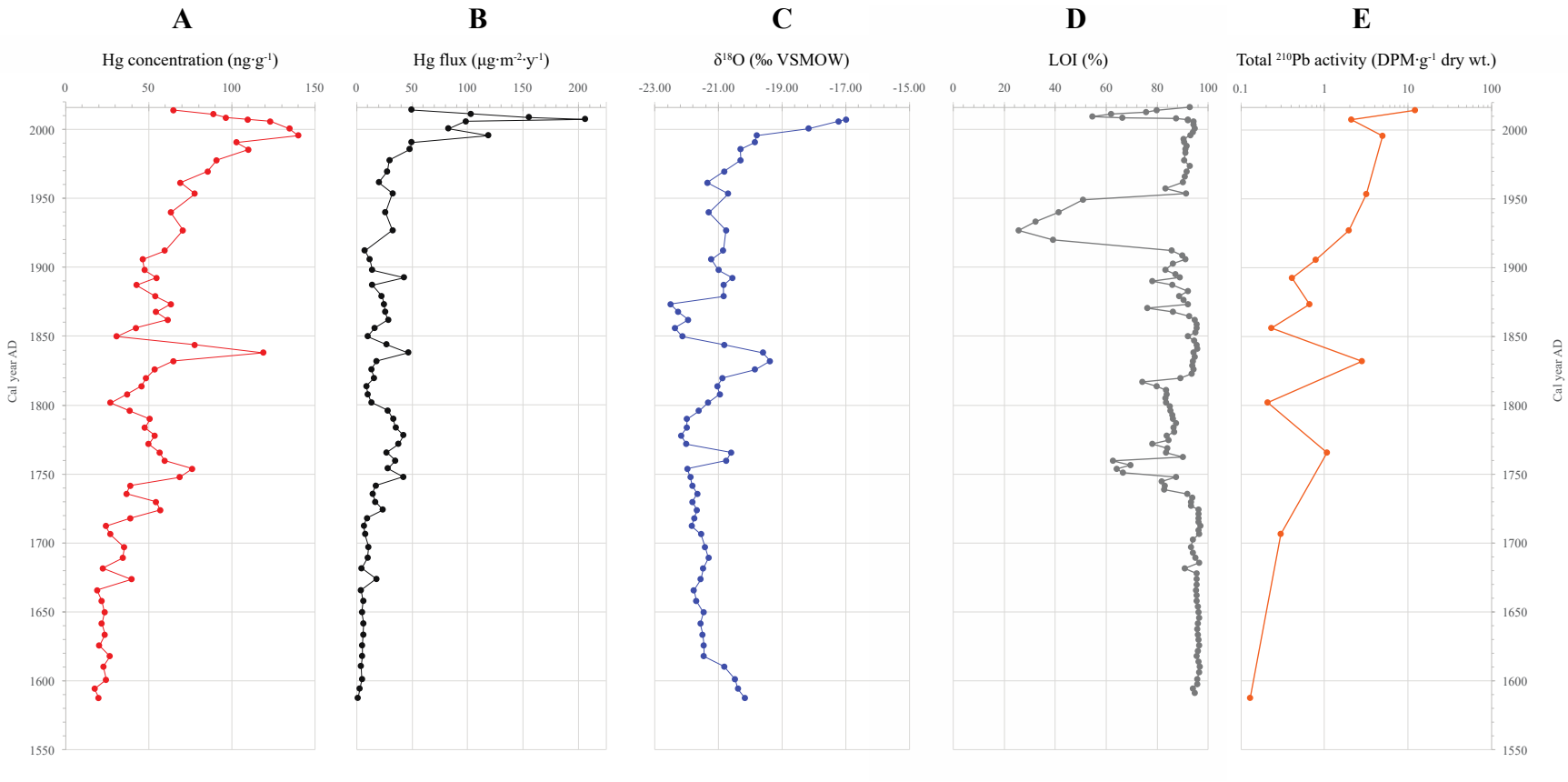

Figure 3.2 Analytical results from the study core. (A) Hg concentration (ng·g^{-1}), (B) Hg flux (µg·m^{-2}y^{-1}), (C) $\delta^{18}O$ (‰VSMOW), (D) LOI (%), and (E) total Pb-210 activity (DPM/g dry wt.).

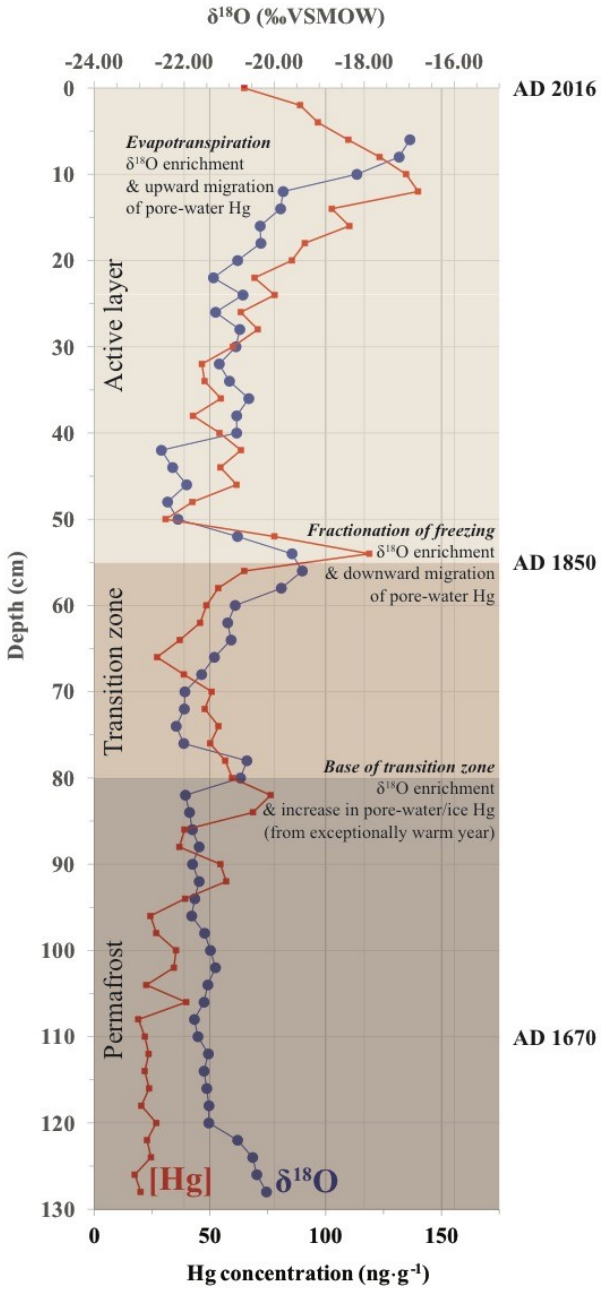

Figure 3.3 Correlation between [Hg] and $\delta^{18}O$ in the study core. Evaporative enrichment of $\delta^{18}O$ occurs in the uppermost 20 cm; late-summer/autumn meteoric water $\delta^{18}O$ signatures are evident from 20-40 cm and 58-129 cm; the depleted $\delta^{18}O$ signature from 40-50 cm is due to fractionation during freeze-up, which also results in a corresponding enrichment centred at 55 cm depth; and enriched $\delta^{18}O$ values at the base of the transition zone (~80 cm depth) is due to an exceptionally warm year.

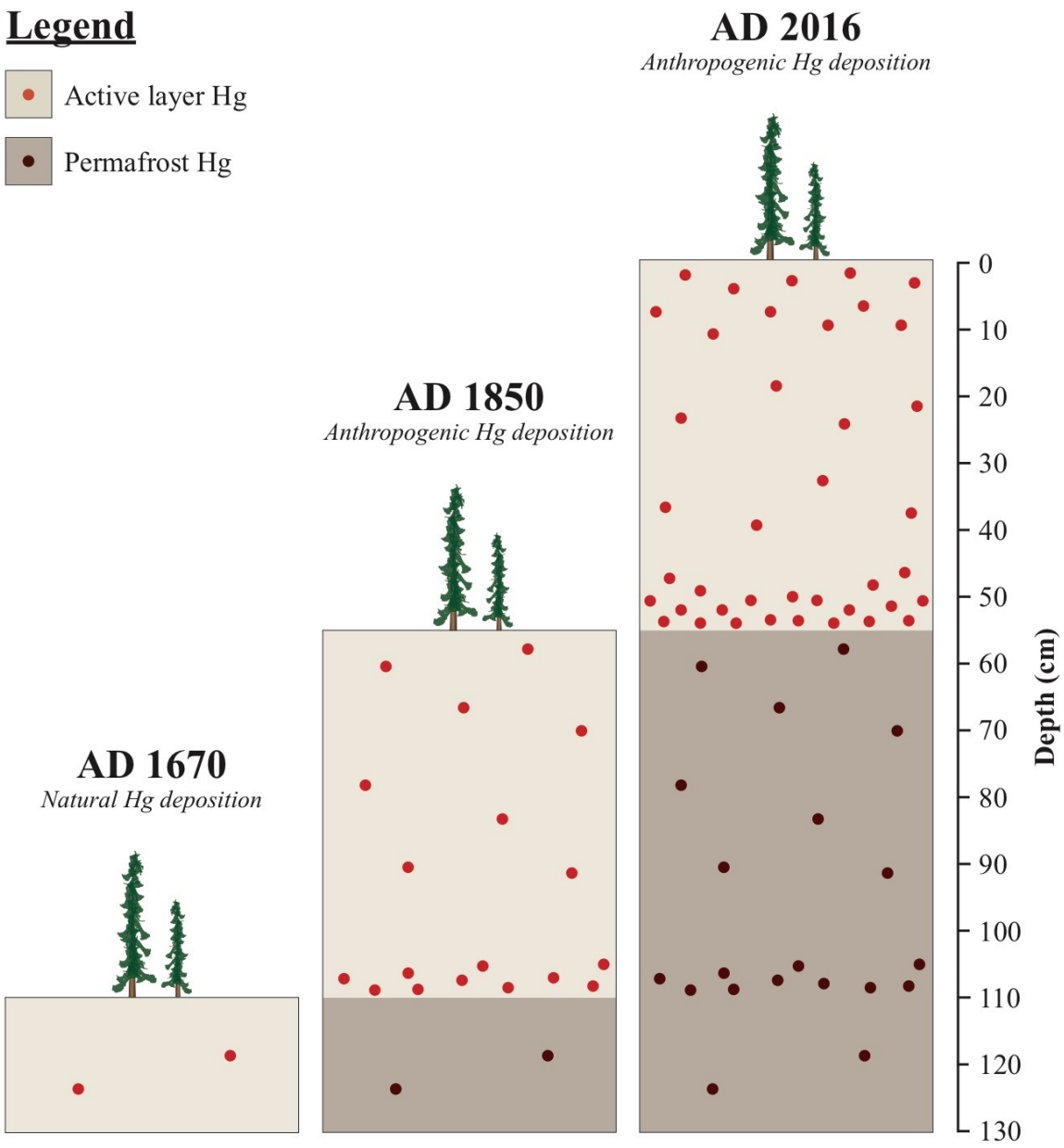

Figure 3.4 Atmospheric Hg deposition and peat plateau development over time. Natural Hg deposition rates persist until AD 1850, following which Hg deposition rates increase due to human activities. Elevated Hg concentrations from industrial emissions since AD 1850 are mobile within the annually thawed active layer. As permafrost aggrades, Hg at the base of the active layer/top of permafrost gets frozen-in (or "cryosequestered") to long-term storage in the absence of thaw.

REFERENCES

(1) Givelet, N.; Roos-Barraclough, F.; Shotyk, W. Predominant Anthropogenic Sources and Rates of Atmospheric Mercury Accumulation in Southern Ontario Recorded by Peat Cores from Three Bogs: Comparison with Natural "background" values (Past 8000 Years). *J. Environ. Monit.* **2003**, *5* (6), 935–949.

(2) Givelet, N.; Roos-Barraclough, F.; Goodsite, M. E.; Cheburkin, A. K.; Shotyk, W. Atmospheric Mercury Accumulation between 5900 and 800 Calibrated Years BP in the High Arctic of Canada Recorded by Peat Hummocks. *Environ. Sci. Technol.* **2004**, *38* (19), 4964–4972.

(3) Roos-Barraclough, F.; Martinez-Cortizas, A.; García-Rodeja, E.; Shotyk, W. A 14 500 Year Record of the Accumulation of Atmospheric Mercury in Peat: Volcanic Signals, Anthropogenic Influences and a Correlation to Bromine Accumulation. *Earth Planet. Sci. Lett.* **2002**, *202* (2), 435–451.

(4) Gustin, M. S.; Lindberg, S. E.; Weisberg, P. J. An Update on the Natural Sources and Sinks of Atmospheric Mercury. *Appl. Geochemistry* **2008**, *23* (3), 482–493.

(5) Engstrom, D. R.; Fitzgerald, W. F.; Cooke, C. A.; Lamborg, C. H.; Drevnick, P. E.; Swain, E. B.; Balogh, S. J.; Balcom, P. H. Atmospheric Hg Emissions from Preindustrial Gold and Silver Extraction in the Americas: A Reevaluation from Lake-Sediment Archives. *Environ. Sci. Technol.* **2014**, *48* (12), 6533–6543.

(6) Schroeder, W. H.; Munthe, J. Atmospheric Mercury - An Overview. *Atmos. Environ.* **1998**, *32* (5), 809–822.

(7) Mason, R.; Fitzgerald, W.; Morel, F. The Biogeochemical Cycling of Elemental Mercury: Anthropogenic Influences. *Geochim. Cosmochim. Acta* **1994**, *58* (15), 3191–3198.

(8) Phillips, V. J. A.; St. Louis, V. L.; Cooke, C. A.; Vinebrooke, R. D.; Hobbs, W. O. Increased Mercury Loadings to Western Canadian Alpine Lakes over the Past 150 Years. *Environ. Sci. Technol.* **2011**, *45* (6), 2042–2047.

(9) Driscoll, C. T.; Mason, R. P.; Chan, H. M.; Jacob, D. J.; Pirrone, N. Mercury as a Global Pollutant: Sources, Pathways, and Effects. *Environmental Science and Technology*. **2013**, pp 4967–4983.

(10) Pacyna, E. G.; Pacyna, J. M. Global Emission of Mercury from Anthropogenic Sources in 1995. *Water. Air. Soil Pollut.* **2002**, *137* (1–4), 149–165.

(11) Lamborg, C. H.; Fitzgerald, W. F.; Damman, A. W. H.; Benoit, J. M.; Balcom, P. H.; Engstrom, D. R. Modern and Historic Atmospheric Mercury Fluxes in Both Hemispheres: Global and Regional Mercury Cycling Implications. *Global Biogeochem. Cycles* **2002**, *16* (4), 51.

(12) Jensen, S.; Jernelöv, a. Biological Methylation of Mercury in Aquatic Organisms. *Nature* **1969**, *223* (5207), 753–754.

(13) Compeau, G. C.; Bartha, R. Sulfate-Reducing Bacteria: Principal Methylators of Mercury in Anoxic Estuarine Sediment. *Applied and Environmental Microbiology*. 1985, pp 498–502.

(14) Kerin, E. J.; Gilmour, C. C.; Roden, E.; Suzuki, M. T.; Coates, J. D.; Mason, R. P. Mercury Methylation by Dissimilatory Iron-Reducing Bacteria. *Appl. Environ. Microbiol.* **2006**, *72* (12), 7919–7921.

(15) Poulain, A. J.; Barkay, T. Cracking the Mercury Methylation Code. *Science.* **2013**, *339* (6125), 1280–1281.

(16) Harris, R. C.; Rudd, J. W. M.; Amyot, M.; Babiarz, C. L.; Beaty, K. G.; Blanchfield, P. J.; Bodaly, R. a; Branfireun, B. a; Gilmour, C. C.; Graydon, J. a; et al. Whole-Ecosystem Study Shows Rapid Fish-Mercury Response to Changes in Mercury Deposition. *Proc. Natl. Acad. Sci. U. S. A.* **2007**, *104* (42), 16586–16591.

(17) Swain, E. B.; Jakus, P. M.; Rice, G.; Lupi, F.; Maxson, P. a; Pacyna, J. M.; Penn, A.; Spiegel, S. J.; Veiga, M. M. Socioeconomic Consequences of Mercury Use and Pollution. *Ambio* **2007**, *36* (1), 45–61.

(18) Roos-Barraclough, F.; Givelet, N.; Cheburkin, A. K.; Shotyk, W.; Norton, S. A. Use of Br and Se in Peat to Reconstruct the Natural and Anthropogenic Fluxes of Atmospheric Hg: A 10000-Year Record from Caribou Bog, Maine. *Environ. Sci. Technol.* **2006**, *40* (10), 3188–3194.

(19) Amirbahman, A.; Ruck, P. L.; Fernandez, I. J.; Haines, T. A.; Kahl, J. S. The Effect of Fire on Mercury Cycling in the Soils of Forested Watersheds: Acadia National Park, Maine, USA. *Water, Air, and Soil Pollution.* **2004**, *152* (1–4), 313–331.

(20) Beal, S.; Osterberg, E. C.; Zdanowicz, C.; Fisher, D. An Ice Core Perspective on Mercury Pollution during the Past 600 Years. *Environ. Sci. Technol.* **2015**, *49*, 7641–7647.

(21) Schuster, P. F.; Krabbenhoft, D. P.; Naftz, D. L.; Cecil, L. D.; Olson, M. L.; Dewild, J. F.; Susong, D. D.; Green, J. R.; Abbott, M. L. Atmospheric Mercury Deposition during the Last 270 Years: A Glacial Ice Core Record of Natural and Anthropogenic Sources. *Environ. Sci. Technol.* **2002**, *36* (11), 2303–2310.

(22) Cooke, C. A.; Wolfe, A. P.; Michelutti, N.; Balcom, P. H.; Briner, J. P. A Holocene Perspective on Algal Mercury Scavenging to Sediments of an Arctic Lake. *Environ. Sci. Technol.* **2012**, *46* (13), 7135–7141.

(23) Roos-Barraclough, F.; Shotyk, W. Millennial-Scale Records of Atmospheric Mercury Deposition Obtained from Ombrotrophic and Minerotrophic Peatlands in the Swiss Jura Mountains. *Environ. Sci. Technol.* **2003**, *37* (2), 235–244.

(24) Shotyk, W.; Goodsite, M. E.; Roos-Barraclough, F.; Frei, R.; Heinemeier, J.; Asmund, G.; Lohse, C.; Hansen, T. S. Anthropogenic Contributions to Atmospheric Hg, Pb and As Accumulation Recorded by Peat Cores from Southern Greenland and Denmark Dated Using the 14C "bomb Pulse Curve." *Geochim. Cosmochim. Acta* **2003**, *67* (21), 3991–4011.

(25) Pheiffer-Madsen, P. Peat Bog Records of Atmospheric Mercury Deposition. *Nature* **1981**, *293*, 127–130.

(26) Jensen, A.; Jensen, A. Historical Deposition Rates of Mercury in Scandinavia Estimated by Dating and Measurement of Mercury in Cores of Peat Bogs. *Water Air Soil Pollut.* **1991**, *56* (1), 769–777.

(27) Benoit, J. M.; Fitzgerald, W. F.; Damman, a W. The Biogeochemistry of an Ombrotrophic Bog: Evaluation of Use as an Archive of Atmosphere Mercury Deposition. *Environ. Res.* **1998**, *78* (2), 118–133.

(28) Martinez-Cortizas, A. Mercury in a Spanish Peat Bog: Archive of Climate Change and Atmospheric Metal Deposition. *Science (80-.).* **1999**, *284* (1999), 939–942.

(29) Biester, H.; Kilian, R.; Franzen, C.; Woda, C.; Mangini, A.; Schöler, H. F. Elevated Mercury Accumulation in a Peat Bog of the Magellanic Moorlands, Chile (53°S) - An Anthropogenic Signal from the Southern Hemisphere. *Earth Planet. Sci. Lett.* **2002**, *201* (3–4), 609–620.

(30) Grigal, D. F. Mercury Sequestration in Forests and Peatlands: A Review. *J. Environ. Qual.* **2003**, *32* (2), 393–405.

(31) Biester, H.; Bindler, R.; Martinez-Cortizas, A.; Engstrom, D. R. Modeling the Past Atmospheric Deposition of Mercury Using Natural Archives. *Environ. Sci. Technol.* **2007**, *41* (14), 4851–4860.

(32) Outridge, P. M.; Sanei, H. Does Organic Matter Degradation Affect the Reconstruction of Pre-Industrial Atmospheric Mercury Deposition Rates from Peat Cores? - A Test of the Hypothesis Using a Permafrost Peat Deposit in Northern Canada. *Int. J. Coal Geol.* **2010**, *83* (1), 73–81.

(33) Yukon Ecoregions Working Group. *Klondike Plateau. In: Ecoregions of the Yukon Territory: Biophysical Properties of Yukon Landscapes,*; Smith, C. A. S., Meikle, J. C., Roots, C. F., Eds.; Agriculture and Agri-Food Canada, PARC Technical Bulletin No. 04-01, **2004**.
(34) Mortensen, J. K. Pre-mid-Mesozoic Tectonic Evolution of the Yukon-Tanana Terrane, Yukon and Alaska. *Tectonics* **1992**, *11* (4), 836–853.
(35) Environment Canada - Government of Canada. Canadian Climate Normals 1981-2010 Station Data "Dawson A - Yukon Territory" http://climate.weather.gc.ca/climate_normals/results_1981_2010_e.html?stnID=1535&lang=e&StationName=dawson&SearchType=Contains&stnNameSubmit=go&dCode=0 (accessed May 9, **2016**).
(36) Klock, R.; Hudson, E.; Aihoshi, D.; Mullock, J. The Weather of the Yukon, Northwest Territories and Western Nunavut: Graphic Area Forecast 35. **2001**.
(37) Calmels, F.; Gagnon, O.; Allard, M. A Portable Earth-Drill System for Permafrost Studies. *Permafr. Periglac. Process.* **2005**, *16* (3), 311–315.
(38) Bronk Ramsey, C. Bayesian Analysis of Radiocarbon Dates. *Radiocarbon* **2009**, *51* (1), 337–360.
(39) Reimer, P. J.; Bard, E.; Bayliss, A.; Beck, J. W.; Blackwell, P. G.; Bronk, M.; Grootes, P. M.; Guilderson, T. P.; Haflidason, H.; Hajdas; et al. IntCal 13 and Marine 13 Radiocarbon Age Calibration Curves 0–50,000 Years Cal BP. *Radiocarbon* **2013**, *55*, 1869–1887.
(40) Hua, Q.; Barbetti, M.; Rakowski, a Z. Atmospheric Radiocarbon for the Period 1950-2010. *Radiocarbon* **2013**, *55* (4), 2059–2072.
(41) Appleby, P. G.; Oldfield, F. The Calculation of Lead-210 Dates Assuming a Constant Rate of Supply of Unsupported 210Pb to the Sediment. *Catena* **1978**, *5* (1), 1–8.
(42) Murton, J. B.; French, H. M. Cryostructures in Permafrost, Tuktoyaktuk Coastlands, Western Arctic Canada. *Can. J. Earth Sci.* **1994**, *31* (4), 737–747.
(43) US EPA (US Environmental Protection Agency). Mercury in Solids and Solutions by Thermal Decomposition, Amalgamation, and Atomic Absorption Spectrophotometry - Method 7473 - Total Mercury. *SW-846, Test Methods Eval. Solid Waste, Phys. Methods* **2007**, 1–17.
(44) Streets, D. G.; Devane, M. K.; Lu, Z.; Bond, T. C.; Sunderland, E. M.; Jacob, D. J. All-Time Releases of Mercury to the Atmosphere from Human Activities. *Environ. Sci. Technol.* **2011**, *45* (24), 10485–10491.
(45) Horowitz, H. M.; Jacob, D. J.; Amos, H. M.; Streets, D. G.; Sunderland, E. M. Historical Mercury Releases from Commercial Products: Global Environmental Implications. *Environ. Sci. Technol.* **2014**, *48* (17), 10242–10250.
(46) Streets, D. G.; Horowitz, H. M.; Jacob, D. J.; Lu, Z.; Levin, L.; Schure, A. F. H.; Sunderland, E. M. Total Mercury Released to the Environment by Human Activities. **2017**, *51* (11), 5969–5977.
(47) Shackleton, N. J.; Opdyke, N. D. Oxygen Isotope and Palaeomagnetic Stratigraphy of Equatorial Pacific Core V28-238: Oxygen Isotope Temperatures and Ice Volumes on a 105 Year and 106 Year Scale. *Quat. Res.* **1973**, *3* (1), 39–55.
(48) Petit, R. J.; Raynaud, D.; Basile, I.; Chappellaz, J.; Ritz, C.; Delmotte, M.; Legrand, M.; Lorius, C.; Pe, L. Climate and Atmospheric History of the Past 420,000 Years from the Vostok Ice Core, Antarctica. *Nature* **1999**, *399*, 429–413.
(49) Mahony, M. E. 50,000 Years of Paleoenvironmental Change Recorded in Meteoric Waters and Coeval Paleoecological and Cryostratigraphic Indicators from the Klondike Goldfields, Yukon, Canada, University of Alberta, **2015**.

(50) Bandara, S.; Froese, D. G.; Porter, T. J.; Calmels, F.; Sanborn, P. Holocene Climate Change and Thermokarst Activity as Recorded by Stable Isotopes in Drained Thermokarst Lake Basin Permafrost from the Old Crow Flats, Yukon, Canada. *Manuscript in preparation*. **2017**.
(51) Craig, H. Isotopic Variations in Meteoric Waters. *Science* **1961**, *133* (3465), 1702–1703.
(52) Dansgaard, W. Stable Isotopes in Precipitation. *Tellus A* **1964**.
(53) Bockheim, J. G.; Hinkel, K. M. Characteristics and Significance of the Transition Zone in Drained Thaw-Lake Basins of the Arctic Coastal Plain , Alaska. *Arctic* **2005**, *58* (4), 406–417.
(54) Bowen, G. J. The Online Isotopes in Precipitation Calculator, version 3.1. http://www.waterisotopes.org (accessed Jun 22, **2017**).
(55) Bowen, G. J.; Revenaugh, J. Interpolating the Isotopic Composition of Modern Meteoric Precipitation. **2003**, *39* (10), 1–13.
(56) IAEA/WMO. Global Network of Isotopes in Precipitation. The GNIP Database. https://nucleus.iaea.org/wiser (accessed Jun 22, **2017**).
(57) Lapp, A. Seasonal Variability of Groundwater Contribution to Watershed Discharge in Discontinuous Permafrost in the North Klondike River Valley, Yukon, University of Ottawa, **2015**.
(58) Anderson, L.; Abbott, M. B.; Finney, B. P.; Burns, S. J. Regional Atmospheric Circulation Change in the North Pacific during the Holocene Inferred from Lacustrine Carbonate Oxygen Isotopes, Yukon Territory, Canada. *Quat. Res.* **2005**, *64* (1), 21–35.
(59) Tranter, M. Isotopic Fractionation of Freezing Water. In *Encyclopedia of Snow, Ice and Glaciers*; Singh, V. P., Singh, P., Haritashya, U. K., Eds.; Springer Netherlands: Dordrecht, **2011**; pp 668–669.
(60) Indian and Northern Affairs Canada. *Yukon Placer Mining Industry 1991-1992*; **1992**.
(61) Allen, D. W. Information Sharing during the Klondike Gold Rush. *J. Econ. Hist.* **2007**, *67* (4), 944–967.
(62) Van Loon, S.; Bond, J. D. *Yukon Placer Mining Industry 2010-2014*; **2014**.
(63) Osler, T. *Study of Mercury Usage in Placer Mining Operations in the Yukon Territory and North Western British Columbia*; **1983**.
(64) Willis, B. L. The Environmental Effects of the Yukon Gold Rush 1896 - 1906: Alterations to Land, Destruction of Wildlife, and Disease, **1997**.
(65) Ram, N.; Verloo, M. Effect of Various Organic Materials on the Mobility of Heavy Metals in Soil. *Environ. Pollut. (Series B)* **1985**, *10*, 241–248.
(66) Novak, M.; Pacherova, P. Mobility of Trace Metals in Pore Waters of Two Central European Peat Bogs. **2008**, *4*.
(67) Novak, M.; Zemanova, L.; Voldrichova, P.; Stepanova, M.; Adamova, M.; Pacherova, P.; Komarek, A.; Krachler, M.; Prechova, E. Experimental Evidence for Mobility / Immobility of Metals in Peat. **2011**, 7180–7187.
(68) Obrist, D.; Agnan, Y.; Jiskra, M.; Olson, C. L.; Dominique, P. Tundra Uptake of Atmospheric Elemental Mercury Drives Arctic Mercury Pollution. *Nature* **2017**, *547* (7662), 201–204.
(69) Enrico, M.; Le Roux, G.; Marusczak, N.; Heimbu, L.; Claustres, A. Atmospheric Mercury Transfer to Peat Bogs Dominated by Gaseous Elemental Mercury Dry Deposition. **2016**, *50* (5), 2405–2412.
(70) Schuster, E. The Behavior of Mercury in the Soil with Special Emphasis on Complexation and Adsorption Processes - A Review of the Literature. *Water, Air, Soil Pollut.* **1991**, *56* (1), 667–680.
(71) Jonasson, I. R. *Mercury in the Natural Environment: A Review of Recent Work.*; **1970**.
(72) Klusman, R. W.; Jaacks, J. Environmental Influences upon Mercury, Radon and Helium Concentrations in Soil Gases at a Site near Denver, Colorado. **1987**, *27*, 259–280.
(73) Evans, L. J. Chemistry of Metal Retention. *Environ. Sci. Technol.* **1989**, *23* (9), 1046–1056.

(74) Nriagu, J. O. *Biogeochemistry of Mercury in the Environment*; Elsevier/North-Holland Biomedical Press, **1979**.
(75) Lodenius, M.; Seppanen, A.; Uusi-Rauva, A. Sorption and Mobilization of Mercury in Peat Soil. *Chemosphere* **1983**, *12* (ll), 1575–1581.
(76) Rasmussen, P. E. Current Methods of Estimating Atmospheric Mercury Fluxes in Remote Areas. **1994**, No. 13, 2233–2241.
(77) Lodenius, M.; Seppanen, A.; Autio, S. Leaching of Mercury from Peat Soil. *Cheosphere* **1987**, *16* (6), 1215–1220.
(78) Lodenius, M.; Sepp, A.; Autio, S. Sorption of Mercury in Soils with Different Humus Content. *Bull. Environ. Contam. Toxicol.* **1987**, 593–600.
(79) Biester, H. U.; Muller, G.; Scholer, H. F. Binding and Mobility of Mercury in Soils Contaminated by Emissions from Chlor-Alkali Plants. *Sci. Total Environ.* **2002**, 191–203.
(80) Allard, B.; Arsenie, I. Abiotic Reduction of Mercury by Humic Substances in Aquatic System - an Important Process for the Mercury Cycle. *Water, Air, Soil Pollut.* **1991**, *56* (1), 457–464.
(81) Harvey, E. T.; Kratzer, S.; Andersson, A. Relationships between Colored Dissolved Organic Matter and Dissolved Organic Carbon in Different Coastal Gradients of the Baltic Sea. *Ambio* **2015**, *44* (3), 392–401.
(82) Green, S. A.; Blough, N. V. Optical Absorption and Fluorescence Properties of Chromophoric Dissolved Organic Matter in Natural Waters. *Limnol. Oceanogr.* **1994**, *39* (8), 1903–1916.
(83) Norton, S. A.; Dillon, P. J.; Evans, R. D.; Mierle, G.; Kahl, J. S. The History of Atmospheric Deposition of Cd, Hg, and Pb in North America: Evidence from Lake and Peat Bog Sediments. In *Acidic Precipitation: Sources, Deposition, and Canopy Interactions*; Lindberg, S. E., Page, A. L., Norton, S. A., Eds.; Springer New York: New York, NY, **1990**; pp 73–102.
(84) Urban, N. R.; Eisenreich, S. J.; Grigal, D. F.; Schurr, K. T. Mobility and Diagenesis of Pb and Diagenesis of Pb in Peat. *Geochim. Cosmochim. Acta* **1990**, *54*, 3329–3346.
(85) Damman, A. W. H. Distribution and Movement of Elements in Ombrotrophic Peat Bogs. **1978**, *30* (3), 480–495.
(86) Jones, J. M.; Hao, J. Ombrotrophic Peat as a Medium for Historical Monitoring of Heavy Metal Pollution. *Environ. Geochem. Health* **1993**, *15* (2–3), 67–74.
(87) Cooke, C. A.; Hobbs, W. O.; Neal, M.; Wolfe, A. P. Reliance on 210Pb Chronology Can Compromise the Inference of Preindustrial Hg Flux to Lake Sediments. *Environ. Sci. Technol.* **2010**, *44* (6), 1998–2003.
(88) Carpenter, R.; Peterson, M. L.; Bennett, J. T. 210Pb-Derived Sediment Accumulation and Mixing Rates for the Washington Continental Slope. *Mar. Geol.* **1982**, *48* (1–2), 135–164.
(89) Steinnes, E.; Sjøbakk, T. E. Order-of-Magnitude Increase of Hg in Norwegian Peat Profiles since the Outset of Industrial Activity in Europe. **2005**, *137*, 365–370.
(90) Branfireun, B. A.; Krabbenhoft, D. P.; Hintelmann, H.; Hunt, R. J.; Hurley, J. P.; Rudd, J. W. M. Speciation and Transport of Newly Deposited Mercury in a Boreal Forest Wetland : A Stable Mercury Isotope Approach. **2005**, *41*, 1–11.
(91) Froese, D.; Westgate, J.; Preece, S.; Storer, J. Age and Significance of the Late Pleistocene Dawson Tephra in Eastern Beringia. **2002**, *21*, 2137–2142.

Chapter 4: 10,000 years of atmospherically deposited mercury in peat permafrost archives from central and northern Yukon, Canada

ABSTRACT

Environmental archives are used to understand the influence of recent human activities and climate change on biogeochemical cycling of mercury (Hg). Arctic and subarctic cryosols, including ice-rich peat permafrost, have sequestered large quantities of organic carbon and Hg for thousands of years. However, with continued climate warming, it is hypothesized that these northern circumpolar soils will shift from stable C/Hg sinks to C/Hg sources through permafrost degradation. Accelerated release of Hg from thawing permafrost to downstream aquatic environments may pose a threat to both wildlife and humans. Here, we reconstruct millennial-scale atmospheric Hg deposition from Holocene (10,000-year old) permafrost peat plateaus (n = 2) along the Dempster Highway in central Yukon and Drained Thermokarst Lake Basin peat deposits (n = 5) in northern Yukon, Canada. Our findings provide a fundamental framework for future studies aimed at assessing (a) the significance of anthropogenic Hg emissions since the Industrial Revolution and (b) the inventory of Hg that may be released to downstream ecosystems with continued climate warming and permafrost degradation.

INTRODUCTION

Mercury (Hg) has been at the forefront of heavy metal contamination research in recent decades. The debilitating, and sometimes fatal, effects of Hg poisoning have been globally recognized since the well-documented Hg disaster of 1965 in Minamata, Japan. Ecological and societal implications of environmental Hg contamination have prompted intergovernmental initiatives, including the Minamata Convention (www.mercuryconvention.org), aimed at reducing Hg emissions from human activities. Such international agreements, and scientific findings regarding Hg biogeochemistry, have led to significant reductions in global anthropogenic Hg emissions since the 1970s.[1,2] Despite emissions reductions, Hg concentrations are rising among many arctic and subarctic biota.[3–5] This finding, coupled with the bioaccumulating and biomagnifying nature of methylmercury (MeHg),[6,7] threatens northern residents whose traditional diets include fish and other wildlife.[4,8–10] Many hypotheses have been proposed to explain the observed increase in Hg concentrations among northern circumpolar ecosystems including (a) the cold-condensation hypothesis,[11,12] (b) mercury depletion events during polar sunrise,[13–16] and (c) efficient scavenging of atmospheric Hg by arctic tundra vegetation and subsequent export of Hg to connected aquatic ecosystems.[17]

The absence of long-term monitoring data from the northern circumpolar region means that contextualizing recent increases in Hg loading requires the use of natural archives. Records based on lake sediments and ombrotrophic peat bogs have shown that post-industrial atmospheric Hg deposition fluxes are at least 3-fold,[18,19] and perhaps as much as an order of magnitude,[20] greater than pre-industrial background values. Reconstructing past deposition fluxes using environmental archives can be challenging; however, long-term accounts are important for advancing our

understanding of the natural Hg biogeochemical cycle and for assessing the significance of anthropogenic influences, especially since industriaization.[21]

Ombrotrophic peat bogs, which receive moisture and nutrient inputs solely from the atmosphere,[22] have been used to reconstruct atmospheric Hg deposition fluxes.[12,23–28] Recent studies have shown that atmospheric Hg inputs to these systems are primarily (~80%) due to dry deposition of gaseous elemental mercury (GEM; Hg^0), followed by Hg wet deposition (~20%), and particulate-bound Hg deposition (<1%).[17,29,30] While some post-depositional mobility may occur within seasonally thawed active layers, export of Hg from these peat archives is not expected provided that the system remains undisturbed over time. For this reason, many peatlands have served as sinks for both organic carbon (OC) and Hg over centennial to millennial timescales.[12,26] However, the fate of these long-term Hg reservoirs is uncertain, particularly in regions undergoing environmental change due to climate warming.

Globally, peatlands cover about 3.556×10^6 km^2, or approximately 19%, of the northern circumpolar permafrost region.[31] Many of these peat deposits are perennially frozen, ice-rich, and therefore particularly susceptible to thaw under warming scenarios. Research suggests that the northern circumpolar permafrost zone will undergo a reduction in areal extent between 37% and 81% by the end of the 21st century.[32] Rapid and widespread permafrost degradation is likely to have far-reaching implications. For instance, recent studies reveal that large quantities of labile OC will become biologically available and be released to aquatic and atmospheric systems as a result of permafrost thaw.[33–35] Similarly, it is hypothesized that permafrost degradation will also release large quantities of archived Hg to downstream aquatic systems[36–40] where it may be converted to methylmercury (MeHg) by methylating bacteria[41–43] and subsequently biomagnify through foodchains.[44] The projected transformation of northern peatlands and other organic-rich

cryosols from OC and Hg sinks to OC and Hg sources presents a timely concern that warrants further scientific investigation.[16]

To assess the potential for Hg release from permafrost thaw, cryosol Hg stocks must first be quantified. At present, there are several estimates of permafrost OC budgets based on empirical measurements from multiple depositional settings within the northern circumpolar region.[31,45–47] However, comparable estimates do not exist for permafrost-bound heavy metals such as Hg. In this study, we quantify concentrations of Hg in peat plateaus along the Dempster Highway in central Yukon and Drained Thermokarst Lake Basin (DTLB) peat deposits in northern Yukon, Canada. The objective is to provide a millennial-scale account of atmospheric Hg deposition fluxes during the Holocene (last 10,000 years) using seven peat permafrost archives from the Yukon Territory. Additionally, we demonstrate how these reconstructions may be used to estimate total Hg stocks in shallow peat permafrost deposits at the local scale. Our findings are intended to serve as a foundation for future investigations concerning cryosol Hg budgets and assessments of potential Hg release by permafrost thaw under projected climate warming scenarios.

MATERIALS AND METHODS

Study sites

Peat plateaus DHP170 and 174 (informal names) are located along the Dempster Highway in central Yukon, Canada (Figure 4.1). These sites lie in the North Ogilvie Mountains Ecoregion, which consists of unglaciated periglacial terrain within the continuous permafrost zone. In this ecoregion, surficial deposits of colluvium, tussock tundra, peat plateaus, and palsa bogs are underlain almost entirely by sedimentary rocks of the Keele Range and Taiga-Nahonni Fold Belt.[48] Regional soils are typically thick with humus-rich near-surface horizons which support white spruce (*Picea glauca*) shrub-forb communities on well drained southerly aspects, and black spruce

(*Picea mariana*) shrub-sedge tussock types on poorly drained gentle slopes. Mean annual temperature (MAT) is -7 to -10 °C and mean annual precipitation (MAP) is 300 to 450 mm.[48] Coring locations were broadly characterized by sphagnum moss (*Sphagnum spp.*) dominated peat deposits with well-established ice-wedge polygon networks. At both sites, surface vegetation also consisted of black spruce, white spruce, dwarf birch (*Betula nana*), Labrador tea (*Rhododendron tomentosum*), kinnikinnick (*Arctostaphylos uva-ursi*), cloudberry (*Rubus chamaemorus*), and reindeer lichen (*Cladonia rangifernia*). Precise coring location information and field images from DHP170 and 174 are available in the supporting information (Figure A2.1).

Peat deposits OCP9, 11, 14, and BFP16 and 19 (informal names) are from the Old Crow Flats Ecoregion in northern Yukon, Canada (Figure 4.1). This region contains up to 1200 m of Tertiary and Quaternary glaciolacustrine and fluvial sediments overlain by ~9 m of Late Pleistocene silts and clays deposited by glacial lake Old Crow.[49] The Old Crow Flats, which lies within the continuous permafrost zone, is poorly drained and contains ~2700 thermokarst lakes[50] collectively covering about 35% of the landscape.[51,52] Regional vegetation varies from shallow water-emergent communities to graminoid meadows, tussock tundra, polygonal peat plateau bogs, and sparsely-treed, shrub tundra.[49] MAT is -9 °C and MAP is 266 mm within the region.[53] Cores were collected from the centres of DTLBs containing peat plateaus with large (~25 m diameter) ice-wedge polygons. Surface vegetation at coring locations included dwarf birch, Labrador tea, cottongrass (*Eriophorum vaginatum*), kinnikinnick, cloudberry, and reindeer lichen. Precise coring location information and field images from OCP9, 11, 14, and BFP16 and 19 are available in the supporting information (Figure A2.1).

Core collection and dating

Shallow peat cores were recovered from the seven study sites using a portable gas-powered earth-drill equipped with a 40 cm long, 10 cm diameter core barrel.[54] The DHP174 core was collected in June 2013. All other cores were collected in late June/early July 2015 (Table A2.1). Thaw depths at the time of core collection are listed in Table A2.1. Core segments were individually sealed in clean polyethylene bags and kept frozen during transport to the University of Alberta. Terrestrial plant macrofossils were chemically pretreated using a standard acid-base-acid (ABA) protocol and submitted for ^{14}C dating at the University of California, Irvine, Keck Carbon Cycle AMS Facility and the University of Ottawa André E. Lalonde AMS Laboratory (Table A2.2). Radiocarbon dates were calibrated using OxCal v4.2.[55] and the IntCal13[56] calibration curve. Simple Bayesian age models were generated for each site using OxCal v4.2 (Appendix 2).

Sample processing and analysis

Core segments were cut in half lengthwise using a diamond-bladed rock saw. Split cores were cleaned using stainless steel razor blades, then imaged and characterized (Table A2.1) following the cryostratigraphic classification scheme of Murton and French (1994).[57] Subsamples were taken from each core at 10-cm intervals. Working in a cold-room at -5 °C to prevent thaw, cuboid aliquots were cut from each subsample to calculate (dry) bulk density (Figure A2.2). Unaltered frozen peat aliquots from each depth were individually freeze-dried, homogenized using a Retsch RM 200 automated agate mortar and pestle (Figure A2.3), and analyzed for total Hg concentration (THg; all forms of Hg) using a Dual-cell Milestone DMA-80 (US EPA Method 7473).[58] Accuracy and precision of instrument blanks, boat blanks, duplicates, quality controls, and the certified standard reference material (MESS-3 [marine sediment, certified value: 91 ± 9

ng·g^{-1}]) associated with DMA-80 measurements are presented in Table A2.3. All aforementioned sample processing and analyses were conducted at the University of Alberta.

RESULTS

Core stratigraphy and chronology

Peat monoliths that were thawed at the time of core collection were excluded from our analyses. Cryostratigraphic observations revealed that both central Yukon cores (DHP170 and 174) were entirely comprised of ice-rich peat (Figure 4.2). Each of the five DTLB cores (OCP9, 11, 14, and BFP16 and 19) from northern Yukon contained grey ice-rich silts (lacustrine sediments) that were overlain by ice-rich peat as shown in Figure 4.2. Peat was dominated by well-preserved *Sphagnum spp.* moss in all seven cores. AMS ^{14}C dates (n = 18) obtained from terrestrial plant macrofossils indicate that all seven cores are of Holocene age (Figure 4.2). While cores OCP9, 11, 14, and BFP16 mostly contain middle- to late-Holocene records, cores DHP170, 174, and BFP19 contain peat that dates back to the early Holocene (ca. 10,000 cal BP). Figure 4.2 also highlights the variability in peat accumulation rates, which is likely a function of local environmental conditions at each study site. For instance, DHP170 and 174 are only 4 km apart, but the latter site accumulated approximately twice as much peat in 9000 years.

Total Hg concentration

Total Hg concentrations are greatest (up to 103 ng·g^{-1}) in lacustrine silts underlying DTLB peat (Figure 4.2). Holocene peat permafrost contains much lower Hg concentrations. If we assume an active layer thickness of 60 cm for each site, average Hg concentrations for each of the seven peat permafrost sequences range from 11.2 to 28.8 ng·g^{-1} (Figure 4.2). The overall average Holocene peat permafrost Hg concentration was 20.7 ± 9.8 ng·g^{-1} (n = 79; Figure 4.3A).

Millennial-scale Hg flux

Millennial-scale Hg accumulation rates (or fluxes) were estimated for each core using the following equation:

$$\text{Hg flux} = 10 \cdot [\text{Hg}] \cdot \text{BD} \cdot \text{AR}$$

where [Hg] is the Hg concentration in $ng \cdot g^{-1}$ (Table A2.4), BD is the peat bulk density in $g \cdot cm^{-3}$ (Table A2.4), and AR is the peat accumulation rate in $cm \cdot y^{-1}$ based on ^{14}C Bayesian age-depth models (Appendix 2; Table A2.4). Peat permafrost background Hg accumulation rates were 510 ± 390 $\mu g \cdot m^{-2} \cdot 1000 y^{-1}$ (n = 79) during the Holocene (Figure 4.3B). Therefore, 5100 ± 3900 μg of Hg is expected to be sequestered in each square meter of a typical 10,000-year old peat permafrost deposit from central or northern Yukon, Canada.

DISCUSSION

Natural Hg accumulation

We calculated an average annual Hg flux rate of 0.51 ± 0.39 $\mu g \cdot m^{-2} \cdot y^{-1}$ (Figure 4.3B), which compares well with preindustrial background Hg accumulation rates of about 1 $\mu g \cdot m^{-2} \cdot y^{-1}$ quantified from other ombrotrophic peatlands in the northern hemisphere (Table 4.1). This is the first account of a preindustrial atmospheric Hg flux estimation from peat archives in Yukon, Canada. The most similar reconstruction, both in terms of archive type and geographic setting, comes from a 6000-year old permafrost peat deposit near Inuvik, NWT.[59] Average preindustrial Hg flux in the Inuvik study was 0.82 ± 0.36 $\mu g \cdot m^{-2} \cdot y^{-1}$ (Table 4.1), which is comparable to Holocene Hg flux estimates from our cores. Also important is the similarity between natural Hg fluxes from our study and those reconstructed from temperate bogs (Table 4.1).[27,30,60–64] This consistency suggests that cold climates have not necessarily promoted enhanced Hg accumulation

over millennial timescales as previously suggested.[12] Alternatively, natural Hg accumulation rates during the Holocene were too small to reveal a significantly greater sequestration of Hg in archives from colder regions.

Our previous work[65] demonstrated that atmospherically deposited Hg may be mobile within active layer pore-waters until becoming "cryosequestered" as permafrost slowly aggrades over centennial to millennial timescales. Such post-depositional mobility within the active layer is expected to dampen any original variability in Hg deposition rates that would otherwise be preserved in the permafrost record. Therefore, the stability and smoothness of Holocene Hg fluxes reconstructed by the seven peat archives in this study may also stem from post-depositional Hg mobility within active layers prior to eventual long-term immobilization in aggrading peat permafrost.

Anthropogenic Hg accumulation

The focus of our study was to quantify naturally deposited Hg concentrations and millennial-scale fluxes. However, thawed monoliths that were excluded from our study presumably contain the greatest concentrations and fluxes due to anthropogenic Hg deposition during recent centuries. Biester et al. (2007)[19] showed that anthropogenic Hg fluxes in a given peat archive are, on average, ~40x greater than natural background fluxes from the same archive. This implies that anthropogenic Hg fluxes should exceed millennial-scale background fluxes estimated from our study cores as shown in Figure 4.4. Figure 4.4 also highlights that (a) despite biophysical differences among our seven sites, natural Hg flux estimates are consistently low for the Holocene, (b) natural Hg accumulation rates, such as those quantified by our cores, demonstrate the significance of recent anthropogenic Hg contamination, and (c) near-surface peat and growing-layer moss contains large quantities of atmospherically deposited Hg. The final point is especially

important given that these uppermost sediments, and their Hg stocks, will be the first impacted by climatic and environmental change.

Estimating permafrost Hg stocks

Our results suggest that perennially frozen peat deposits from unglaciated central and northern Yukon contain similar concentrations of atmospherically deposited Hg (20.7 ± 9.8 $ng \cdot g^{-1}$; Figure 4.3A). Considering the consistency in Hg concentrations among our seven study cores, it may be feasible to apply this empirical Hg concentration average to derive first-order approximations of Holocene peat permafrost Hg stocks in the Yukon. For example, a relatively small (500 m x 500 m x 1.5 m) DTLB peat deposit with an average BD of 0.1 $g \cdot cm^{-3}$ (Table A2.4) would contain a total Hg inventory of 776 ± 368 g (Appendix 2). This is in fact an underestimation because it does not incorporate near-surface peat, which presumably contains significantly large Hg stocks (Figure 4.4). Nonetheless, extrapolating similar calculations to preexisting peatland thickness and coverage databases may aid in deriving first-order estimations of Hg stocks at local to regional scales. The utility of this approximation method is not limited to peat deposits within the continuous permafrost zone. Provided additional empirical data from a sufficient selection of sites, future studies may use the same technique to estimate Hg stocks in cryosols from the discontinuous permafrost zone, which is experiencing permafrost thaw at an alarming rate due to climate warming.[40,66–68]

Climate warming and the fate of permafrost Hg

Although studies have demonstrated the strong capacity of northern circumpolar soils to sequester Hg over millennial timescales,[69] the quantity of Hg in permafrost and its fate with future environmental change remains unclear.[16] It is hypothesized that continued global climate warming and consequent permafrost degradation will mobilize OC and Hg that has been effectively frozen

for thousands of years.[38,68,70,71] However, similar to how lability affects the rate of OC release from thawing permafrost,[35] the form of Hg and its complexation with organic matter will influence rates of Hg export. For instance, Hg that was incorporated into plant matter through foliar uptake of GEM (Hg^0) dry deposition will likely remain within litterfall and peat fibers until they are mobilized to the aquatic system following decomposition. Alternatively, Hg bound to cell structures of near-surface peat and growing-layer moss may be volatilized by wildfires, which have been recognized as effective transferring agents of Hg from organic soils and plants to the atmosphere (i.e. pyroreduction of Hg).[69,72] Permafrost Hg that has been acquired by wet deposition is typically complexed with soluble anionic ligands, such as OH^- and Cl^-, and dissolved organic matter in pore-waters.[40,73–77] Presumably, this aqueous Hg will be readily mobilized by pore-water export from permafrost thaw[38,40,44,70,71] and subsequently become converted to MeHg by methylating bacteria in anoxic settings,[41–43] such as sediments of nearby thermokarst lakes.[78] Methylmercury may then bioaccumulate in local biota and biomagnify in the food chain.[6,7,44] Future assessments of potential Hg release from permafrost with continued climate warming warrants not only estimates of cryosol Hg stocks, but also improved understanding of Hg partitioning within these northern circumpolar deposits.

ASSOCIATED CONTENT

Supporting Information (Appendix 2)

Coring location details (Figure A2.1), Bayesian age-depth models (Appendix 2), bulk density measurement method (Figure A2.2), peat homogenization method (Figure A2.3), cryostratigraphic classification of cores (Table A2.1), AMS ^{14}C dating results (Table A2.2), DMA-80 data quality (Table A2.3), modelled age, AR, BD, Hg concentration, and Hg flux results (Table A2.4), and example Hg stock calculation for a Holocene DTLB peat deposit (Appendix 2).

ACKNOWLEDGMENTS

Funding for this research was provided by The W. Garfield Weston Foundation, EnviroNorth, the Geological Society of America, and NSERC. Special thanks to Dr. Trevor Porter, Joel Pumple, Matt Mahony, Lauren Davies, Kasia Stanizewska, Hector Martinez, Sydney Clackett, and Jonny Vandewint for assistance with core collection. Thanks also to Mark Labbe and Crystal Dodge for technical support with sample processing.

FIGURES AND TABLES

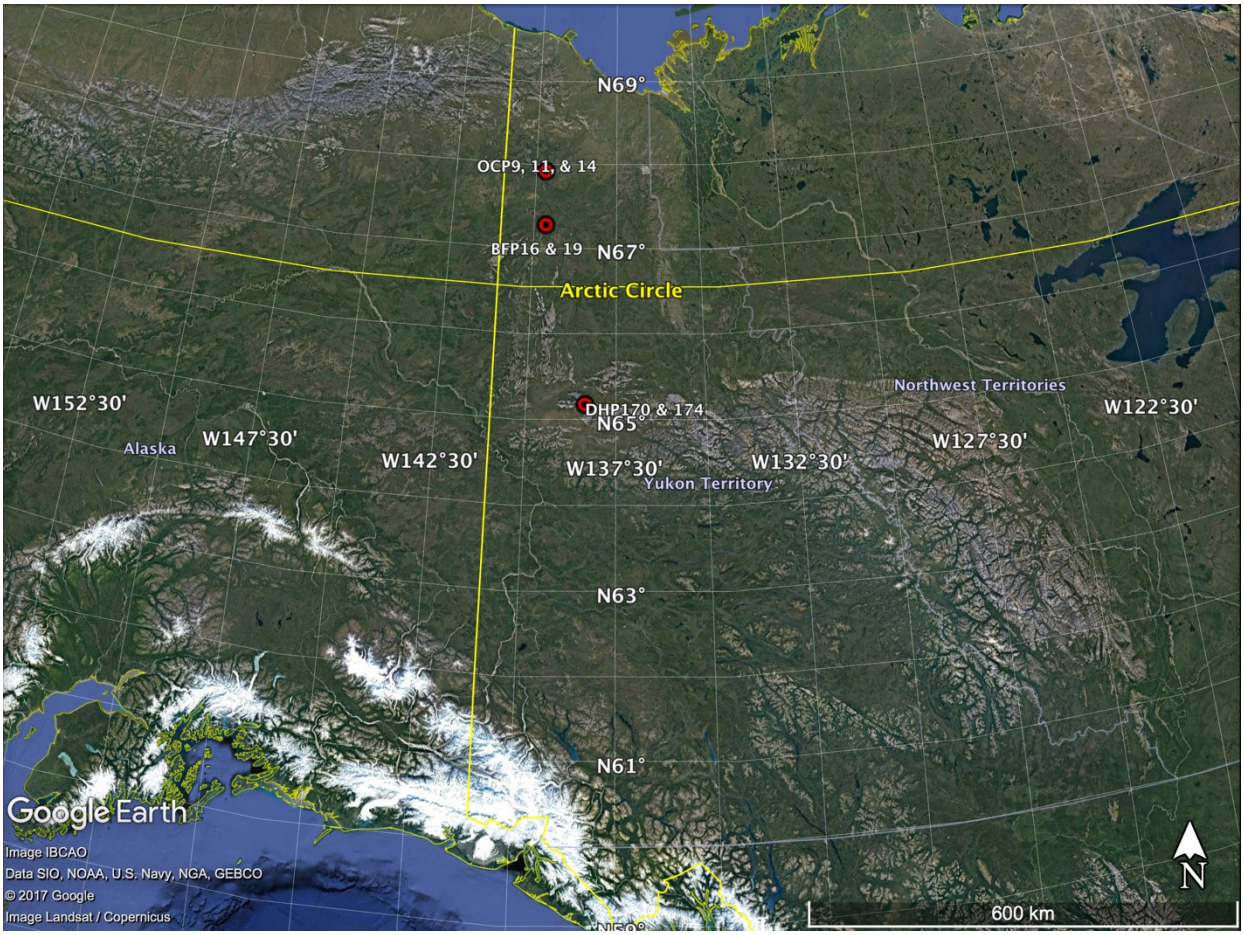

Figure 4.1 Map showing study sites in central and northern Yukon. Cores DHP170 and 174 were collected from peat plateaus within the North Ogilvie Mountains Ecoregion. Cores OCP9, 11, 14, and BFP16 and 19 were collected from the Old Crow Flats Ecoregion. Precise coring location information and field images from each of the seven sites are available in the supporting information (Figure A2.1).

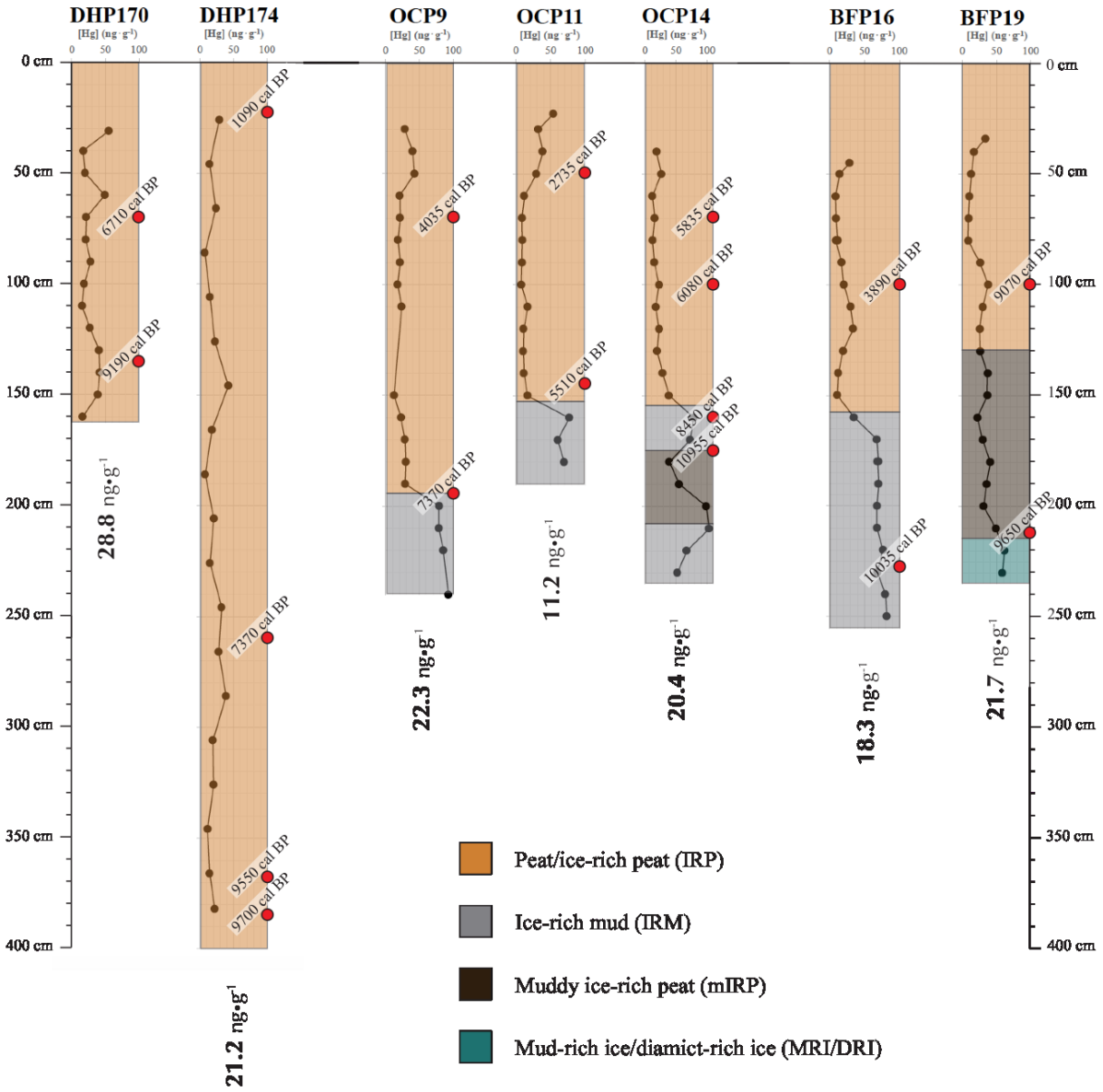

Figure 4.2 Cryostratigraphic profiles with Hg concentration data for each of the seven study cores. Median calibrated ^{14}C dates are marked by red dots. Average Hg concentrations for peat permafrost from each core are listed below the respective profiles; this is based on an assumed active layer thickness of 60 cm for each site.

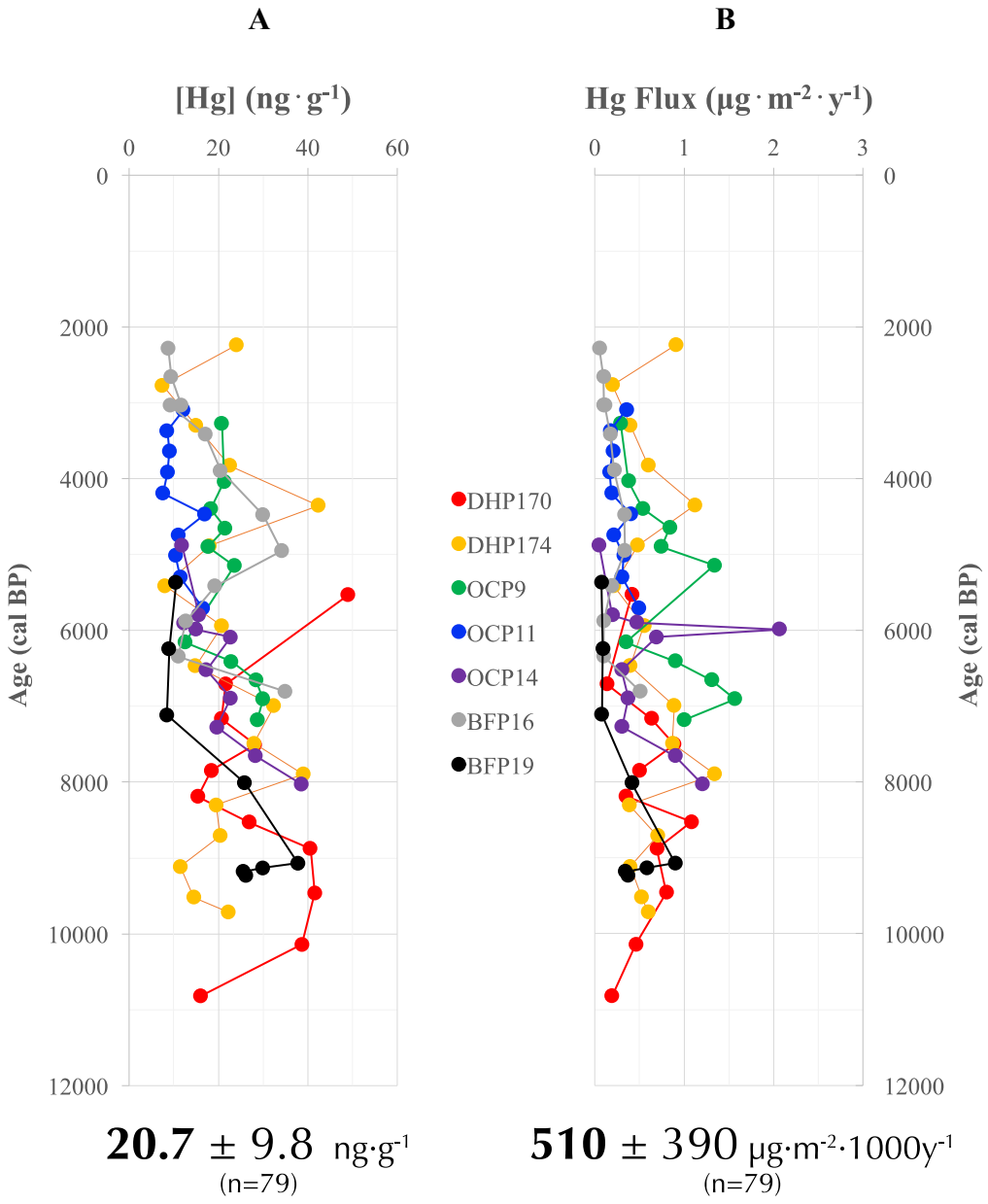

Figure 4.3 Total Hg concentrations (A) and fluxes (B) plotted by calibrated age for each of the seven study cores. Holocene average Hg concentration and flux values are listed below the respective panels.

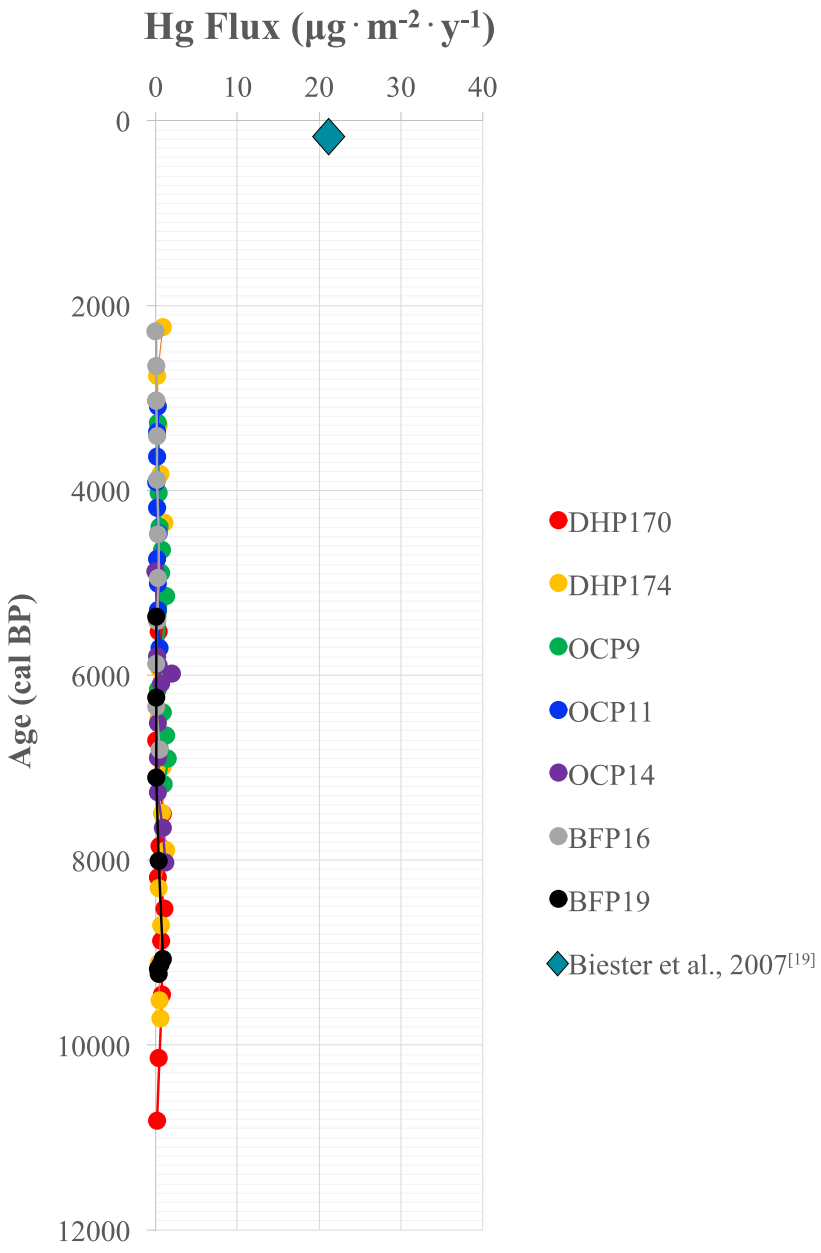

Figure 4.4 Natural atmospheric Hg deposition flux estimated by Holocene peat permafrost (~0.51 ± 0.39 µg·m^{-2}·y^{-1}) from this study in the context of hypothesized anthropogenic Hg fluxes according to Biester et al. (2007).[19]

Table 4.1 Preindustrial atmospheric Hg accumulation rates from Northern Hemisphere ombrotrophic peat archives. Modified from Outridge and Sanei (2010).[59]

Site/region	Time period*	Hg Flux ($\mu g \cdot m^{-2} \cdot y^{-1}$)	Reference
Pinet peat bog and Estibere peatland, France	8000 BC - 1000 BC	1.5 ± 1.0	Enrico et al. (2017)[30]
Misten peat bog, Belgium	1300 AD - 500 AD	1.8 ± 1.0	Allan et al. (2013)[60]
Tanghongling peat, Heilongjiang, China	3150 BC - 2550 BP	2.2 ± 1.0	Tang et al. (2012)[61]
Lindow Bog, England	2050 BC - 50 BC	~1.5 (unpublished)	De Vleeschouwer et al. (2010)[62]
Inuvik, NWT, Canada	4320 BC - 1770 AD	0.82 ± 0.36	Outridge and Sanei (2010)[59]
Red moss of Balerno, Scotland	800 AD - 1800 AD	3.7	Farmer et al. (2009)[63]
Flanders moss, Scotland	1 AD - 1800 AD	4.5	Farmer et al. (2009)[63]
Caribou bog, Maine, USA	8000 BC - 1800 AD	1.7 ± 1.3	Roos-Barraclough et al. (2006)[64]
Five peat bogs, Norway	~1000 BC - ~1200 AD	0.23 - 0.72	Steinnes and Sjobakk (2005)[79]
Faroe Islands, North Atlantic Ocean	1520 BC - 1385 AD	1.27 ± 0.38	Shotyk et al. (2005)[10]
Bathurst Island, Nunavut, Canada	4000 BC - 1200 AD	0.5 - 1.5	Givelet et al. (2004)[15]
Luther Bog, Ontario, Canada	5700 BC - 1470 AD	1.4 ± 1.0	Givelet et al. (2003)[21]
"ERG" site, Jura Mountains, Switzerland	0 AD - 1150 AD	1.0 ± 0.3	Roos-Barraclough and Shotyk (2003)[27]
Dumme Mosse and Store Mosse, Sweden	~2000 BC - 1500 AD	0.5 - 1	Bindler (2003)[26]
"TGE" site, Jura Mountains, Switzerland	1200 BC - 1150 AD	1.6 ± 0.4	Roos-Barraclough and Shotyk (2003)[27]
Tasiusaq, Greenland	~1400 BC - 1750 AD	0.3 - 3.0	Shotyk et al. (2003)[28]

*All calibrated (cal BP/AD) dates from literature have been converted to calendar years BC/AD to facilitate comparison

REFERENCES

(1) Horowitz, H. M.; Jacob, D. J.; Amos, H. M.; Streets, D. G.; Sunderland, E. M. Historical Mercury Releases from Commercial Products: Global Environmental Implications. *Environ. Sci. Technol.* **2014**, *48* (17), 10242–10250.

(2) Hylander, L. D.; Meili, M. 500 Years of Mercury Production: Global Annual Inventory by Region until 2000 and Associated Emissions. *Sci. Total Environ.* **2003**, *304* (1–3), 13–27.

(3) AMAP. Arctic Monitoring and Assessment Program (AMAP) Arctic Pollution Issues: A State of the Arctic Environment Report; Oslo, 1998.

(4) Johansen, P.; Pars, T.; Bjerregaard, P. Lead , Cadmium , Mercury and Selenium Intake by Greenlanders from Local Marine Food. *Sci. Total Environ.* **2000**, *245* (1), 187–194.

(5) NCP. *Canadian Arctic Contaminants Assessment Report II. Ottawa: Northern Contaminants Program (NCP)*; **2003**.

(6) Mason, R. P.; Reinfelder, J. R.; Morel, F. M. M. Bioaccumulation of Mercury and Methylmercury. *Water, Air, Soil Pollut.* **1995**, *80* (1), 915–921.

(7) Morel, F.; Kraepiel, A. M. L.; Amyot, M. The Chemical Cycle and Bioaccumulation of Mercury. *Annu. Rev. Ecol. Syst. 29.1* **1998**, *29* (1), 543–566.

(8) Grandjean, P.; Weihe, P. A. L.; White, R. F.; Debes, F. Cognitive Deficit in 7-Year-Old Children with Prenatal Exposure to Methylmercury. **1997**, *19* (6), 417–428.

(9) Wheatley, U. B.; Wheatley, M. A. Methylmercury and the Health of Indigenous Peoples : A Risk Management Challenge for Physical and Social Sciences and for Public Health Policy. **2000**, 23–29.

(10) Shotyk, W.; Goodsite, M. E.; Roos-Barraclough, F.; Givelet, N.; Le Roux, G.; Weiss, D.; Cheburkin, A. K.; Knudsen, K.; Heinemeier, J.; van Der Knaap, W. O.; et al. Accumulation Rates and Predominant Atmospheric Sources of Natural and Anthropogenic Hg and Pb on the Faroe Islands. *Geochim. Cosmochim. Acta* **2005**, *69* (1), 1–17.

(11) Mackay, D.; Wania, F.; Schroeder, W. H. Prospects for Modeling the Behavior and Fate of Mercury, Globally and in Aquatic Systems. *Water. Air. Soil Pollut.* **1995**, *80* (1–4), 941–950.

(12) Martinez-Cortizas, A.; Pontevedra-Pombal, X.; García-Rodeja, E.; Novoa-Munoz, C.; Shotyk, W. Mercury in a Spanish Peat Bog: Archive of Climate Change and Atmospheric Metal Deposition. *Science (80-.).* **1999**, *284* (1999), 939–942.

(13) Schroeder, W. H.; Anlauf, K. G.; Barrie, L. A.; Lu, J. Y.; Steffen, A.; Schneeberger, D. R.; Berg, T. Arctic Springtime Depletion of Mercury. *Nature* **1998**, *394* (6691), 331–332.

(14) Schroeder, W. H.; Munthe, J. Atmospheric Mercury - An Overview. *Atmos. Environ.* **1998**, *32* (5), 809–822.

(15) Givelet, N.; Roos-Barraclough, F.; Goodsite, M. E.; Cheburkin, A. K.; Shotyk, W. Atmospheric Mercury Accumulation between 5900 and 800 Calibrated Years BP in the High Arctic of Canada Recorded by Peat Hummocks. *Environ. Sci. Technol.* **2004**, *38* (19), 4964–4972.

(16) Steffen, A.; Lehnherr, I.; Cole, A.; Ariya, P.; Dastoor, A.; Durnford, D.; Kirk, J.; Pilote, M. Atmospheric Mercury in the Canadian Arctic. Part I: A Review of Recent Field Measurements. *Sci. Total Environ.* **2015**, *509*, 3–15.

(17) Obrist, D.; Agnan, Y.; Jiskra, M.; Olson, C. L.; Dominique, P. Tundra Uptake of Atmospheric Elemental Mercury Drives Arctic Mercury Pollution. *Nature* **2017**, *547* (7662), 201–204.

(18) Engstrom, D. R.; Fitzgerald, W. F.; Cooke, C. A.; Lamborg, C. H.; Drevnick, P. E.; Swain, E. B.; Balogh, S. J.; Balcom, P. H. Atmospheric Hg Emissions from Preindustrial Gold and Silver

Extraction in the Americas: A Reevaluation from Lake-Sediment Archives. *Environ. Sci. Technol.* **2014**, *48* (12), 6533–6543.
(19) Biester, H.; Bindler, R.; Martinez-Cortizas, A.; Engstrom, D. R. Modeling the Past Atmospheric Deposition of Mercury Using Natural Archives. *Environ. Sci. Technol.* **2007**, *41* (14), 4851–4860.
(20) Amos, H. M.; Sonke, J. E.; Obrist, D.; Robins, N.; Hagan, N.; Horowitz, H. M.; Mason, R. P.; Witt, M.; Hedgecock, I. M.; Corbitt, E. S.; et al. Observational and Modeling Constraints on Global Anthropogenic Enrichment of Mercury. **2015**.
(21) Givelet, N.; Roos-Barraclough, F.; Shotyk, W. Predominant Anthropogenic Sources and Rates of Atmospheric Mercury Accumulation in Southern Ontario Recorded by Peat Cores from Three Bogs: Comparison with Natural "background" values (Past 8000 Years). *J. Environ. Monit.* **2003**, *5* (6), 935–949.
(22) Clymo, R. S. The Limits to Peat Bog Growth. *Philos. Trans. R. Soc. London B Biol. Sci.* **1984**, *303* (1117), 605–654.
(23) Pheiffer-Madsen, P. Peat Bog Records of Atmospheric Mercury Deposition. *Nature* **1981**, *293*, 127–130.
(24) Jensen, A.; Jensen, A. Historical Deposition Rates of Mercury in Scandinavia Estimated by Dating and Measurement of Mercury in Cores of Peat Bogs. *Water Air Soil Pollut.* **1991**, *56* (1), 769–777.
(25) Benoit, J. M.; Fitzgerald, W. F.; Damman, a W. The Biogeochemistry of an Ombrotrophic Bog: Evaluation of Use as an Archive of Atmosphere Mercury Deposition. *Environ. Res.* **1998**, *78* (2), 118–133.
(26) Bindler, R. Estimating the Natural Background Atmospheric Deposition Rate of Mercury Utilizing Ombrotrophic Bogs in Southern Sweden. *Environ. Sci. Technol.* **2003**, *37* (1), 40–46.
(27) Roos-Barraclough, F.; Shotyk, W. Millennial-Scale Records of Atmospheric Mercury Deposition Obtained from Ombrotrophic and Minerotrophic Peatlands in the Swiss Jura Mountains. *Environ. Sci. Technol.* **2003**, *37* (2), 235–244.
(28) Shotyk, W.; Goodsite, M. E.; Roos-Barraclough, F.; Frei, R.; Heinemeier, J.; Asmund, G.; Lohse, C.; Hansen, T. S. Anthropogenic Contributions to Atmospheric Hg, Pb and As Accumulation Recorded by Peat Cores from Southern Greenland and Denmark Dated Using the 14C "bomb Pulse Curve." *Geochim. Cosmochim. Acta* **2003**, *67* (21), 3991–4011.
(29) Enrico, M.; Le Roux, G.; Marusczak, N.; Heimbu, L.; Claustres, A.; Fu, X.; Sun, R.; Sonke, J. E. Atmospheric Mercury Transfer to Peat Bogs Dominated by Gaseous Elemental Mercury Dry Deposition. **2016**, *50* (5), 2405–2412.
(30) Enrico, M.; Beek, P. Van; Souhaut, M.; Sonke, J. E. Holocene Atmospheric Mercury Levels Reconstructed from Peat Bog Mercury Stable Isotopes. **2017**, *51* (11), 5899–5906.
(31) Tarnocai, C.; Canadell, J. G.; Schuur, E. a. G.; Kuhry, P.; Mazhitova, G.; Zimov, S. Soil Organic Carbon Pools in the Northern Circumpolar Permafrost Region. *Global Biogeochem. Cycles* **2009**, *23* (2).
(32) Stocker, T. F.; Qin, D.; Plattner, G.-K.; Tignor, M.; Allen, S. K.; Boschung, J.; Nauels, A.; Xia, Y.; Bex, V.; Midgley, P. M. *IPCC, 2013: Climate Change 2013: The Physical Science Basis. Contributions of Working Group I to the Fifth Assessment Report of the Intergovernmental Panel on Climate Change*; Cambridge University Press: Cambridge, UK and New York, USA, **2014**.
(33) Battle, M.; Bender, M. L.; Tans, P. P.; White, J. W. C.; Ellis, J. T.; Conway, T.; Francey, R. J. Global Carbon Sinks and Their Variability Inferred from Atmospheric O2 and d13C. **2000**, *287* (5462), 2467–2471.

(34) Knoblauch, C.; Beer, C.; Sosnin, A.; Wagner, D. Predicting Long-Term Carbon Mineralization and Trace Gas Production from Thawing Permafrost of Northeast Siberia. **2013**, 1160–1172.
(35) Schadel, C.; Schuur, E. A. G.; Bracho, R.; Elberling, B. O.; Knoblauch, C.; Lee, H.; Luo, Y.; Shaver, G. R.; Turetsky, M. R. Circumpolar Assessment of Permafrost C Quality and Its Vulnerability over Time Using Long-Term Incubation Data. *Glob. Chang. Biol.* **2014**, *20* (2), 641–652.
(36) MacDonald, R. W.; Harner, T.; Fyfe, J.; Loeng, H.; Weingartner, T. *AMAP Assessment 2002: The Influence of Global Change on Contaminant Patways To, Within, and from the Arctic*; **2003**.
(37) MacDonald, R. W.; Harner, T.; Fyfe, J. Recent Climate Change in the Arctic and Its Impact on Contaminant Pathways and Interpretation of Temporal Trend Data. **2005**, *342*, 5–86.
(38) Klaminder, J.; Yoo, K.; Rydberg, J.; Giesler, R. An Explorative Study of Mercury Export from a Thawing Palsa Mire. **2008**, *113* (October), 1–9.
(39) Braune, B. M.; Outridge, P. M.; Fisk, A. T.; Muir, D. C. G.; Helm, P. A.; Hobbs, K.; Hoekstra, P. F.; Kuzyk, Z. A.; Kwan, M.; Letcher, R. J.; et al. Persistent Organic Pollutants and Mercury in Marine Biota of the Canadian Arctic : An Overview of Spatial and Temporal Trends. **2005**, *352*, 4–56.
(40) Gordon, J.; Quinton, W.; Bran, B. A.; Olefeldt, D. Mercury and Methylmercury Biogeochemistry in a Thawing Permafrost Wetland Complex , Northwest Territories , Canada. **2016**, *3638* (August), 3627–3638.
(41) Compeau, G. C.; Bartha, R. Sulfate-Reducing Bacteria: Principal Methylators of Mercury in Anoxic Estuarine Sediment. *Applied and Environmental Microbiology*. **1985**, pp 498–502.
(42) Kerin, E. J.; Gilmour, C. C.; Roden, E.; Suzuki, M. T.; Coates, J. D.; Mason, R. P. Mercury Methylation by Dissimilatory Iron-Reducing Bacteria. *Appl. Environ. Microbiol.* **2006**, *72* (12), 7919–7921.
(43) Poulain, A. J.; Barkay, T. Cracking the Mercury Methylation Code. *Science (80-.).* **2013**, *339* (6125), 1280–1281.
(44) Chételat, J.; Braune, B.; Stow, J.; Tomlinson, S. Special Issue on Mercury in Canada' S North : Summary and Recommendations for Future Research. *Sci. Total Environ.* **2015**, *510*, 260–262.
(45) McGuire, A. D.; Anderson, L. G.; Christensen, T. R.; Dallimore, S.; Guo, L.; Hayes, D. J.; Heimann, M.; Lorenson, T. D.; MacDonald, R. W.; Poulet, N. Sensitivity of the Carbon Cycle in the Arctic to Climate Change. *Ecol. Monogr.* **2009**, *79* (4), 523–555.
(46) Strauss, J.; Schirrmeister, L.; Grosse, G.; Wetterich, S.; Ulrich, M.; Herzschuh, U.; Hubberten, H. The Deep Permafrost Carbon Pool of the Yedoma Region in Siberia and Alaska. *Geophys. Res. Lett.* **2013**, *40* (23), 6165–6170.
(47) Hugelius, G.; Strauss, J.; Zubrzycki, S.; Harden, J. W.; Schuur, E. A. G.; Ping, C.; Schirrmeister, L.; Grosse, G.; Michaelson, G. J.; Koven, C. D.; et al. Estimated Stocks of Circumpolar Permafrost Carbon with Quantified Ranges and Identified Data Gaps. *Biogeosciences* **2014**, *11* (23), 6573–6593.
(48) Yukon Ecoregions Working Group. *North Ogilvie Mountains. In: Ecoregions of the Yukon Territory: Biophysical Properties of Yukon Landscapes,*; C. Smirh, J. Meikle, C. R., Ed.; Agriculture and Agri-Food Canada, PARC Technical Bulletin No. 04-01, **2004**.
(49) Yukon Ecoregions Working Group. *Old Crow Flats. In: Ecoregions of the Yukon Territory: Biophysical Properties of Yukon Landscapes,*; C. Smith, J. Meikle, C. R., Ed.; Agriculture and Agri-Food Canada, PARC Technical Bulletin No. 04-01, **2004**.
(50) Turner, K. W.; Wolfe, B. B.; Edwards, T. W. D. Characterizing the Role of Hydrological Processes on Lake Water Balances in the Old Crow Flats, Yukon Territory, Canada, Using Water Isotope Tracers. *J. Hydrol.* **2010**, *386* (1–4), 103–117.

(51) Roy-Léveillée, P.; Burn, C. R. Permafrost Conditions near Shorelines of Oriented Lakes in Old Crow Flats , Yukon Territory. **2010**, No. August.
(52) Lauriol, B.; Lacelle, D.; Labrecque, S.; Duguay, C. R.; Telka, A. Holocene Evolution of Lakes in the Bluefish Basin , Northern Yukon , Canada. **2009**, *62* (2), 212–224.
(53) Canada, E. C.-G. of. Canadian Climate Normals 1971 - 2000 Station Data "Old Crow A - Yukon Territory" http://climate.weather.gc.ca/climate_normals/results_e.html?stnID=1582&lang=e&StationName=Old+Crow+&SearchType=Contains&stnNameSubmit=go&dCode=5&dispBack=1 (accessed Jul 27, **2017**).
(54) Calmels, F.; Gagnon, O.; Allard, M. A Portable Earth-Drill System for Permafrost Studies. *Permafr. Periglac. Process.* **2005**, *16* (3), 311–315.
(55) Bronk Ramsey, C. Bayesian Analysis of Radiocarbon Dates. *Radiocarbon* **2009**, *51* (1), 337–360.
(56) Reimer, P. J.; Bard, E.; Bayliss, A.; Beck, J. W.; Blackwell, P. G.; Bronk, M.; Grootes, P. M.; Guilderson, T. P.; Haflidason, H.; Hajdas; et al. IntCal 13 and Marine 13 Radiocarbon Age Calibration Curves 0–50,000 Years Cal BP. *Radiocarbon* **2013**, *55*, 1869–1887.
(57) Murton, J. B.; French, H. M. Cryostructures in Permafrost, Tuktoyaktuk Coastlands, Western Arctic Canada. *Can. J. Earth Sci.* **1994**, *31* (4), 737–747.
(58) US EPA (US Environmental Protection Agency); EPA; US EPA (US Environmental Protection Agency). Mercury in Solids and Solutions by Thermal Decomposition, Amalgamation, and Atomic Absorption Spectrophotometry - Method 7473 - Total Mercury. *SW-846, Test Methods Eval. Solid Waste, Phys. Methods* **2007**, 1–17.
(59) Outridge, P. M.; Sanei, H. Does Organic Matter Degradation Affect the Reconstruction of Pre-Industrial Atmospheric Mercury Deposition Rates from Peat Cores? - A Test of the Hypothesis Using a Permafrost Peat Deposit in Northern Canada. *Int. J. Coal Geol.* **2010**, *83* (1), 73–81.
(60) Allan, M.; Le Roux, G.; Sonke, J. E.; Piotrowska, N.; Streel, M.; Fagel, N. Reconstructing Historical Atmospheric Mercury Deposition in Western Europe Using: Misten Peat Bog Cores, Belgium. *Sci. Total Environ.* **2013**, *442*, 290–301.
(61) Tang, S.; Zhongwei, H.; Jun, L.; Zaichan, Y.; Qinhua, L. Atmospheric Mercury Deposition Recorded in an Ombrotrophic Peat Core from Xiaoxing'an Mountain, Northeast China. *Environ. Res.* **2012**, *118*, 145–148.
(62) De Vleeschouwer, F.; Le Roux, G.; Shotyk, W. Peat as an Archive of Atmospheric Pollution and Environmental Change : A Case Study of Lead in Europe. *PAGES Mag.* **2010**, *18* (1), 20–22.
(63) Farmer, J. G.; Anderson, P.; Cloy, J. M.; Graham, M. C.; Mackenzie, A. B.; Cook, G. T. Science of the Total Environment Historical Accumulation Rates of Mercury in Four Scottish Ombrotrophic Peat Bogs over the Past 2000 Years. *Sci. Total Environ.* **2009**, *407* (21), 5578–5588.
(64) Roos-Barraclough, F.; Givelet, N.; Cheburkin, A. K.; Shotyk, W.; Norton, S. A. Use of Br and Se in Peat to Reconstruct the Natural and Anthropogenic Fluxes of Atmospheric Hg: A 10000-Year Record from Caribou Bog, Maine. *Environ. Sci. Technol.* **2006**, *40* (10), 3188–3194.
(65) Bandara, S.; Froese, D. G.; St. Louis, V. L.; Cooke, C. A.; Calmels, F. Post-Depositional Mercury Mobility in Active Layers of Peat Permafrost from Central Yukon: Implications for Reconstructing Historic Mercury Deposition Fluxes Using Permafrost Archives. *Manuscript in preparation.* **2017**.
(66) AMAP/CAFF/IASC. Arctic Climate Impact Assessment; Cambridge, UK, **2005**; p 1042.
(67) IPCC. Climate Change 2007: The Physical Science Basis. In: Solomon S, Qin D, Manning M, Chen Z, Marquis M, Averyt KB, Tignor M, Miller HL, Editors. Contributions of Working Group I to the

Fourth Assessment Report of the Intergovernmental Panel on Climate Change; Cambridge, UK and New York, USA, **2007**; p 996.

(68) Stern, G. A.; MacDonald, R. W.; Outridge, P. M.; Wilson, S.; Chételat, J.; Cole, A.; Hintelmann, H.; Loseto, L. L.; Steffen, A.; Wang, F.; et al. Science of the Total Environment How Does Climate Change in Fl Uence Arctic Mercury ? *Sci. Total Environ.* **2012**, *414*, 22–42.

(69) Giesler, R.; Clemmensen, K. E.; Wardle, D. A.; Klaminder, J.; Bindler, R. Boreal Forests Sequester Large Amounts of Mercury over Millennial Time Scales in the Absence of Wildfire. **2017**.

(70) Rydberg, J.; Klaminder, J.; Rosén, P.; Bindler, R. Climate Driven Release of Carbon and Mercury from Permafrost Mires Increases Mercury Loading to Sub-Arctic Lakes. *Sci. Total Environ.* **2010**, *408* (20), 4778–4783.

(71) Korosi, J. B.; Mcdonald, J.; Coleman, K. A.; Palmer, M. J.; Smol, J. P.; Simpson, M. J.; Blais, J. M. Long-Term Changes in Organic Matter and Mercury Transport to Lakes in the Sporadic Discontinuous Permafrost Zone Related to Peat Subsidence. **2015**, 1550–1561.

(72) Turetsky, M. R.; Harden, J. W.; Friedli, H. R.; Flannigan, M.; Payne, N.; Crock, J.; Radke, L. Wildfires Threaten Mercury Stocks in Northern Soils. **2006**, *33* (February), 1–6.

(73) Schuster, E. The Behavior of Mercury in the Soil with Special Emphasis on Complexation and Adsorption Processes - A Review of the Literature. *Water, Air, Soil Pollut.* **1991**, *56* (1), 667–680.

(74) Lodenius, M.; Seppanen, A.; Uusi-Rauva, A. Sorption and Mobilization of Mercury in Peat Soil. *Chemosphere* **1983**, *12* (ll), 1575–1581.

(75) Rasmussen, P. E. Current Methods of Estimating Atmospheric Mercury Fluxes in Remote Areas. **1994**, No. 13, 2233–2241.

(76) Biester, H. U.; Muller, G.; Scholer, H. F. Binding and Mobility of Mercury in Soils Contaminated by Emissions from Chlor-Alkali Plants. *Sci. Total Environ.* **2002**, 191–203.

(77) Norton, S. A.; Dillon, P. J.; Evans, R. D.; Mierle, G.; Kahl, J. S. The History of Atmospheric Deposition of Cd, Hg, and Pb in North America: Evidence from Lake and Peat Bog Sediments. In *Acidic Precipitation: Sources, Deposition, and Canopy Interactions*; Lindberg, S. E., Page, A. L., Norton, S. A., Eds.; Springer New York: New York, NY, **1990**; pp 73–102.

(78) St. Louis, V. L.; Sharp, M. J.; Steffen, A.; May, A.; Barker, J.; Kirk, J. L.; Kelly, D. J. A.; Arnott, S. E.; Keatley, B.; Smol, J. P. Some Sources and Sinks of Monomethyl and Inorganic Mercury on Ellesmere Island in the Canadian High Arctic. **2005**, *39* (8), 2686–2701.

(79) Steinnes, E.; Sjøbakk, T. E. Order-of-Magnitude Increase of Hg in Norwegian Peat Profiles since the Outset of Industrial Activity in Europe. **2005**, *137*, 365–370.

Chapter 5: General Discussion and Conclusions

The influences of human activities and climate warming on the Hg cycle in northern circumpolar regions remains unclear. Although understudied, peat permafrost archives from these settings may aid in improving our understanding of past, present, and future Hg biogeochemical cycling. This thesis represents the first comprehensive examination of natural and anthropogenic atmospheric Hg deposition as recorded by peat permafrost archives in central and northern Yukon, Canada. The objectives of this research were to (1) develop an effective protocol for processing peat permafrost samples for inorganic geochemical analysis, (2) reconstruct anthropogenic atmospheric Hg deposition fluxes and test for a hypothesized increase in Hg pollution from Klondike gold mining, and (3) quantify millennial-scale natural atmospheric Hg deposition using Holocene (10,000-year old) peat deposits from the Yukon and demonstrate how such data may be used to estimate local peat permafrost Hg stocks.

Summary of work

Chapter 1 introduced the use of natural environmental archives for reconstructing past atmospheric deposition of Hg. The technical communication in Chapter 2 described important considerations for reconstructing Hg deposition fluxes using peat permafrost archives. Site selection, field planning, core collection, core subsampling, dating/age-modelling, pore-water/ice geochemistry, and total Hg concentration measurements were among the topics covered in Chapter 2. Additionally, new strategies were developed for effectively homogenizing and accurately calculating densities of fibrous, ice-rich, peat permafrost.

The case for post-depositional Hg mobility in active layers

In Chapter 3, an active layer/shallow permafrost core from a rapidly aggrading peat plateau near Dawson, Yukon, was carefully analyzed in effort to reconstruct local anthropogenic Hg deposition fluxes. The hypothesized increase in Hg deposition corresponding to the timing of extensive placer gold mining in the Klondike (ca. AD 1896 – 1920) was not observed. Instead, results from the study suggested that anthropogenic Hg concentrations and fluxes began to increase around AD 1670, which is much earlier than expected (Biester et al., 2007; Streets et al., 2011; Horowitz et al., 2014; Streets et al., 2017). This discrepancy was investigated using pore-water/ice stable isotopes ($\delta^{18}O$). A positive correlation between $\delta^{18}O$ and total Hg concentration was recognized, and interpreted to result from common chemo-physical processes affecting both variables simultaneously. This correlation suggested that atmospherically deposited Hg was mobile within active layer pore-waters prior to being "cryosequestered" by (frozen into) underlying permafrost. Mechanistic details relating to post-depositional mobility were also discussed in Chapter 3. In light of earlier research, it appears that anionic ligands and organic host molecules facilitate the mobility of Hg in acidic, dissolved organic matter (DOM) enriched pore-waters (Biester et al., 2002; Rasmussen, 1994; Schuster et al., 1991; Norton et al., 1990; Evans, 1989; Klusman and Jaacks, 1987; Nriagu, 1979; Jonasson, 1970). The findings from Chapter 3 indicate that ombrotrophic peat permafrost archives may not contain straightforward records of atmospheric Hg deposition, and hence, caution must be exercised when using such archives for reconstructing past deposition fluxes.

Estimating Hg fluxes and stocks in Holocene peat permafrost

Despite the discovery of post-depositional Hg mobility within annually thawed active layers, Hg is expected to remain cryosequestered in peat permafrost in the absence of significant

disturbance. Therefore, peat permafrost can be used to reconstruct millennial-scale Hg deposition fluxes as shown in Chapter 4. Findings from this chapter highlight that natural Hg fluxes were ~0.51 ± 0.39 $\mu g \cdot m^{-2} \cdot y^{-1}$ (n = 79) during the Holocene in central and northern Yukon, which is similar to temperate and boreal peat-based reconstructions from the same period (~1 $\mu g \cdot m^{-2} \cdot y^{-1}$; Table 4.1). Also discussed are uncertainties surrounding the quantity of Hg stored in northern circumpolar permafrost and the fate of these Hg inventories with continued climatic and environmental change. The chapter concludes with a local-scale demonstration of how empirical Hg concentration and bulk density data may be used in conjunction with pre-existing cryosol thickness and coverage maps to estimate total Hg inventories.

Future research

The evidence of post-depositional Hg mobility within active layers (Chapter 3) raises several important questions. Firstly, how does partitioning of Hg between the solid and aqueous phases vary with time in ombrotrophic peat permafrost archives? Secondly, which chemo-physical factors are the most influential in governing post-depositional Hg mobility in active layers? Finally, are some northern peat permafrost archives more reliable for reconstructing atmospheric deposition fluxes than others?

Although post-depositional Hg mobility in DOM-rich pore-waters hinders detailed deposition reconstructions, millennial-scale Hg fluxes may provide useful information about climate-permafrost-Hg interactions. This insight is integral for estimating cryosol Hg stocks and assessing their vulnerability to future climate warming. Given the limited number of study sites, it is unclear whether Holocene Hg concentration and flux results from Chapter 4 are unique to peat permafrost from Yukon, Canada. Empirical data from a more representative selection of sites within the circumpolar north is warranted for better constraining natural deposition rates and

estimating cryosol Hg stocks at the regional to global scale. In light of this discussion, future research should consider the following themes.

Post-depositional Hg mobility may be further investigated using Hg isotope tracing techniques employed in previous studies (i.e. Branfireun et al., 2005). If Hg is mobile within seasonally-thawed peat as suggested by Chapter 3, experimentally applied ^{202}Hg should migrate down to the base of the active layer within one full thaw cycle. Failing to satisfy this hypothesis will imply that the concept of post-depositional Hg mobility needs to be revised.

Peat permafrost may be analyzed to test for a correlation between total Hg concentration and chromophoric DOM. If post-depositional Hg mobility is facilitated by DOM and anionic ligands in solution as discussed in Chapter 3, then a positive correlation is expected between the abundance of these constituents and total Hg concentrations. Presumably, this correlation should also exist for other commonly occurring divalent heavy metals, including Pb, Cd, Cu, and Zn, which are also expected be mobile within pore-waters.

Enrico et al. (2016) and Obrist et al. (2017) showed that ombrotrophic peatlands acquire ~80% of their Hg by dry deposition of gaseous elemental Hg, ~20% by wet deposition of Hg^{2+}, and <1% by particulate-bound Hg. However, the evolution of Hg partitioning in annually thawed active layers of northern circumpolar peat deposits remains unclear. As litterfall and peat decompose with time in the active layer, Hg partitioning into the aqueous phase should gradually increase. Quantitative evidence demonstrating this phenomenon would further support the notion of Hg mobility within active layer pore-waters presented in Chapter 3.

As mentioned in Chapter 4, estimating cryosol Hg stocks and evaluating the potential vulnerability of Hg release from thawing permafrost requires improved empirical datasets. Fortunately, direct mercury analyzer (DMA) instruments can quickly generate total Hg

concentration data from peat and other sediments. Collaborative research utilizing a DMA and pre-existing samples (i.e. from studies involving the Northern Circumpolar Soil Carbon Database and Permafrost Carbon Network) may provide a feasible means of quantifying Hg stocks in northern circumpolar cryosols. Such estimates may then be used in conjunction with climate models and projected permafrost degradation maps to assess the vulnerability of Hg release from thawing permafrost to aquatic environments.

References

Biester, H., Müller, G., & Schöler, H. F. (2002). Binding and mobility of mercury in soils contaminated by emissions from chlor-alkali plants. *Science of the Total Environment*, *284*(1), 191-203.

Biester, H., Bindler, R., Martinez-Cortizas, A., & Engstrom, D. R. (2007). Modeling the past atmospheric deposition of mercury using natural archives. *Environmental science & technology*, *41*(14), 4851-4860.

Enrico, M., Le Roux, G., Marusczak, N., Heimbürger, L. E., Claustres, A., Fu, X., ... & Sonke, J. E. (2016). Atmospheric mercury transfer to peat bogs dominated by gaseous elemental mercury dry deposition. *Environmental science & technology*, *50*(5), 2405-2412.

Evans, L. J. (1989). Chemistry of metal retention by soils. *Environmental Science & Technology*, *23*(9), 1046-1056.

Horowitz, H. M., Jacob, D. J., Amos, H. M., Streets, D. G., & Sunderland, E. M. (2014). Historical mercury releases from commercial products: Global environmental implications. *Environmental science & technology*, *48*(17), 10242-10250.

Jonasson, I. R. (1970). Mercury in the natural environment: a review of recent work. *Mercury in the natural environment: a review of recent work.*, (70-57).

Klusman, R. W., & Jaacks, J. A. (1987). Environmental influences upon mercury, radon and helium concentrations in soil gases at a site near Denver, Colorado. *Journal of Geochemical Exploration*, *27*(3), 259-280.

Norton, S. A., Dillon, P. J., Evans, R. D., Mierle, G., & Kahl, J. S. (1990). The history of atmospheric deposition of Cd, Hg, and Pb in North America: evidence from lake and peat bog sediments. In *Acidic Precipitation* (pp. 73-102). Springer New York.

Nriagu, J. O. (1979). *Biogeochemistry of Mercury in the Environment*. Elsevier/North-Holland Biomedical Press.

Obrist, D., Agnan, Y., Jiskra, M., Olson, C. L., Colegrove, D. P., Hueber, J., ... & Helmig, D. (2017). Tundra uptake of atmospheric elemental mercury drives Arctic mercury pollution. *Nature*, *547*, 201-204.

Rasmussen, P. E. (1994). Current methods of estimating atmospheric mercury fluxes in remote areas. *Environmental science & technology*, *28*(13), 2233-2241.

Schuster, E. (1991). The behavior of mercury in the soil with special emphasis on complexation and adsorption processes-a review of the literature. *Water, Air, & Soil Pollution*, *56*(1), 667-680.

Streets, D. G., Devane, M. K., Lu, Z., Bond, T. C., Sunderland, E. M., & Jacob, D. J. (2011). All-time releases of mercury to the atmosphere from human activities. *Environmental science & technology*, *45*(24), 10485-10491.

Streets, D. G., Horowitz, H. M., Jacob, D. J., Lu, Z., Levin, L., Ter Schure, A. F., & Sunderland, E. M. (2017). Total Mercury Released to the Environment by Human Activities. *Environmental Science & Technology*, *51*(11), 5969-5977.

Bibliography

Allan, M., Le, G., Sonke, J. E., Piotrowska, N., Streel, M., & Fagel, N. (2013). Science of the Total Environment Reconstructing historical atmospheric mercury deposition in Western Europe using : Misten peat bog cores , Belgium. *Science of the Total Environment, The*, *442*, 290–301. http://doi.org/10.1016/j.scitotenv.2012.10.044

Allard, B., & Arsenie, I. (1991). Abiotic reduction of mercury by humic substances in aquatic system - an important process for the mercury cycle. *Water, Air, & Soil Pollution*, *56*(1), 457–464. http://doi.org/10.1007/BF00342291

Allen, D. W. (2007). Information Sharing during the Klondike Gold Rush. *The Journal of Economic History*, *67*(4), 944–967.

AMAP. (1998). Arctic Monitoring and Assessment Program (AMAP) Arctic Pollution Issues: A state of the Arctic environment report. Oslo.

AMAP. (2002). Arctic pollution 2002 Arctic Monitoring and Assessment Program (AMAP). Oslo, Norway. 112 pp.

AMAP/CAFF/IASC. (2005). Arctic climate impact assessment. Cambridge, UK. Cambridge University Press. 1042 pp.

Amirbahman, A., Ruck, P. L., Fernandez, I. J., Haines, T. A., & Kahl, J. S. (2004). The effect of fire on mercury cycling in the soils of forested watersheds: Acadia National Park, Maine, USA. *Water, Air, and Soil Pollution*, *152*(1–4), 313–331. http://doi.org/10.1023/b:wate.0000015369.02804.15

Amos, H. M., Sonke, J. E., Obrist, D., Robins, N., Hagan, N., Horowitz, H. M., … Sunderland, E. M. (2015). Observational and Modeling Constraints on Global Anthropogenic Enrichment of Mercury. http://doi.org/10.1021/es5058665

Anderson, L., Abbott, M. B., Finney, B. P., & Burns, S. J. (2005). Regional atmospheric circulation change in the North Pacific during the Holocene inferred from lacustrine carbonate oxygen isotopes, Yukon Territory, Canada. *Quaternary Research*, *64*(1), 21–35. http://doi.org/10.1016/j.yqres.2005.03.005

Appleby, P. G., & Oldfield, F. (1978). The calculation of lead-210 dates assuming a constant rate of supply of unsupported 210Pb to the sediment. *Catena*, *5*(1), 1–8. http://doi.org/10.1016/S0341-8162(78)80002-2

Appleby, P.G., Nolan, P.J., Oldfield, F., Richardson, N., and Higgitt, S.R. (1988). 210 Pb dating of lake sediments and ombrotrophic peats by gamma essay. *Science*, v. 69, p. 157–177.

Bandara, S., Froese, D.G., Porter, T.J., Calmels, F., and Sanborn, P. (2017). Holocene climate change and thermokarst activity as recorded by stable isotopes in drained thermokarst lake basin permafrost from the Old Crow Flats, Yukon, Canada. *Manuscript in preparation.*

Barber, K.E., Chambers, F.M., and Maddy, D. (2003). Holocene palaeoclimates from peat stratigraphy: Macrofossil proxy climate records from three oceanic raised bogs in England and Ireland. *Quaternary Science Reviews*, v. 22, p. 521–539, doi: 10.1016/S0277-3791(02)00185-3.

Battle, M., Bender, M. L., Tans, P. P., White, J. W. C., Ellis, J. T., Conway, T., & Francey, R. J. (2000). Global Carbon Sinks and Their Variability Inferred from Atmospheric O2 and d13C, *287*(March), 2467–2471.

Beal, S. A., Osterberg, E. C., Zdanowicz, C. M., & Fisher, D. A. (2015). Ice core perspective on mercury pollution during the past 600 years. *Environmental science & technology*, 49(13), 7641-7647.

Benoit, J. M., Fitzgerald, W. F., & Damman, a W. (1998). The biogeochemistry of an ombrotrophic bog: evaluation of use as an archive of atmosphere mercury deposition. *Environmental Research*, *78*(2), 118–133. http://doi.org/10.1006/enrs.1998.3850

Biester, H., Bindler, R., Martinez-Cortizas, A., & Engstrom, D. R. (2007). Modeling the past atmospheric deposition of mercury using natural archives. *Environmental science & technology*, 41(14), 4851-4860.

Biester, H., Kilian, R., Franzen, C., Woda, C., Mangini, A., and Schöler, H.F. (2002). Elevated mercury accumulation in a peat bog of the Magellanic Moorlands, Chile (53°S) - An anthropogenic signal from the Southern Hemisphere. *Earth and Planetary Science Letters*, v. 201, p. 609–620, doi: 10.1016/S0012-821X(02)00734-3.

Biester, H., Müller, G., & Schöler, H. F. (2002). Binding and mobility of mercury in soils contaminated by emissions from chlor-alkali plants. *Science of the Total Environment*, 284(1), 191-203.

Bindler, R. (2003). Estimating the natural background atmospheric deposition rate of mercury utilizing ombrotrophic bogs in southern Sweden. *Environmental science & technology*, 37(1), 40-46.

Bindler, R., Klarqvist, M., Klaminder, J., and Förster, J. (2004). Does within-bog spatial variability of mercury and lead constrain reconstructions of absolute deposition rates from single peat records? The example of Store Mosse, Sweden. *Global Biogeochemical Cycles*, v. 18, doi: 10.1029/2004GB002270.

Bindler, R., Renberg, I., Klaminder, J., & Emteryd, O. (2004). Tree rings as Pb pollution archives? A comparison of 206 Pb/207 Pb isotope ratios in pine and other environmental media. *Science of the Total Environment*, 319(1), 173-183.

Bockheim, J. G., & Hinkel, K. M. (2005). Characteristics and Significance of the Transition Zone in Drained Thaw-Lake Basins of the Arctic Coastal Plain, Alaska. *Arctic*, *58*(4), 406–417.

Boutron, C. F., Vandal, G. M., Fitzgerald, W. F., & Ferrari, C. P. (1998). A forty-year record of mercury in central Greenland snow. *Geophysical Research Letters*, 25(17), 3315-3318.

Bowen, G. J. (2017). The Online Isotopes in Precipitation Calculator, version 3.1. Retrieved June 22, 2017, from http://www.waterisotopes.org

Bowen, G. J., & Revenaugh, J. (2003). Interpolating the isotopic composition of modern meteoric precipitation, *39*(10), 1–13. http://doi.org/10.1029/2003WR002086

Branfireun, B. A., Krabbenhoft, D. P., Hintelmann, H., Hunt, R. J., Hurley, J. P., & Rudd, J. W. M. (2005). Speciation and transport of newly deposited mercury in a boreal forest wetland : A stable mercury isotope approach, *41*, 1–11. http://doi.org/10.1029/2004WR003219

Brännvall, M.L., Bindler, R., Emteryd, O., Nilsson, M., and Renberg, I. (1997). Stable isotope and concentration records of atmospheric lead pollution in peat and lake sediments in Sweden. *Water, Air, and Soil Pollution*, v. 100, p. 243–252, doi: 10.1023/A:1018360106350.

Braune, B. M., Outridge, P. M., Fisk, A. T., Muir, D. C. G., Helm, P. A., Hobbs, K., … Stirling, I. (2005). Persistent organic pollutants and mercury in marine biota of the Canadian Arctic : An overview of spatial and temporal trends, *352*, 4–56. http://doi.org/10.1016/j.scitotenv.2004.10.034

Brimblecombe, P., Tranter, M., Abrahams, P. W., Blackwood, I., Davies, T. D., & Vincent, C. E. (1985). Relocation and preferential elution of acidic solute through the snowpack of a small, remote, high-altitude Scottish catchment. *Annals of Glaciology*, 7, 141-147.

Bronk Ramsey, C. (2009). Bayesian Analysis of Radiocarbon Dates. *Radiocarbon*, v. 51, p. 337–360, doi: 10.2458/azu_js_rc.v51i1.3494.

Brooks, S., Arimoto, R., Lindberg, S., & Southworth, G. (2008). Antarctic polar plateau snow surface conversion of deposited oxidized mercury to gaseous elemental mercury with fractional long-term burial. *Atmospheric Environment*, 42(12), 2877-2884.

Burn, C. R. (1997). Cryostratigraphy, paleogeography, and climate change during the early Holocene warm interval, western Arctic coast, Canada. *Canadian Journal of Earth Sciences*, 34(7), 912-925.

Calmels, F., Gagnon, O., and Allard, M. (2005). A portable Earth-drill system for permafrost studies. *Permafrost and Periglacial Processes*, v. 16, p. 311–315, doi: 10.1002/ppp.529.

Canada, E. C.-G. of. (n.d.). Canadian Climate Normals 1971 - 2000 Station Data "Old Crow A - Yukon Territory." Retrieved July 27, 2017, from http://climate.weather.gc.ca/climate_normals/results_e.html?stnID=1582&lang=e&StationName=Old+Crow+&SearchType=Contains&stnNameSubmit=go&dCode=5&dispBack=1

Carpenter, R., Peterson, M. L., & Bennett, J. T. (1982). 210Pb-derived sediment accumulation and mixing rates for the Washington continental slope. *Marine Geology*, *48*(1–2), 135–164. http://doi.org/10.1016/0025-3227(82)90133-5

Charman, D.J., Blundell, A., Chiverrell, R.C., Hendon, D., and Langdon, P.G. (2006). Compilation of non-annually resolved Holocene proxy climate records: Stacked Holocene peatland palaeo-water table reconstructions from northern Britain. *Quaternary Science Reviews*, v. 25, p. 336–350, doi: 10.1016/j.quascirev.2005.05.005.

Chételat, J., Braune, B., Stow, J., & Tomlinson, S. (2015). Special issue on mercury in Canada' s North : Summary and recommendations for future research. *Science of the Total Environment*, *510*, 260–262.

Clymo, R. S. (1984). The limits to peat bog growth. *Philosophical Transactions of the Royal Society of London B: Biological Sciences, 303*(1117), 605–654.

Clymo, R. S. (1987). The ecology of peatlands. *Science Progress (Oxford)*, 71, 593-614.

Compeau, G. C., & Bartha, R. (1985). Sulfate-reducing bacteria: principal methylators of mercury in anoxic estuarine sediment. *Applied and environmental microbiology*, 50(2), 498-502.

Cooke, C. A., Hobbs, W. O., Neal, M., & Wolfe, A. P. (2010). Reliance on 210pb chronology can compromise the inference of preindustrial hg flux to lake sediments. *Environmental Science and Technology*, *44*(6), 1998–2003. http://doi.org/10.1021/es9027925

Cooke, C. A., Wolfe, A. P., Michelutti, N., Balcom, P. H., & Briner, J. P. (2012). A Holocene perspective on algal mercury scavenging to sediments of an arctic lake. *Environmental science & technology*, 46(13), 7135-7141.

Craig, H. (1961). Isotopic Variations in Meteoric Waters. *Science (New York, N.Y.)*, *133*(3465), 1702–1703. http://doi.org/10.1126/science.133.3465.1702

Damman, A. W. H. (1978). Distribution and Movement of Elements in Ombrotrophic Peat Bogs, *30*(3), 480–495. http://doi.org/10.2307/3543344

Dansgaard, W. (1964). Stable isotopes in precipitation. *Tellus A*. http://doi.org/10.3402/tellusa.v16i4.8993

Day, J.H., Rennie, P.J., Stanek, W., and Raymond, G.P. (1979). Peat Testing Manual: Technical Memorendum: National Research Council of Canada - Muskeg Subcommittee.

De Vleeschouwer, F., Le Roux, G., & Shotyk, W. (2010). Peat as an archive of atmospheric pollution and environmental change : A case study of lead in Europe. *PAGES Magazine*, *18*(1), 20–22.

De Vleeschouwer, F., Piotrowska, N., Sikorski, J., Pawlyta, J., Cheburkin, a., Le Roux, G., Lamentowicz, M., Fagel, N., and Mauquoy, D. (2009). Multiproxy evidence of `Little Ice Age' palaeoenvironmental changes in a peat bog from northern Poland: *The Holocene*, v. 19, p. 625–637, doi: 10.1177/0959683609104027.

Dillon, P. J., Scholer, P. J., & Evans, H. E. (1986). 210Pb fluxes in acidified lakes. In Sediments and Water Interactions (pp. 491-499). Springer New York.

Driscoll, C. T., Mason, R. P., Chan, H. M., Jacob, D. J., & Pirrone, N. (2013). Mercury as a global pollutant: sources, pathways, and effects. *Environmental science & technology*, 47(10), 4967-4983.

Durnford, D., Dastoor, A., Figueras-Nieto, D., & Ryjkov, A. (2010). Long range transport of mercury to the Arctic and across Canada. *Atmospheric Chemistry and Physics*, 10(13), 6063-6086.

Duruibe, J. O., Ogwuegbu, M. O. C., & Egwurugwu, J. N. (2007). Heavy metal pollution and human biotoxic effects. *International Journal of Physical Sciences*, 2(5), 112-118.

Ebinghaus, R., Kock, H. H., Temme, C., Einax, J. W., Löwe, A. G., Richter, A., ... & Schroeder, W. H. (2002). Antarctic springtime depletion of atmospheric mercury. *Environmental science & technology*, 36(6), 1238-1244.

Engstrom, D. R., Fitzgerald, W. F., Cooke, C. A., Lamborg, C. H., Drevnick, P. E., Swain, E. B., ... & Balcom, P. H. (2014). Atmospheric Hg emissions from preindustrial gold and silver extraction in the Americas: A reevaluation from lake-sediment archives. Envir*onmental science & technology*, 48(12), 6533-6543.

Enrico, M., Beek, P. Van, Souhaut, M., and Sonke, J.E., 2017, Holocene Atmospheric Mercury Levels Reconstructed from Peat Bog Mercury Stable Isotopes:, doi: 10.1021/acs.est.6b05804.

Enrico, M., Le Roux, G., Marusczak, N., Heimbürger, L. E., Claustres, A., Fu, X., ... & Sonke, J. E. (2016). Atmospheric mercury transfer to peat bogs dominated by gaseous elemental mercury dry deposition. *Environmental science & technology*, 50(5), 2405-2412.

Environment Canada - Government of Canada. (n.d.). Canadian Climate Normals 1981-2010 Station Data "Dawson A - Yukon Territory." Retrieved May 9, 2016, from http://climate.weather.gc.ca/climate_normals/results_1981_2010_e.html?stnID=1535&lang=e&StationName=dawson&SearchType=Contains&stnNameSubmit=go&dCode=0

Evans, L. J. (1989). Chemistry of metal retention by soils. *Environmental Science & Technology*, 23(9), 1046-1056.

Farmer, J. G., Anderson, P., Cloy, J. M., Graham, M. C., Mackenzie, A. B., & Cook, G. T. (2009). Science of the Total Environment Historical accumulation rates of mercury in four Scottish ombrotrophic peat bogs over the past 2000 years. *Science of the Total Environment*, *407*(21), 5578–5588. http://doi.org/10.1016/j.scitotenv.2009.06.014

Fitzgerald, W. F., Engstrom, D. R., Mason, R. P., & Nater, E. A. (1998). The case for atmospheric mercury contamination in remote areas. *Environmental Science & Technology*, 32(1), 1-7.

French, H., and Shur, Y. (2010). The principles of cryostratigraphy. *Earth-Science Reviews*, v. 101, p. 190–206, doi: 10.1016/j.earscirev.2010.04.002.

Froese, D.G., Davies, L.J., Appleby, P., Bandara, S., van Bellen, S., Magnan, G., Mullan-Boudreau, G., Noernberg, T., Shotyk, W., Staniszewska, K., and Zaccone, C. (2016). High-resolution age modelling of peat bog profiles using pre and postbomb 14C, 210Pb and cryptotephra data from Alberta and Yukon peatlands. *Dating the Anthropocene in Environmental Archives Workshop*.

Froese, D., Westgate, J., Preece, S., & Storer, J. (2002). Age and significance of the Late Pleistocene Dawson tephra in eastern Beringia, *21*, 2137–2142.

Giesler, R., Clemmensen, K. E., Wardle, D. A., Klaminder, J., & Bindler, R. (2017). Boreal Forests Sequester Large Amounts of Mercury over Millennial Time Scales in the Absence of Wildfire. http://doi.org/10.1021/acs.est.6b06369

Givelet, N. (2004). Long-term Records of Atmospheric Deposition of Mercury in Peat Cores from Arctic, and Comparison with Bogs in the Temperate Zone. *Doctoral dissertation*.

Givelet, N., Le Roux, G., Cheburkin, A., Chen, B., Frank, J., Goodsite, M. E., ... & Rheinberger, S. (2004). Suggested protocol for collecting, handling and preparing peat cores and peat samples for physical, chemical, mineralogical and isotopic analyses. *Journal of Environmental Monitoring*, 6(5), 481-492.

Givelet, N., Roos-Barraclough, F., & Shotyk, W. (2003). Predominant anthropogenic sources and rates of atmospheric mercury accumulation in southern Ontario recorded by peat cores from three bogs: comparison with natural "background" values (past 8000 years). *Journal of Environmental Monitoring*, 5(6), 935-949.

Givelet, N., Roos-Barraclough, F., Goodsite, M. E., Cheburkin, A. K., & Shotyk, W. (2004). Atmospheric mercury accumulation rates between 5900 and 800 calibrated years BP in the High Arctic of Canada recorded by peat hummocks. *Environmental science & technology*, 38(19), 4964-4972.

Gordon, J., Quinton, W., Bran, B. A., & Olefeldt, D. (2016). Mercury and methylmercury biogeochemistry in a thawing permafrost wetland complex , Northwest Territories , Canada, *3638*(August), 3627–3638. http://doi.org/10.1002/hyp.10911

Grandjean, P., Weihe, P. A. L., White, R. F., & Debes, F. (1997). Cognitive Deficit in 7-Year-Old Children with Prenatal Exposure to Methylmercury, *19*(6), 417–428.

Green, S. A., & Blough, N. V. (1994). Optical absorption and fluorescence properties of chromophoric dissolved organic matter in natural waters. *Limnology and Oceanography*, *39*(8), 1903–1916. http://doi.org/10.4319/lo.1994.39.8.1903

Grigal, D. F. (2003). Mercury sequestration in forests and peatlands: a review. *Journal of Environmental Quality*, *32*(2), 393–405. http://doi.org/10.2134/jeq2003.3930

Gustin, M. S., Lindberg, S. E., & Weisberg, P. J. (2008). An update on the natural sources and sinks of atmospheric mercury. *Applied Geochemistry*, *23*(3), 482–493. http://doi.org/10.1016/j.apgeochem.2007.12.010

Harris, R. C., Rudd, J. W., Amyot, M., Babiarz, C. L., Beaty, K. G., Blanchfield, P. J., ... & Heyes, A. (2007). Whole-ecosystem study shows rapid fish-mercury response to changes in mercury deposition. *Proceedings of the National Academy of Sciences*, 104(42), 16586-16591.

Harvey, E. T., Kratzer, S., & Andersson, A. (2015). Relationships between colored dissolved organic matter and dissolved organic carbon in different coastal gradients of the Baltic Sea. *Ambio*, *44*(3), 392–401. http://doi.org/10.1007/s13280-015-0658-4

Heiri, O., Lotter, A. F., & Lemcke, G. (2001). Loss on ignition as a method for estimating organic and carbonate content in sediments: reproducibility and comparability of results. *Journal of Paleolimnology*, *25*(1), 101–110.

Hermanson, M. H. (1998). Anthropogenic mercury deposition to Arctic lake sediments. *Water, Air, and Soil Pollution*, 101(1-4), 309-321.

Horowitz, H. M., Jacob, D. J., Amos, H. M., Streets, D. G., & Sunderland, E. M. (2014). Historical mercury releases from commercial products: Global environmental implications. *Environmental science & technology*, 48(17), 10242-10250.

Hua, Q., Barbetti, M., & Rakowski, a Z. (2013). Atmospheric radiocarbon for the period 1950-2010. *Radiocarbon*, *55*(4), 2059–2072. http://doi.org/10.2458/azu_js_rc.v55i2.16177

Hugelius, G., Strauss, J., Zubrzycki, S., Harden, J. W., Schuur, E. A. G., Ping, C., … Kuhry, P. (2014). Estimated stocks of circumpolar permafrost carbon with quantified ranges and identified data gaps. *Biogeosciences*, *11*(23), 6573–6593. http://doi.org/10.5194/bg-11-6573-2014

Hylander, L. D., & Meili, M. (2003). 500 Years of mercury production: Global annual inventory by region until 2000 and associated emissions. *Science of the Total Environment*, *304*(1–3), 13–27. http://doi.org/10.1016/S0048-9697(02)00553-3

IAEA/WMO. (2015). Global Network of Isotopes in Precipitation. The GNIP Database. Retrieved June 22, 2017, from https://nucleus.iaea.org/wiser

Indian and Northern Affairs Canada. (1992). *Yukon Placer Mining Industry 1991-1992*.

IPCC. (2007). Climate change 2007: the physical science basis. In: Solomon S, Qin D, Manning M, Chen Z, Marquis M, Averyt KB, Tignor M, Miller HL, editors. Contributions of Working Group I to the Fourth Assessment Report of the Intergovernmental Panel on Climate Change (p. 996). Cambridge, UK and New York, USA.

Jensen, A., & Jensen, A. (1991). Historical deposition rates of mercury in scandinavia estimated by dating and measurement of mercury in cores of peat bogs. *Water Air & Soil Pollution*, *56*(1), 769–777. http://doi.org/10.1007/BF00342315

Jensen, S., & Jernelöv, A. (1969). Biological methylation of mercury in aquatic organisms. *Nature*, 233, 753-754.

Johansen, P., Pars, T., & Bjerregaard, P. (2000). Lead , cadmium , mercury and selenium intake by Greenlanders from local marine food. *Science of the Total Environment*, *245*(1), 187–194.

Jonasson, I. R. (1970). Mercury in the natural environment: a review of recent work. Mercury in the natural environment: a review of recent work., (70-57).

Jones, J. M., & Hao, J. (1993). Ombrotrophic peat as a medium for historical monitoring of heavy metal pollution. *Environmental Geochemistry and Health*, *15*(2–3), 67–74. http://doi.org/10.1007/BF02627824

Jones, M.C., Grosse, G., Jones, B.M., and Walter Anthony, K. (2012). Peat accumulation in drained thermokarst lake basins in continuous, ice-rich permafrost, northern Seward Peninsula, Alaska: Journal of Geophysical Research. *Biogeosciences*, v. 117, doi: 10.1029/2011JG001766.

Kaufman, D. S., Ager, T. A., Anderson, N. J., Anderson, P. M., Andrews, J. T., Bartlein, P. J., ... & Dyke, A. S. (2004). Holocene thermal maximum in the western Arctic (0–180 W). *Quaternary Science Reviews*, 23(5), 529-560.

Kempter, H., Görres, M., and Frenzel, B. (1997). Ti and Pb Concentrations in rainwater-fed bogs in Europe as indicators of past anthropogenic activities. *Water, Air, and Soil Pollution*, v. 100, p. 367–377, doi: 10.1023/A:1018376509985.

Kerin, E. J., Gilmour, C. C., Roden, E., Suzuki, M. T., Coates, J. D., & Mason, R. P. (2006). Mercury methylation by dissimilatory iron-reducing bacteria. *Applied and environmental microbiology*, 72(12), 7919-7921.

Kirk, J. L., St. Louis, V. L., & Sharp, M. J. (2006). Rapid reduction and reemission of mercury deposited into snowpacks during atmospheric mercury depletion events at Churchill, Manitoba, Canada. *Environmental science & technology*, 40(24), 7590-7596.

Klaminder, J., Renberg, I., Bindler, R., and Emteryd, O. (2003). Isotopic trends and background fluxes of atmospheric lead in northern Europe: Analyses of three ombrotrophic bogs from south Sweden. *Global Biogeochemical Cycles*, v. 17, doi: 10.1029/2002gb001921.

Klaminder, J., Yoo, K., Rydberg, J., & Giesler, R. (2008). An explorative study of mercury export from a thawing palsa mire, *113*(October), 1–9. http://doi.org/10.1029/2008JG000776

Klock, R., Hudson, E., Aihoshi, D., & Mullock, J. (2001). The Weather of the Yukon, Northwest Territories and Western Nunavut. *Graphic Area Forecast* 35.

Klusman, R. W., & Jaacks, J. A. (1987). Environmental influences upon mercury, radon and helium concentrations in soil gases at a site near Denver, Colorado. *Journal of Geochemical Exploration*, 27(3), 259-280.

Knoblauch, C., Beer, C., Sosnin, A., & Wagner, D. (2013). Predicting long-term carbon mineralization and trace gas production from thawing permafrost of Northeast Siberia, 1160–1172. http://doi.org/10.1111/gcb.12116

Korosi, J. B., Mcdonald, J., Coleman, K. A., Palmer, M. J., Smol, J. P., Simpson, M. J., & Blais, J. M. (2015). Long-term changes in organic matter and mercury transport to lakes in the sporadic discontinuous permafrost zone related to peat subsidence, 1550–1561. http://doi.org/10.1002/lno.10116

Kylander, M.E., Klaminder, J., Bindler, R., and Weiss, D.J. (2010). Natural lead isotope variations in the atmosphere. *Earth and Planetary Science Letters*, v. 290, p. 44–53, doi: 10.1016/j.epsl.2009.11.055.

Lalonde, J. D., Poulain, A. J. M., & Amyot, M. (2000). Mercury dynamics in snow. In *Proceedings of the 11th Annual International Conference on Heavy Metals in the Environment*. School of Public Health, University of Michigan, Ann Arbor, MI.

Lamborg, C. H., Fitzgerald, W. F., Damman, A. W. H., Benoit, J. M., Balcom, P. H., & Engstrom, D. R. (2002). Modern and historic atmospheric mercury fluxes in both hemispheres: Global and regional mercury cycling implications. *Global Biogeochemical Cycles*, *16*(4), 51. http://doi.org/10.1029/2001GB001847

Lapp, A. (2015). Seasonal Variability of Groundwater Contribution to Watershed Discharge in Discontinuous Permafrost in the North Klondike River Valley, Yukon. University of Ottawa.

Lauriol, B., Lacelle, D., Labrecque, S., Duguay, C. R., & Telka, A. (2009). Holocene evolution of lakes in the Bluefish Basin, northern Yukon, Canada. *Arctic, 62*(2), 212-224.

Le Roux, G., & De Vleeschouwer, F. (2010). Preparation of peat samples for inorganic geochemistry used as palaeoenvironmental proxies. *Mires and Peat*, 7, 1–9.

Lindberg, S., Bullock, R., Ebinghaus, R., Engstrom, D., Feng, X., Fitzgerald, W., ... & Seigneur, C. (2007). A synthesis of progress and uncertainties in attributing the sources of mercury in deposition. *Ambio: A Journal of the Human Environment*, 36(1), 19-33.

Lockhart, W. L., MacDonald, R. W., Outridge, P. M., Wilkinson, P., DeLaronde, J. B., & Rudd, J. W. M. (2000). Tests of the fidelity of lake sediment core records of mercury deposition to known histories of mercury contamination. *Science of the Total Environment*, 260(1), 171-180.

Lockhart, W. L., Wilkinson, P., Billeck, B. N., Hunt, R. V., Wagemann, R., & Brunskill, G. J. (1995). Current and historical inputs of mercury to high-latitude lakes in Canada and to Hudson Bay. *Water, Air, and Soil Pollution*, 80(1-4), 603-610.

Lodenius, M., Seppanen, A., & Autio, S. (1987). Leaching of mercury from peat soil. *Cheosphere*, *16*(6), 1215–1220.

Lodenius, M., Seppanen, A., & Autio, S. (1987). Sorption of Mercury in Soils with Different Humus Content. *Bulletin of Environmental Contamination and Toxicology*, 593–600.

Lodenius, M., Seppanen, A., & Uusi-Rauva, A. (1983). Sorption and mobilization of mercury in peat soil. *Chemosphere*, *12*(ll), 1575–1581.

MacDonald, R. W., Harner, T., & Fyfe, J. (2005). Recent climate change in the Arctic and its impact on contaminant pathways and interpretation of temporal trend data. *Science of the total environment*, 342(1), 5-86.

MacDonald, R. W., Harner, T., Fyfe, J., Loeng, H., & Weingartner, T. (2003). AMAP Assessment 2002: The Influence of Global Change on Contaminant Patways to, within, and from the Arctic.

Mackay, D., Wania, F., & Schroeder, W. H. (1995). Prospects for modeling the behavior and fate of mercury, globally and in aquatic systems. In *Mercury as a Global Pollutant* (pp. 941-950). Springer Netherlands.

Mahony, M. E. (2015). 50,000 years of paleoenvironmental change recorded in meteoric waters and coeval paleoecological and cryostratigraphic indicators from the Klondike goldfields, Yukon, Canada. University of Alberta.

Martinez-Cortizas, A. (1999). Mercury in a Spanish Peat Bog: Archive of Climate Change and Atmospheric Metal Deposition. *Science*, v. 284, p. 939–942, doi: 10.1126/science.284.5416.939.

Martınez-Cortizas, A., Pontevedra-Pombal, X., Garcıa-Rodeja, E., Novoa-Munoz, J. C., & Shotyk, W. (1999). Mercury in a Spanish peat bog: archive of climate change and atmospheric metal deposition. *Science*, 284(5416), 939-942.

Martínez-Cortizas, A., Pontevedra-Pombal, X., Nóvoa Muñoz, J.C., and García-Rodeja, E. (1997). Four thousand years of atmospheric Pb, Cd and Zn deposition recorded by the ombrotrophic peat bog of Penido Vello (Northwestern Spain). *Water, Air, and Soil Pollution*, v. 100, p. 387–403, doi: 10.1023/A:1018312223189.

Mason, R. P., Fitzgerald, W. F., & Morel, F. M. (1994). The biogeochemical cycling of elemental mercury: anthropogenic influences. *Geochimica et Cosmochimica Acta*, 58(15), 3191-3198.

Mason, R. P., Reinfelder, J. R., & Morel, F. M. M. (1995). Bioaccumulation of mercury and methylmercury. *Water, Air, & Soil Pollution*, *80*(1), 915–921.

McGuire, A. D., Anderson, L. G., Christensen, T. R., Dallimore, S., Guo, L., Hayes, D. J., … Poulet, N. (2009). Sensitivity of the carbon cycle in the Arctic to climate change. *Ecological Monographs*, *79*(4), 523–555.

Monna, F., Petit, C., Gulllaumet, J.P., Jouffroy-Bapicot, I., Blanchot, C., Dominik, J., Losno, R., Richard, H., Lévêque, J., and Chateau, C. (2004). History and Environmental Impact of Mining Activity in Celtic Aeduan Territory Recorded in a Peat Bog (Morvan, France). *Environmental Science and Technology*, v. 38, p. 665–673, doi: 10.1021/es034704v.

Morel, F., Kraepiel, A. M. L., & Amyot, M. (1998). The Chemical Cycle and Bioaccumulation of Mercury. *Annual Review of Ecology and Systematics 29.1*, *29*(1), 543–566.

Mortensen, J. K. (1992). Pre-mid-Mesozoic tectonic evolution of the Yukon-Tanana terrane, Yukon and Alaska. *Tectonics*, *11*(4), 836–853.

Murton, J.B., and French, H.M. (1994). Cryostructures in permafrost, Tuktoyaktuk coastlands, western arctic Canada. *Canadian Journal of Earth Sciences*, v. 31, p. 737–747, doi: 10.1139/e94-067.

NCP. (2003). Canadian Arctic Contaminants Assessment Report II. Ottawa: Northern Contaminants Program (NCP).

Nørnberg, T., Goodsite, M.E., and Shotyk, W. (2004). An improved motorized corer and sample processing system for frozen peat. *Arctic*, v. 57, p. 242–246.

Norton, S. A., & Kahl, J. S. (1987). A comparison of lake sediments and ombrotrophic peat deposits as long-term monitors of atmospheric pollution. New Approaches to Monitoring Aquatic Ecosystems, 40-57.

Norton, S. A., Dillon, P. J., Evans, R. D., Mierle, G., & Kahl, J. S. (1990). The history of atmospheric deposition of Cd, Hg, and Pb in North America: evidence from lake and peat bog sediments. In *Acidic Precipitation* (pp. 73-102). Springer New York.

Novak, M., & Pacherova, P. (2008). Mobility of trace metals in pore waters of two Central European peat bogs, *4*. http://doi.org/10.1016/j.scitotenv.2008.01.036

Novák, M., Emmanuel, S., Vile, M.A., Erel, Y., Véron, A., Pačes, T., Wieder, R.K., Vaněček, M., Štěpánová, M., Břízová, E., and Hovorka, J. (2003). Origin of lead in eight central European peat bogs determined from isotope ratios, strengths, and operation times of regional pollution sources. *Environmental Science and Technology*, v. 37, p. 437–445, doi: 10.1021/es0200387.

Novak, M., Zemanova, L., Voldrichova, P., Stepanova, M., Adamova, M., Pacherova, P., … Prechova, E. (2011). Experimental Evidence for Mobility / Immobility of Metals in Peat, 7180–7187.

Nriagu, J. O. (1979). Biogeochemistry of Mercury in the Environment. Elsevier/North-Holland Biomedical Press.

Obrist, D., Agnan, Y., Jiskra, M., Olson, C. L., Colegrove, D. P., Hueber, J., ... & Helmig, D. (2017). Tundra uptake of atmospheric elemental mercury drives Arctic mercury pollution. *Nature*, 547, 201-204.

Oldfield, F., Appleby, P.G., Cambray, R.S., Eakins, J.D., Barber, K.E., Battarbee, R.W., Pearson, G.R., and Williams, J.M. (1979). 210 Pb, 137 Cs and 239 Pu Profiles in Ombrotrophic Peat. *Oikos*, v. 33, p. 40–45.

Osler, T. (1983). Study of Mercury Usage in Placer Mining Operations in the Yukon Territory and North Western British Columbia.

Outridge, P. M., & Sanei, H. (2010). Does organic matter degradation affect the reconstruction of pre-industrial atmospheric mercury deposition rates from peat cores? - A test of the hypothesis using a permafrost peat deposit in northern Canada. *International Journal of Coal Geology*, 83(1), 73-81.

Outridge, P. M., Sanei, H., Stern, G. A., Hamilton, P. B., & Goodarzi, F. (2007). Evidence for control of mercury accumulation rates in Canadian High Arctic lake sediments by variations of aquatic primary productivity. *Environmental science & technology*, 41(15), 5259-5265.

Pacyna, E. G., & Pacyna, J. M. (2002). Global emission of mercury from anthropogenic sources in 1995. *Water, Air, and Soil Pollution*, *137*(1–4), 149–165. http://doi.org/10.1023/A:1015502430561

Page, S.E., Wűst, R.A.J., Weiss, D., Rieley, J.O., Shotyk, W., and Limin, S.H. (2004). A record of Late Pleistocene and Holocene carbon accumulation and climate change from an equatorial peat bog (Kalimantan, Indonesia): implications for past, present and future carbon dynamics. *Journal of Quaternary Science*, v. 19, p. 625–635, doi: 10.1002/jqs.884.

Petit, R. J., Raynaud, D., Basile, I., Chappellaz, J., Ritz, C., Delmotte, M., … Pe, L. (1999). Climate and atmospheric history of the past 420,000 years from the Vostok ice core, Antarctica. *Nature*, *399*, 429–413. http://doi.org/10.1038/20859

Pheiffer-Madsen, P. (1981). Peat bog records of atmospheric mercury deposition. *Nature*, v. 293, p. 127–130, doi: 10.1038/293127a0.

Phillips, V. J. A., St. Louis, V. L., Cooke, C. A., Vinebrooke, R. D., & Hobbs, W. O. (2011). Increased mercury loadings to Western Canadian Alpine Lakes over the past 150 years. *Environmental Science and Technology*, *45*(6), 2042–2047. http://doi.org/10.1021/es1031135

Poulain, A. J., & Barkay, T. (2013). Cracking the mercury methylation code. Science, 339(6125), 1280-1281.

Poulain, A. J., Lalonde, J. D., Amyot, M., Shead, J. A., Raofie, F., & Ariya, P. A. (2004). Redox transformations of mercury in an Arctic snowpack at springtime. *Atmospheric Environment*, 38(39), 6763-6774.

Ram, N., & Verloo, M. (1985). Effect of Various Organic Materials on the Mobility of Heavy Metals in Soil. *Environmental Pollution (Series B)*, *10*, 241–248.

Rasmussen, P. E. (1994). Current methods of estimating atmospheric mercury fluxes in remote areas. *Environmental science & technology*, 28(13), 2233-2241.

Reimer, P. J., Bard, E., Bayliss, A., Beck, J. W., Blackwell, P. G., Bronk, M., … van der Plicht, J. (2013). IntCal 13 and Marine 13 radiocarbon age calibration curves 0–50,000 years cal BP. *Radiocarbon*, *55*, 1869–1887.

Riley, J.L. (1989). Laboratory Methods for Testing Peat: Ontario Peatland Inventory Project: Ontario Ministry of Northern Development and Mines, v. 145.

Ritchie, J. C., Cwynar, L. C., and Spear, R. W., 1983: Evidence from north-west Canada for an early Holocene Milankovitch thermal maximum. *Nature*, 305: 126–128.

Roos-Barraclough, F., & Shotyk, W. (2003). Millennial-scale records of atmospheric mercury deposition obtained from ombrotrophic and minerotrophic peatlands in the Swiss Jura Mountains. *Environmental science & technology*, 37(2), 235-244.

Roos-Barraclough, F., Givelet, N., Cheburkin, A. K., Shotyk, W., & Norton, S. A. (2006). Use of Br and Se in peat to reconstruct the natural and anthropogenic fluxes of atmospheric Hg: A 10000-year record from Caribou Bog, Maine. *Environmental Science and Technology*, *40*(10), 3188–3194. http://doi.org/10.1021/es051945p

Roos-Barraclough, F., Givelet, N., Martinez-Cortizas, A., Goodsite, M. E., Biester, H., & Shotyk, W. (2002). An analytical protocol for the determination of total mercury concentrations in solid peat samples. *Science of the total environment*, 292(1), 129-139.

Roos-Barraclough, F., Martinez-Cortizas, A., García-Rodeja, E., & Shotyk, W. (2002). A 14 500-year record of the accumulation of atmospheric mercury in peat: volcanic signals, anthropogenic influences and a correlation to bromine accumulation. *Earth and Planetary Science Letters*, 202(2), 435-451.

Roy-Léveillée, P., & Burn, C. R. (2010). Permafrost conditions near shorelines of oriented lakes in Old Crow Flats , Yukon Territory, (August). http://doi.org/10.13140/2.1.1332.4167

Rydberg, J., Klaminder, J., Rosén, P., & Bindler, R. (2010). Climate driven release of carbon and mercury from permafrost mires increases mercury loading to sub-arctic lakes. *Science of the Total Environment*, *408*(20), 4778–4783. http://doi.org/10.1016/j.scitotenv.2010.06.056

Schadel, C., Schuur, E. A. G., Bracho, R., Elberling, B. O., Knoblauch, C., Lee, H., … Turetsky, M. R. (2014). Circumpolar assessment of permafrost C quality and its vulnerability over time using long-term incubation data. *Global Change Biology*, *20*(2), 641–652. http://doi.org/10.1111/gcb.12417

Schaefer, K., Lantuit, H., Romanovsky, V.E., Schuur, E.A.G., and Witt, R. (2014). The impact of the permafrost carbon feedback on global climate. *Environmental Research Letters*, 9, 085003, doi: 10.1088/1748-9326/9/8/085003.

Schroeder, W. H., & Munthe, J. (1998). Atmospheric mercury—an overview. *Atmospheric Environment*, 32(5), 809-822.

Schroeder, W. H., Anlauf, K. G., Barrie, L. A., Lu, J. Y., Steffen, A., Schneeberger, D. R., & Berg, T. (1998). Arctic springtime depletion of mercury. *Nature*, 394(6691), 331-332.

Schuster, E. (1991). The behavior of mercury in the soil with special emphasis on complexation and adsorption processes-a review of the literature. *Water, Air, & Soil Pollution*, 56(1), 667-680.

Schuster, P. F., Krabbenhoft, D. P., Naftz, D. L., Cecil, L. D., Olson, M. L., Dewild, J. F., ... & Abbott, M. L. (2002). Atmospheric mercury deposition during the last 270 years: a glacial ice core record of natural and anthropogenic sources. *Environmental Science & Technology*, 36(11), 2303-2310.

Shackleton, N. J., & Opdyke, N. D. (1973). Oxygen isotope and palaeomagnetic stratigraphy of Equatorial Pacific core V28-238: Oxygen isotope temperatures and ice volumes on a 105 year and 106 year scale. *Quaternary Research*, *3*(1), 39–55. http://doi.org/10.1016/0033-5894(73)90052-5

Shotyk, W. (2002). The chronology of anthropogenic, atmospheric Pb deposition recorded by peat cores in three minerogenic peat deposits from Switzerland. *Science of the Total Environment*, v. 292, p. 19–31, doi: 10.1016/S0048-9697(02)00030-X.

Shotyk, W., & Steinmann, P. (1994). Pore-water indicators of rainwater-dominated versus groundwater-dominated peat bog profiles (Jura Mountains, Switzerland). *Chemical Geology*, v. 116, p. 137–146, doi: 10.1016/0009-2541(94)90162-7.

Shotyk, W., Goodsite, M. E., Roos-Barraclough, F., Frei, R., Heinemeier, J., Asmund, G., ... & Hansen, T. S. (2003). Anthropogenic contributions to atmospheric Hg, Pb and As accumulation recorded by peat cores from southern Greenland and Denmark dated using the 14 C "bomb pulse curve". *Geochimica et Cosmochimica Acta*, 67(21), 3991-4011.

Shotyk, W., Goodsite, M. E., Roos-Barraclough, F., Givelet, N., Le Roux, G., Weiss, D., … Lohse, C. (2005). Accumulation rates and predominant atmospheric sources of natural and anthropogenic Hg and Pb on the Faroe Islands. *Geochimica et Cosmochimica Acta*, *69*(1), 1–17. http://doi.org/10.1016/j.gca.2004.06.011

Shotyk, W., Weiss, D., Appleby, P.G., Cheburkin, A.K., Frei, R., Kramers, J.D., Reese, S., and Van Der Knaap, W.O. (1998). History of Atmospheric Lead Deposition Since 12,370 14C yr BP from a Peat Bog, Jura Mountains, Switzerland. *Science*, v. 281, p. 1635–1640, doi: 10.1126/science.281.5383.1635.

St. Louis, V. L., Sharp, M. J., Steffen, A., May, A., Barker, J., Kirk, J. L., ... & Smol, J. P. (2005). Some sources and sinks of monomethyl and inorganic mercury on Ellesmere Island in the Canadian High Arctic. *Environmental science & technology*, 39(8), 2686-2701.

Steffen, A., Lehnherr, I., Cole, A., Ariya, P., Dastoor, A., Durnford, D., … Pilote, M. (2015). Atmospheric mercury in the Canadian Arctic. Part I: A review of recent field measurements. *Science of the Total Environment*, *509*, 3–15.

Steinnes, E., & Sjøbakk, T. E. (2005). Order-of-magnitude increase of Hg in Norwegian peat profiles since the outset of industrial activity in Europe, *137*, 365–370. http://doi.org/10.1016/j.envpol.2004.10.008

Stern, G. A., MacDonald, R. W., Outridge, P. M., Wilson, S., Chetelat, J., Cole, A., ... & Zdanowicz, C. (2012). How does climate change influence arctic mercury?. *Science of the total environment*, 414, 22-42.

Stern, G. A., Sanei, H., Roach, P., Delaronde, J., & Outridge, P. M. (2009). Historical interrelated variations of mercury and aquatic organic matter in lake sediment cores from a subarctic lake in Yukon, Canada: further evidence toward the algal-mercury scavenging hypothesis. *Environmental science & technology*, 43(20), 7684-7690.

Stocker, T. F., Qin, D., Plattner, G.-K., Tignor, M., Allen, S. K., Boschung, J., … Midgley, P. M. (2014). IPCC, 2013: Climate Change 2013: The Physical Science Basis. Contributions of Working Group I to the Fifth Assessment Report of the Intergovernmental Panel on Climate Change. Cambridge, UK and New York, USA: Cambridge University Press.

Strauss, J., Schirrmeister, L., Grosse, G., Wetterich, S., Ulrich, M., Herzschuh, U., & Hubberten, H. (2013). The deep permafrost carbon pool of the Yedoma region in Siberia and Alaska. *Geophysical Research Letters*, *40*(23), 6165–6170. http://doi.org/10.1002/2013GL058088

Streets, D. G., Devane, M. K., Lu, Z., Bond, T. C., Sunderland, E. M., & Jacob, D. J. (2011). All-time releases of mercury to the atmosphere from human activities. *Environmental science & technology*, 45(24), 10485-10491.

Streets, D. G., Horowitz, H. M., Jacob, D. J., Lu, Z., Levin, L., Ter Schure, A. F., & Sunderland, E. M. (2017). Total Mercury Released to the Environment by Human Activities. *Environmental Science & Technology*, 51(11), 5969-5977.

Swain, E. B., Engstrom, D. R., Brigham, M. E., Henning, T. A., & Brezonik, P. L. (1992). Increasing rates of atmospheric mercury deposition in midcontinental North America. *Science*, 257(5071), 784-787.

Swain, E. B., Jakus, P. M., Rice, G., Lupi, F., Maxson, P. A., Pacyna, J. M., ... & Veiga, M. M. (2007). Socioeconomic consequences of mercury use and pollution. *Ambio: A Journal of the Human Environment*, 36(1), 45-61.

Swindles, G., Vleeschouwer, F. De, and Plunkett, G. (2010). Dating peat profiles using tephra: stratigraphy, geochemistry and chronology. *Mires and Peat*, v. 7, p. 1–9, http://www.doaj.org/doaj?func=fulltext&aId=896235.

Tang, S., Zhongwei, H., Jun, L., Zaichan, Y., & Qinhua, L. (2012). Atmospheric mercury deposition recorded in an ombrotrophic peat core from Xiaoxing'an Mountain, Northeast China. *Environmental Research*, *118*, 145–148. http://doi.org/10.1016/j.envres.2011.12.009

Tarnocai, C., Canadell, J. G., Schuur, E. a. G., Kuhry, P., Mazhitova, G., & Zimov, S. (2009). Soil organic carbon pools in the northern circumpolar permafrost region. *Global Biogeochemical Cycles*, *23*(2). http://doi.org/10.1029/2008GB003327

Tommasini, S., Davies, G. R., & Elliott, T. (2000). Lead isotope composition of tree rings as bio-geochemical tracers of heavy metal pollution: a reconnaissance study from Firenze, Italy. *Applied Geochemistry*, 15(7), 891-900.

Tranter, M. (2011). Isotopic Fractionation of Freezing Water. In V. P. Singh, P. Singh, & U. K. Haritashya (Eds.), *Encyclopedia of Snow, Ice and Glaciers* (pp. 668–669). Dordrecht: Springer Netherlands. http://doi.org/10.1007/978-90-481-2642-2_310

Turetsky, M. R., Harden, J. W., Friedli, H. R., Flannigan, M., Payne, N., Crock, J., & Radke, L. (2006). Wildfires threaten mercury stocks in northern soils, *33*(February), 1–6. http://doi.org/10.1029/2005GL025595

Turner, K. W., Wolfe, B. B., & Edwards, T. W. D. (2010). Characterizing the role of hydrological processes on lake water balances in the Old Crow Flats, Yukon Territory, Canada, using water isotope tracers. *Journal of Hydrology*, *386*(1–4), 103–117. http://doi.org/10.1016/j.jhydrol.2010.03.012

Urban, N. R., Eisenreich, S. J., Grigal, D. F., & Schurr, K. T. (1990). Mobility and diagenesis of Pb and diagenesis of Pb in peat. *Geochimica et Cosmochimica Acta*, *54*, 3329–3346.

US EPA. (2007). Mercury in solids and solutions by thermal decomposition, amalgamation, and atomic absorption spectrophotometry - method 7473 - total Mercury. *SW-846, Test Methods for Evaluating Solid Waste, Physical/Chemical Methods*, 1–17. Retrieved from http://www.epa.gov/osw/hazard/testmethods/sw846/pdfs/7473.pdf

Van Loon, S., & Bond, J. D. (2014). *Yukon Placer Mining Industry 2010-2014*.

Wania, F., & Mackay, D. (1993). Global fractionation and cold condensation of low volatility organochlorine compounds in polar regions. *Ambio*, 10-18.

Watmough, S. A. (1999). Monitoring historical changes in soil and atmospheric trace metal levels by dendrochemical analysis. *Environmental pollution*, 106(3), 391-403.

Weiss, D., Shotyk, W., Rieley, J., Page, S., Gloor, M., Reese, S., and Martinez-Cortizas, A. (2002). The geochemistry of major and selected trace elements in a forested peat bog, Kalimantan, SE Asia, and its implications for past atmospheric dust deposition. *Geochimica et Cosmochimica Acta*, v. 66, p. 2307–2323, doi: 10.1016/S0016-7037(02)00834-7.

Wheatley, B., & Wheatley, M. A. (2000). Methylmercury and the health of indigenous peoples: a risk management challenge for physical and social sciences and for public health policy. *Science of the Total Environment*, 259(1), 23-29.

Willis, B. L. (1997). The Environmental Effects of the Yukon Gold Rush 1896 - 1906: Alterations to land, destruction of wildlife, and disease.

Wright, G., Woodward, C., Peri, L., Weisberg, P. J., & Gustin, M. S. (2014). Application of tree rings [dendrochemistry] for detecting historical trends in air Hg concentrations across multiple scales. *Biogeochemistry*, 120(1-3), 149-162.

Xia, K., Skyllberg, U. L., Bleam, W. F., Bloom, P. R., Nater, E. A., & Helmke, P. A. (1999). X-ray absorption spectroscopic evidence for the complexation of Hg (II) by reduced sulfur in soil humic substances. *Environmental science & technology*, 33(2), 257-261.

Xie, S., Nott, C.J., Avsejs, L.A., Volders, F., Maddy, D., Chambers, F.M., Gledhill, A., Carter, J.F., and Evershed, R.P. (2000). Palaeoclimate records in compound-specific dD values of a lipid biomarker in ombrotrophic peat. *Organic Geochemistry*, v. 31, p. 1053–1057, doi: 10.1016/S0146-6380(00)00116-9.

Yukon Ecoregions Working Group. (2004a). Klondike Plateau. In *Ecoregions of the Yukon Territory: Biophysical properties of Yukon landscapes,*. (C. A. S. Smith, J. C. Meikle, & C. F. Roots, Eds.). Agriculture and Agri-Food Canada, PARC Technical Bulletin No. 04-01.

Yukon Ecoregions Working Group. (2004b). North Ogilvie Mountains. In *Ecoregions of the Yukon Territory: Biophysical properties of Yukon landscapes,*. (C. R. C. Smirh, J. Meikle, Ed.). Agriculture and Agri-Food Canada, PARC Technical Bulletin No. 04-01.

Yukon Ecoregions Working Group. (2004c). Old Crow Flats. In *Ecoregions of the Yukon Territory: Biophysical properties of Yukon landscapes,*. (C. R. C. Smith, J. Meikle, Ed.). Agriculture and Agri-Food Canada, PARC Technical Bulletin No. 04-01.

Appendix 1: Supporting information for Chapter 3

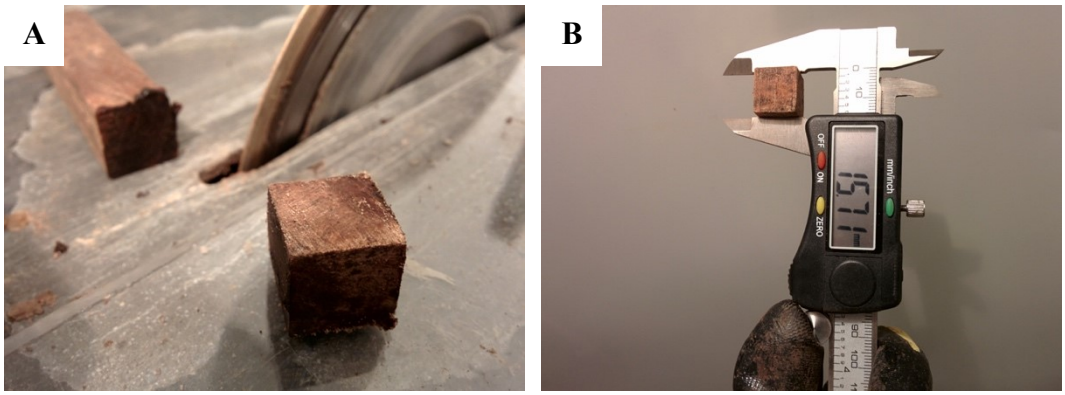

Figure A1.1 Bulk density measurement method. (A) Cuboid subsamples were cut using a diamond-bladed rock saw and (B) their dimensions were measured with a digital caliper (± 0.01 mm) for calculating volume. Subsamples were oven-dried at 80 °C for 24 hours and a digital analytical balance (± 0.0001 g) was used to measure initial (wet) and final (dry) weights of subsamples. Dry bulk density was quantified by dividing the dry weight by wet volume. Subsampling was conducted in a cold-room at -5 °C to prevent thaw. Subsamples taken for density calculation were not used in Hg analyses.

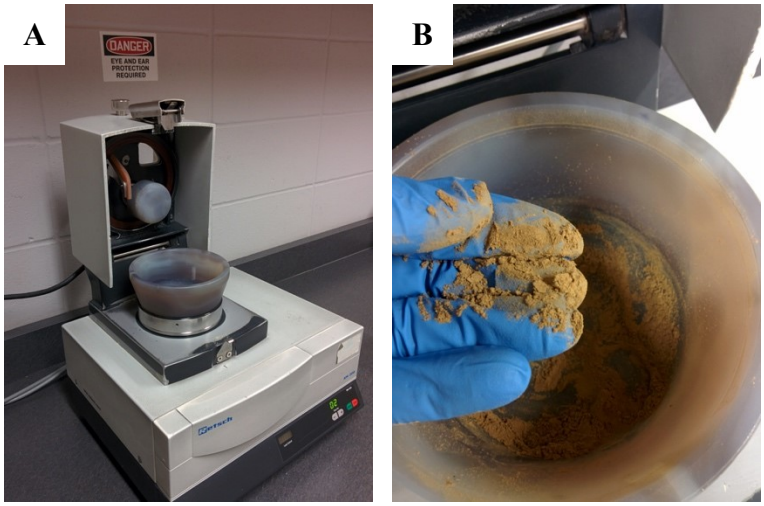

Figure A1.2 Peat homogenization method. (A) A Retsch RM 200 automated agate mortar and pestle was used for homogenizing samples. (B) Freeze-dried samples were individually ground for 2-3 minutes and subsequently brushed into 50 mL centrifuge tubes using a clean nitrile glove. All components of the automated agate mortar and pestle were rinsed with water and thoroughly wiped with paper towels damped with acetone and/or HPLC grade water to prevent cross-contamination.

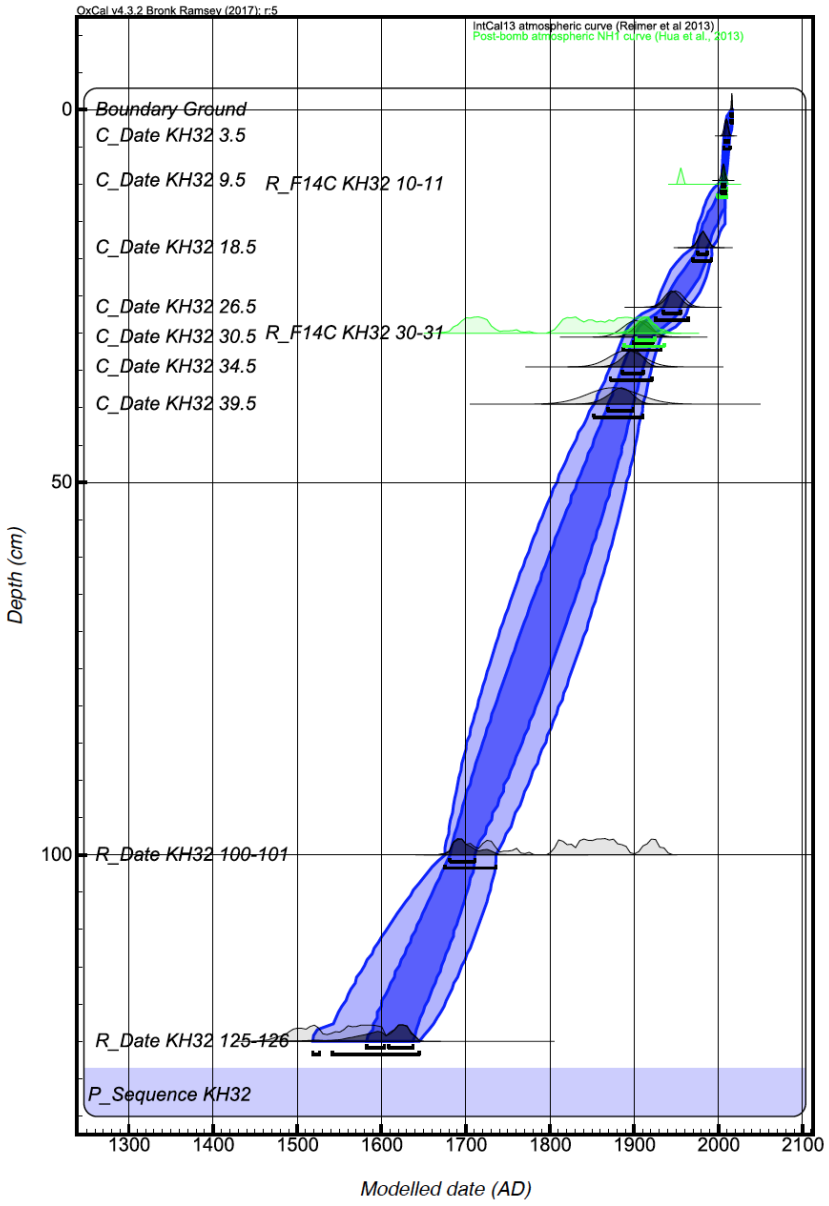

Figure A1.3 Radiocarbon and ^{210}Pb age-depth model for the composite active layer/shallow permafrost core analyzed in our study. This model was produced using the *P_Sequence* function of OxCal v4.2[1]. The IntCal13[2] and Bomb13NH1[3] calibration curves were applied appropriately. Dark blue and light blue areas indicate 68.2 and 95.4% probability age ranges, respectively.

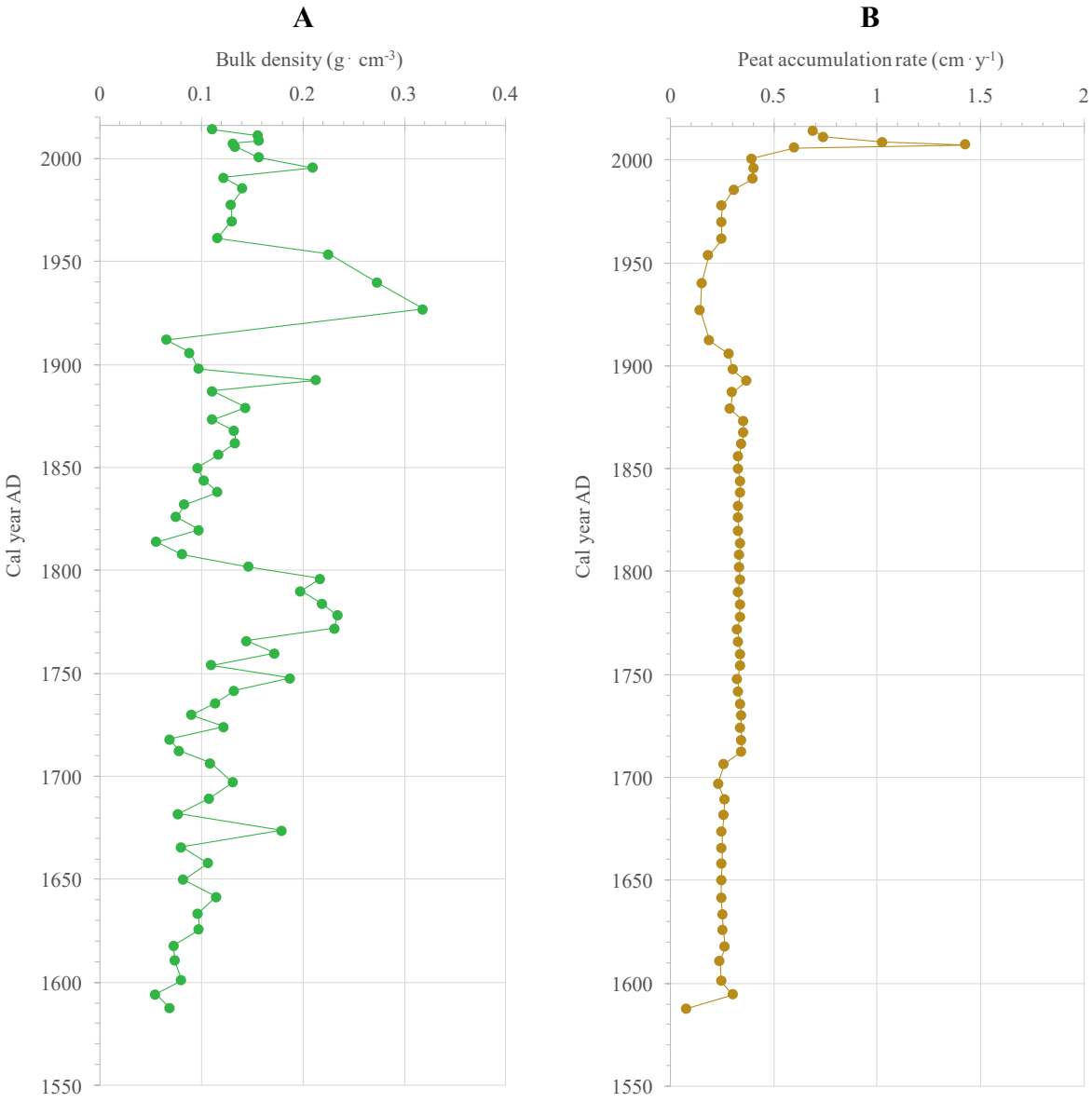

Figure A1.4 (A) bulk density (BD; g·cm^{-3}) and (B) peat accumulation rate (AR; cm·y^{-1}) based on age-depth model from Figure A1.3.

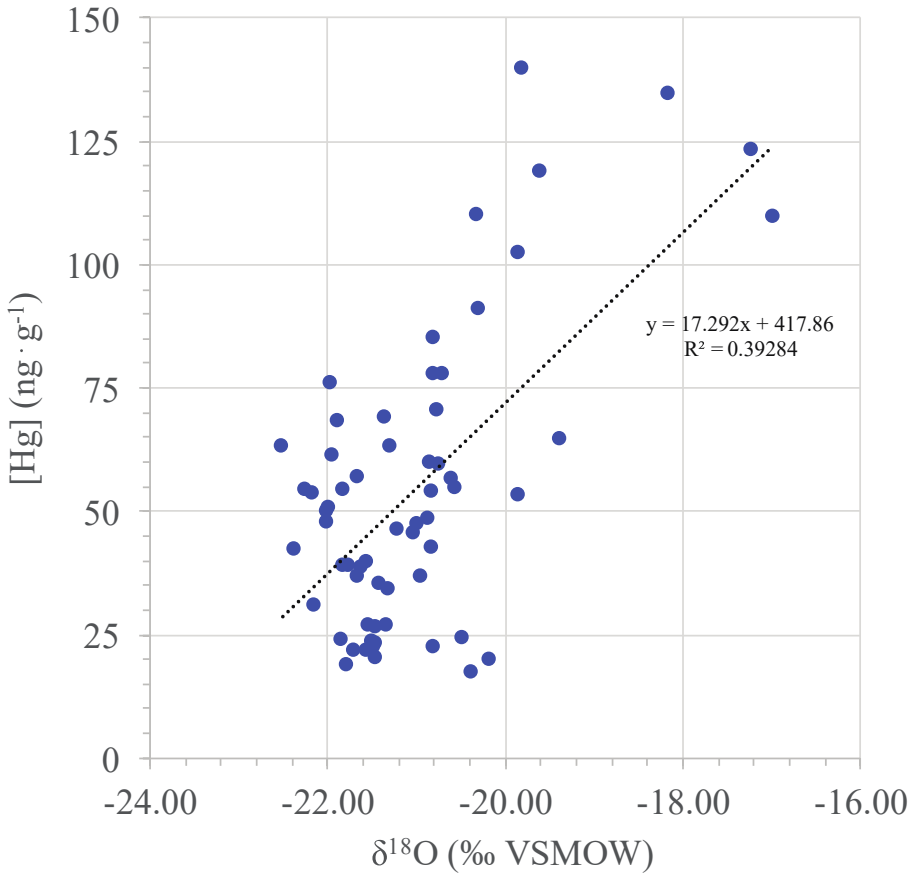

Figure A1.5 Positive correlation between pore-water/ice $\delta^{18}O$ and total Hg concentration from corresponding depths (n = 62; $R^2 = 0.4$).

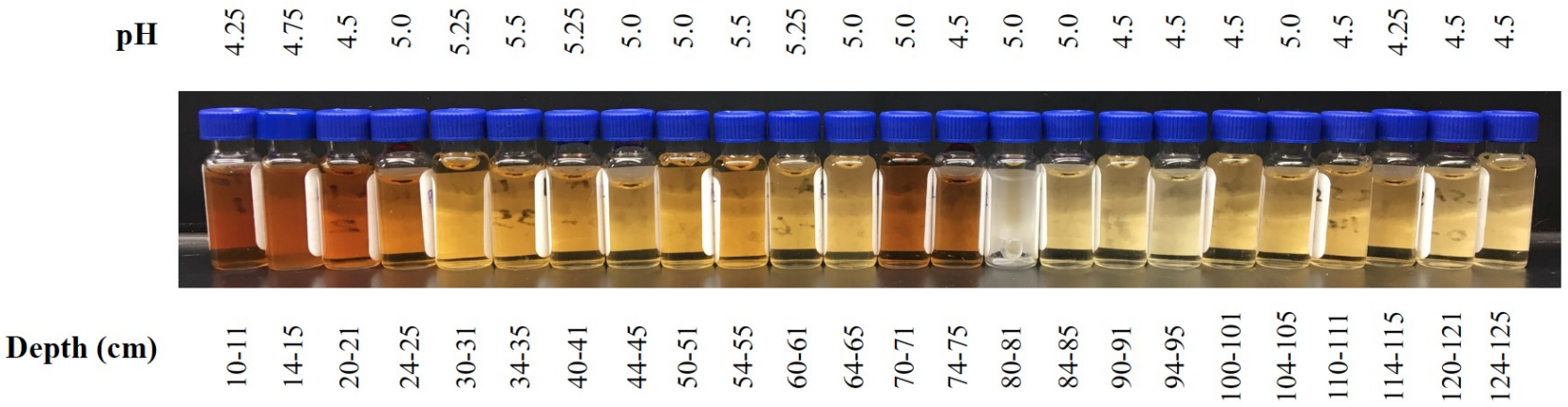

Figure A1.6 Vials containing pore-waters that have been filtered through 0.2 μm nylon membranes. Pore-water pH values range from 4.25 to 5.5 and brown colouration demonstrates the presence of dissolved organic matter.[4,5]

Table A1.1 AMS 14C dates from the André E. Lalonde Laboratory at the University of Ottawa, and ^{210}Pb results (CRS model[6] corroborated by ^{137}Cs and ^{226}Ra) from the Flett Research Ltd. laboratory in Winnipeg, Manitoba, Canada.

	Sample ID	Upper Depth (cm)	Lower Depth (cm)	^{14}C Age (years BP)	1 SD ^{14}C Error (years)	F^{14}C	1 SD F^{14}C Error	Lab ID
^{14}C	KH32 10-11	10	11	Modern	22	1.0551	0.0029	UOC-2658
	KH32 30-31	30	31	90	37	0.9889	0.0045	UOC-2659
	KH32 100-101	100	101	124	22	0.9847	0.0027	UOC-2664
	KH32125-126	125	126	335	22	0.9591	0.0027	UOC-2665
	Sample ID	**Upper Depth (cm)**	**Lower Depth (cm)**	**Total Activity (DPM/g dry wt.)**	**1 SD Activity Error (DPM/g dry wt.)**	**Extrapolated Upper Depth (cm)**	**Unsupported ^{210}Pb Activity (DPM/g dry wt.)**	**CRS Modelled Age at Bottom of Extrapolated Section (years BP)**
^{210}Pb	KH32 0-1	0	1	12.19	0.44	0	11.96	7.2
	KH32 6-7	6	7	2.10	0.20	4	1.87	9.9
	KH32 12-13	12	13	4.94	0.35	10	4.71	33.6
	KH32 24-25	24	25	3.17	0.28	19	2.93	67.1
	KH32 28-29	28	29	1.95	0.24	27	1.72	113.6
	KH32 32-33	32	33	0.79	0.12	31	0.56	124.6
	KH32 36-37	36	37	0.41	0.13	35	0.18	141.1
	KH32 42-43	42	43	0.66	0.11	40	0.43	---
	KH32 48-49	48	49	0.23	0.08	46	0.00	---
	KH32 56-57	56	57	2.81	0.31	53	---	---
	KH32 66-67	66	67	0.21	0.08	62	---	---
	KH32 78-79	78	79	1.08	0.19	73	---	---
	KH32 98-99	98	99	0.30	0.08	89	---	---
	KH32 128-129	128	129	0.13	0.06	114	---	---
^{137}Cs	KH32 16-17	16	17	1.42	0.19	---	---	---
	KH32 18-19	18	19	1.01	0.18	---	---	---
	KH32 20-21	20	21	0.45	0.40	---	---	---
	KH32 22-23	22	23	1.44	0.46	---	---	---
	KH32 26-27	26	27	0.30	0.18	---	---	---
	KH32 38-39	38	39	---	---	---	---	---
^{226}Ra	KH32 56-57	56	57	0.20	0.05	---	---	---
	KH32 76-77	76	77	0.37	0.05	---	---	---

Table A1.2 Cryostratigraphic classification of core segments based on Murton and French (1994).[7]

Core segment ID	Depth range (cm)	Cryofacies	Cryostructures in order of decreasing abundance	Descriptions
KH32 (1)	0-24	Ice-poor peat (monolith)	Structureless	Light brown to brown fibrous peat lacking visible ice. Many (>25) yellow-brown woody macrofossils (2 mm avg. diameter) and dark brown roots scattered throughout
KH32 (2)	24-47	Ice-rich peat	Lenticular (wavy, non-parallel) and structureless	Brown to dark brown ice-rich peat. Some (~10) light brown woody macrofossils (up to 5 mm in diameter) scattered throughout
KH32 (3)	47-78	Ice-rich peat	Structureless and lenticular (wavy, non-parallel)	Orange-brown ice-poor peat from 47-68 cm and dark brown ice-rich peat from 68-78 cm. Many (>25) light brown woody macrofossils (3 mm avg. diameter) scattered throughout. One large (~3.5 cm diameter) tree trunk with ca. 32 tree-rings at 64 cm depth
KH32 (4)	78-105	Ice-rich peat	Lenticular (wavy, non-parallel) and structureless	Dark brown to brown ice-rich peat. Some (~10) light brown woody macrofossils (upto 1 cm long) scattered throughout top half of core segment
KH32 (5)	105-129	Ice-rich peat	Lenticular (wavy, non-parallel)	Brown to orange-brown ice-rich peat. Some black mottles (3 mm avg. diameter) scattered throughout bottom half of core and two (~4 mm diameter) woody macrofossil at 124 and 126 cm depths

Table A1.3 Accuracy and precision of instrument blanks, boat blanks, duplicates, quality controls, and the standard reference material for Hg measurements from DMA-80. MESS-3 (marine sediment, certified value: 91 ± 9 $ng \cdot g^{-1}$).

	Hg Concentration ($ng \cdot g^{-1}$)				Relative standard deviation (%)
	Min	Max	Mean	Standard deviation	
Instrument blank (n=6)	0.0324	0.0623	0.0475	0.0124	26.11
Boat blank total (n=6)	0.0357	0.0656	0.0461	0.0110	23.86
QCSB-DH15 (n=12)	13.1074	14.1946	13.7100	0.3203	2.336
MESS-3 (n=12)	81.8014	89.3468	85.7717	2.0427	2.382

***Duplicate average % difference (*n=11*): 1.54%**

Table A1.4 Compiled geochemical results organized by depth and modelled age.

Sample ID	Upper Depth (cm)	Modelled Age (cal BP)	Modelled Age (cal AD)	Modelled Acc. Rate ($cm \cdot y^{-1}$)	Bulk Density ($g \cdot cm^{-3}$)	Hg Concentration ($ng \cdot g^{-1}$)	Hg Flux ($\mu g \cdot m^{-2} \cdot y^{-1}$)	$\delta^{18}O$ (‰VSMOW)	LOI_{550} (%)
KH32 0-1	0	0	2014	0.69	0.11	64.80	49.59	n/a	92.6
KH32 2-3	2	3	2011	0.74	0.16	88.99	102.95	n/a	75.5
KH32 4-5	4	5	2009	1.03	0.16	96.66	155.20	n/a	54.5
KH32 6-7	6	7	2007	1.43	0.13	109.74	206.18	-16.99	87.4
KH32 8-9	8	8	2006	0.60	0.13	123.33	98.13	-17.23	92.0
KH32 10-11	10	14	2001	0.39	0.16	134.74	82.91	-18.17	94.3
KH32 12-13	12	18	1996	0.40	0.21	139.96	118.69	-19.80	93.9
KH32 14-15	14	23	1991	0.40	0.12	102.70	49.54	-19.86	90.2
KH32 16-17	16	29	1986	0.31	0.14	110.19	47.77	-20.31	91.5
KH32 18-19	18	36	1978	0.25	0.13	91.00	29.45	-20.30	91.0
KH32 20-21	20	45	1970	0.25	0.13	85.42	27.50	-20.82	92.7
KH32 22-23	22	53	1961	0.25	0.12	69.26	19.97	-21.35	90.8
KH32 24-25	24	61	1953	0.18	0.23	77.89	32.38	-20.70	83.1
KH32 26-27	26	74	1940	0.15	0.27	63.28	26.03	-21.31	50.8
KH32 28-29	28	87	1927	0.14	0.32	70.63	32.51	-20.77	32.3
KH32 30-31	30	102	1912	0.19	0.07	59.86	7.45	-20.85	39.0
KH32 32-33	32	108	1906	0.28	0.09	46.50	11.74	-21.22	89.8
KH32 34-35	34	116	1898	0.30	0.10	47.66	14.00	-21.00	86.1
KH32 36-37	36	122	1892	0.37	0.21	54.75	42.80	-20.57	87.0
KH32 38-39	38	127	1887	0.30	0.11	42.67	14.09	-20.84	77.9
KH32 40-41	40	135	1879	0.29	0.14	54.13	22.55	-20.84	92.0
KH32 42-43	42	141	1873	0.35	0.11	63.37	24.75	-22.51	90.3
KH32 44-45	44	146	1868	0.35	0.13	54.47	25.56	-22.26	76.0
KH32 46-47	46	152	1862	0.34	0.13	61.51	28.39	-21.95	92.6
KH32 48-49	48	158	1856	0.33	0.12	42.39	16.38	-22.37	95.4
KH32 50-51	50	164	1850	0.33	0.10	30.87	9.76	-22.14	94.9
KH32 52-53	52	170	1844	0.34	0.10	77.83	27.09	-20.82	94.3
KH32 54-55	54	176	1838	0.34	0.12	118.88	46.48	-19.61	95.6
KH32 56-57	56	182	1832	0.33	0.08	64.82	17.91	-19.38	94.6
KH32 58-59	58	188	1826	0.33	0.08	53.55	13.30	-19.85	93.7
KH32 60-61	60	194	1820	0.33	0.10	48.49	15.73	-20.87	93.4
KH32 62-63	62	200	1814	0.34	0.06	45.73	8.71	-21.04	74.2
KH32 64-65	64	206	1808	0.33	0.08	36.98	10.02	-20.96	83.4
KH32 66-67	66	212	1802	0.33	0.15	27.13	13.26	-21.33	83.2
KH32 68-69	68	218	1796	0.34	0.22	38.70	28.29	-21.62	84.9
KH32 70-71	70	224	1790	0.33	0.20	50.79	32.96	-21.99	85.7
KH32 72-73	72	230	1784	0.34	0.22	47.75	35.23	-22.00	87.4
KH32 74-75	74	236	1778	0.34	0.23	53.70	42.25	-22.18	86.5
KH32 76-77	76	242	1772	0.33	0.23	50.07	37.66	-22.01	84.4
KH32 78-79	78	248	1766	0.33	0.14	56.62	27.01	-20.61	83.8
KH32 80-81	80	254	1760	0.34	0.17	59.59	34.86	-20.75	90.1
KH32 82-83	82	260	1754	0.34	0.11	76.23	28.23	-21.98	69.6
KH32 84-85	84	266	1748	0.33	0.19	68.56	41.87	-21.88	66.5
KH32 86-87	86	272	1742	0.33	0.13	39.02	17.10	-21.82	81.8
KH32 88-89	88	278	1736	0.34	0.11	36.77	14.23	-21.67	82.6
KH32 90-91	90	284	1730	0.34	0.09	54.47	16.86	-21.82	93.8
KH32 92-93	92	290	1724	0.34	0.12	57.00	23.71	-21.67	93.2
KH32 94-95	94	296	1718	0.34	0.07	39.22	9.35	-21.77	96.1
KH32 96-97	96	302	1712	0.34	0.08	24.24	6.53	-21.84	96.2
KH32 98-99	98	308	1706	0.26	0.11	26.86	7.62	-21.55	96.1
KH32 100-101	100	317	1697	0.23	0.13	35.34	10.77	-21.42	93.9
KH32 102-103	102	325	1689	0.26	0.11	34.37	9.73	-21.31	94.0
KH32 104-105	104	332	1682	0.26	0.08	22.52	4.52	-21.48	96.5
KH32 106-107	106	340	1674	0.25	0.18	39.69	17.78	-21.56	95.3
KH32 108-109	108	348	1666	0.25	0.08	19.06	3.85	-21.78	95.4
KH32 110-111	110	356	1658	0.25	0.11	21.89	5.83	-21.70	95.5
KH32 112-113	112	364	1650	0.25	0.08	23.51	4.80	-21.47	95.8
KH32 114-115	114	372	1642	0.25	0.11	21.80	6.18	-21.56	96.3
KH32 116-117	116	381	1634	0.25	0.10	23.68	5.79	-21.50	95.7
KH32 118-119	118	388	1626	0.25	0.10	20.34	5.07	-21.45	96.0
KH32 120-121	120	396	1618	0.26	0.07	26.82	5.16	-21.46	95.8
KH32 122-123	122	404	1611	0.24	0.07	22.79	4.00	-20.82	96.1
KH32 124-125	124	413	1601	0.25	0.08	24.51	4.89	-20.48	96.4
KH32 126-127	126	420	1594	0.30	0.06	17.53	2.92	-20.39	95.7
KH32 128-129	128	426	1588	0.08	0.07	20.03	1.10	-20.17	94.6

Loss on ignition method. Loss on ignition at 550°C was determined similarly to methods outlined in Heiri et al. (2001).[8] In summary, ~1-2 cm^3 of peat was extracted from each depth of interest, oven-dried at 100°C for 24 hours in pre-weighed crucibles, and combusted in a muffle furnace at 550°C for 4 hours. Sample weights were recorded after oven-drying and combusting; LOI (%) was then calculated using the following equation:

$$LOI_{550} = ((DW_{100}-DW_{550})/(DW_{100}))*100$$

where DW_{100} is sample weight following 24 hours of oven-drying at 100°C and DW_{550} is sample weight following 4 hours of combustion at 550°C.

References

(1) Bronk Ramsey, C. Bayesian Analysis of Radiocarbon Dates. *Radiocarbon* **2009**, *51* (1), 337–360.

(2) Reimer, P. J.; Bard, E.; Bayliss, A.; Beck, J. W.; Blackwell, P. G.; Bronk, M.; Grootes, P. M.; Guilderson, T. P.; Haflidason, H.; Hajdas; et al. IntCal 13 and Marine 13 radiocarbon age calibration curves 0–50,000 years cal BP. *Radiocarbon* **2013**, *55*, 1869–1887.

(3) Hua, Q.; Barbetti, M.; Rakowski, a Z. Atmospheric radiocarbon for the period 1950-2010. *Radiocarbon* **2013**, *55* (4), 2059–2072.

(4) Harvey, E. T.; Kratzer, S.; Andersson, A. Relationships between colored dissolved organic matter and dissolved organic carbon in different coastal gradients of the Baltic Sea. *Ambio* **2015**, *44* (3), 392–401.

(5) Green, S. A.; Blough, N. V. Optical absorption and fluorescence properties of chromophoric dissolved organic matter in natural waters. *Limnol. Oceanogr.* **1994**, *39* (8), 1903–1916.

(6) Appleby, P. G.; Oldfield, F. The calculation of lead-210 dates assuming a constant rate of supply of unsupported 210Pb to the sediment. *Catena* **1978**, *5* (1), 1–8.

(7) Murton, J. B.; French, H. M. Cryostructures in permafrost, Tuktoyaktuk coastlands, western arctic Canada. *Can. J. Earth Sci.* **1994**, *31* (4), 737–747.

(8) Heiri, O.; Lotter, A. F.; Lemcke, G. Loss on ignition as a method for estimating organic and carbonate content in sediments: reproducibility and comparability of results. *J. Paleolimnol.* **2001**, *25* (1), 101–110.

Appendix 2: Supporting information for Chapter 4

DHP170
N65°10.497' W138°21.663'

DHP174
N65°12.647' W138°19.588'

OCP9
N67°56.380' W139°40.107'

OCP11
N68°00.507' W139°37.670'

OCP14
N67°55.497' W139°36.400'

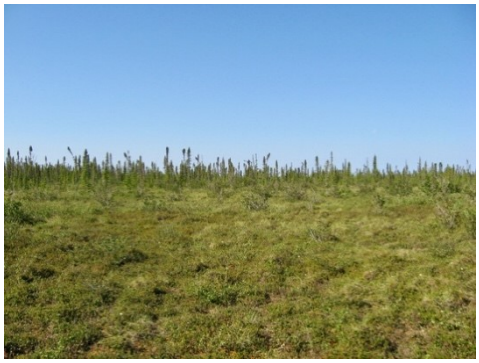

BFP16
N67°28.871' W139°54.005'

BFP19
N67°26.055' W139°36.320'

Figure A2.1 Coring location details and images from each of the seven study sites.

Bayesian age-depth models. Radiocarbon dates were calibrated using OxCal v4.2.[1] and the IntCal13[2] calibration curve. Age-depth models were produced using the *P_Sequence* function of OxCal v4.2[1]. Dark blue and light blue areas indicate 68.2 and 95.4% probability age ranges, respectively.

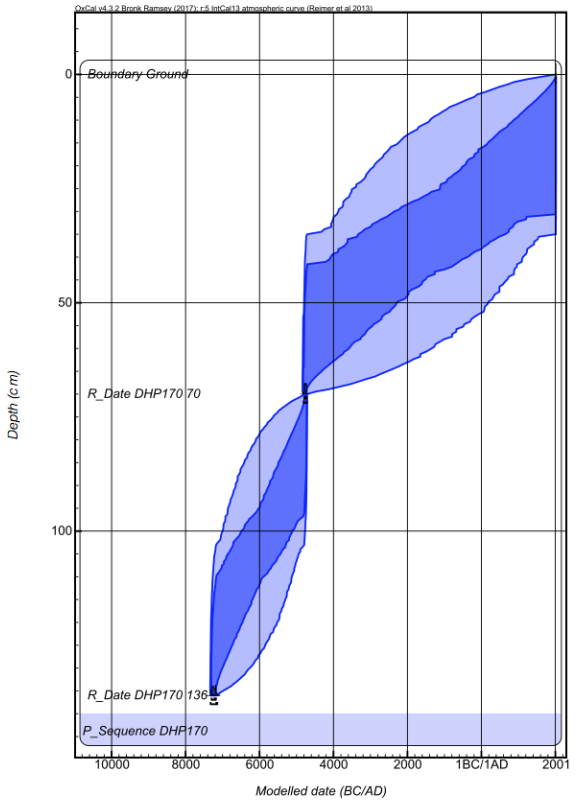

DHP170

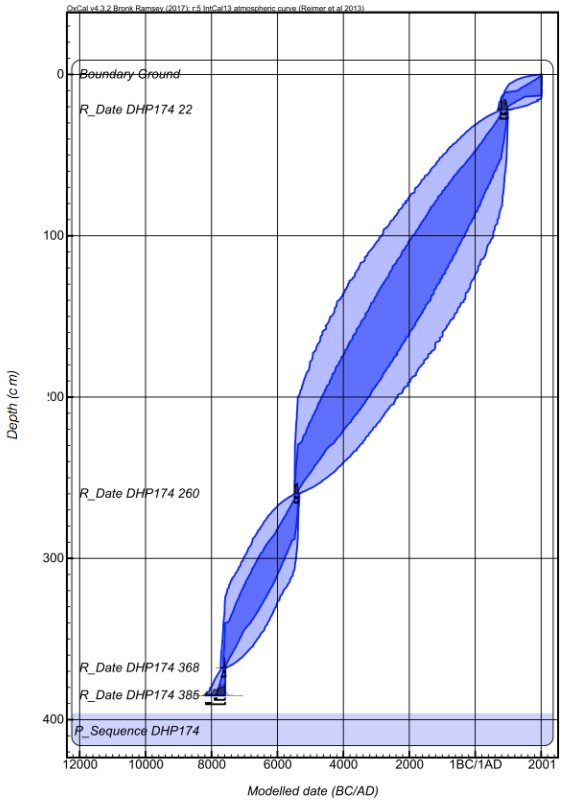

DHP174

Bayesian age-depth models *(continued)*.

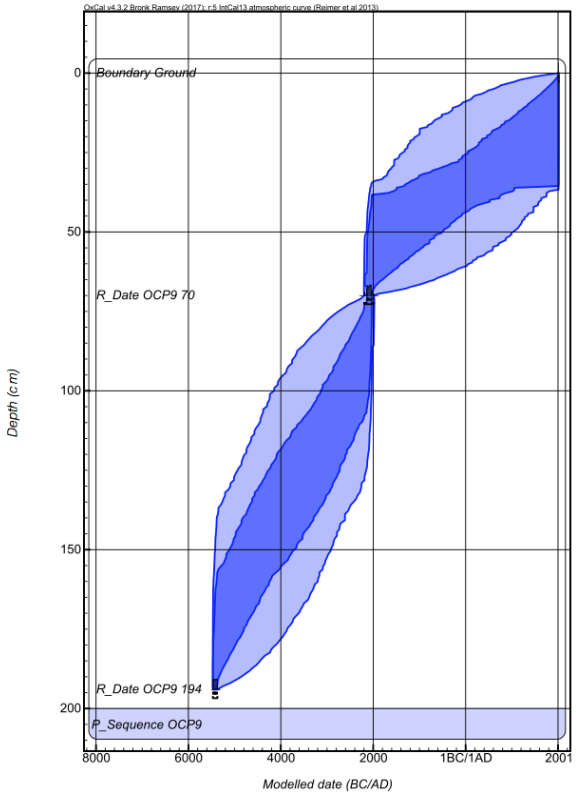

OCP9

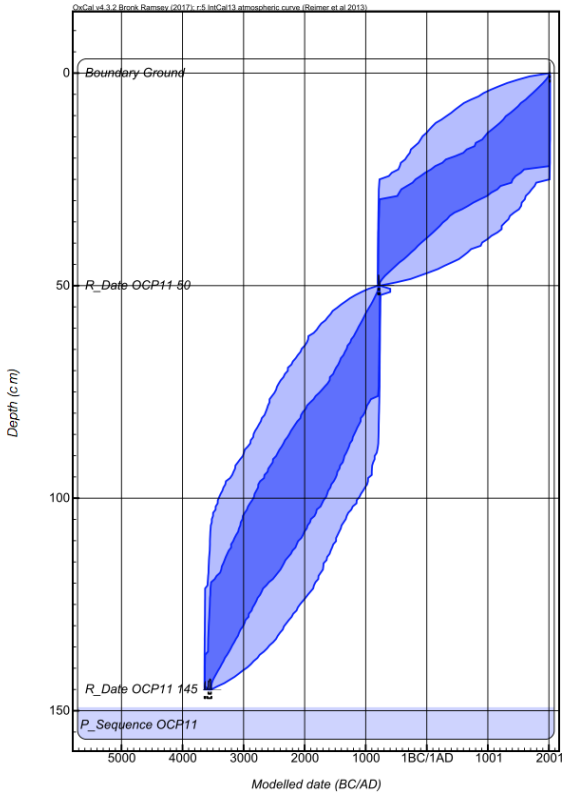

OCP11

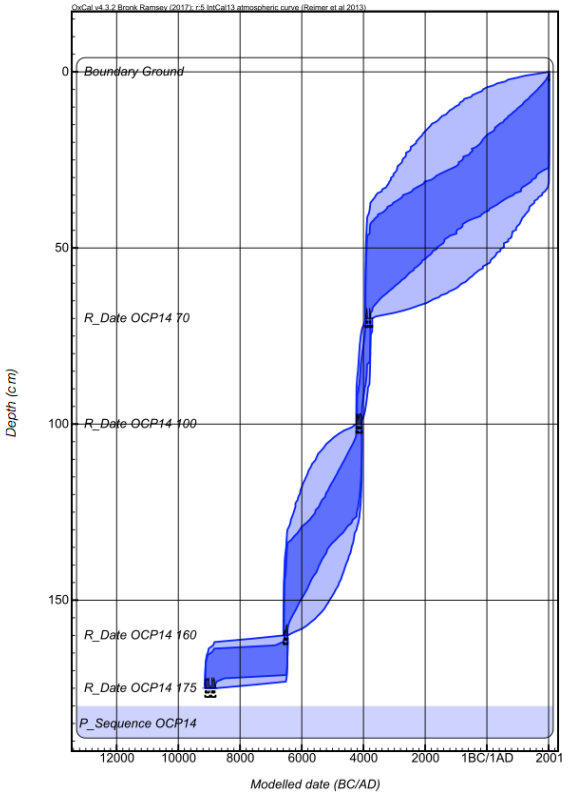

OCP14

Bayesian age-depth models *(continued)*.

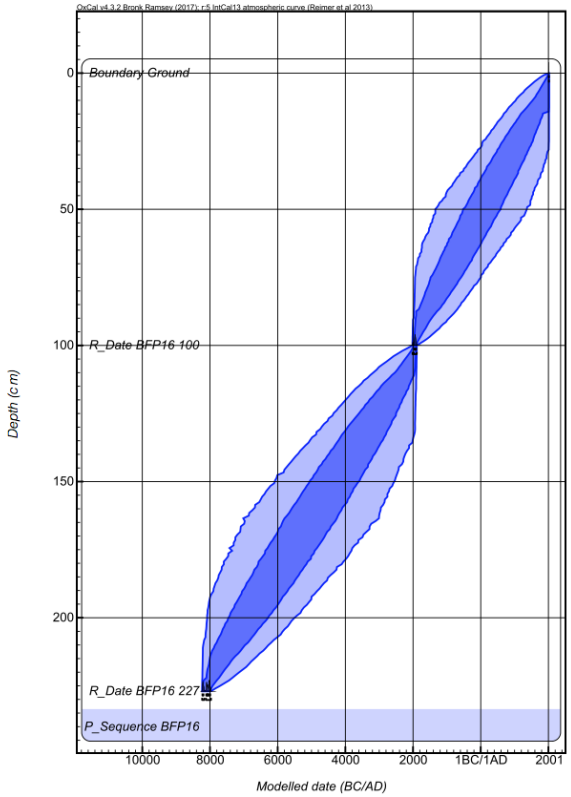

BFP16

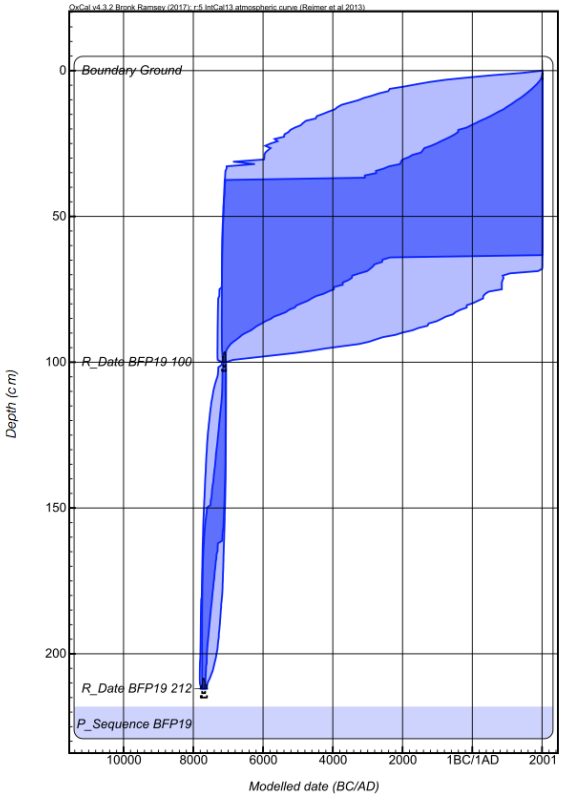

BFP19

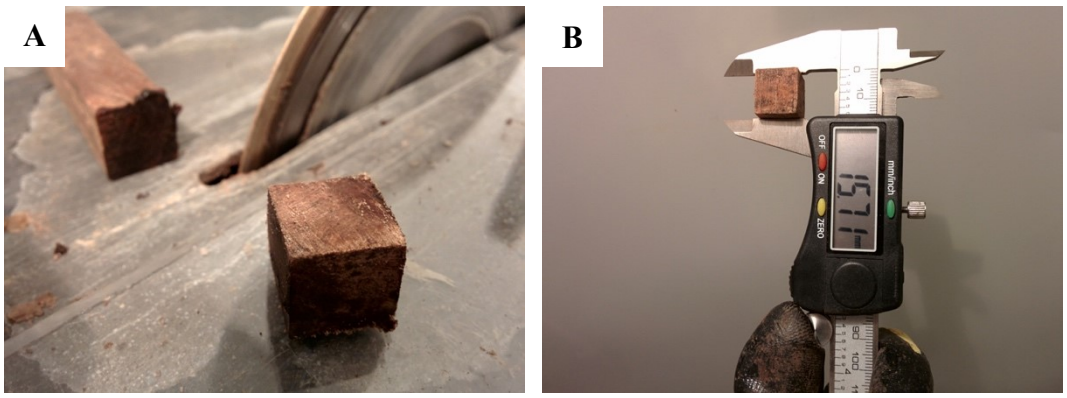

Figure A2.2 Bulk density measurement method. (A) Cuboid subsamples were cut using a diamond-bladed rock saw and (B) their dimensions were measured with a digital caliper (± 0.01 mm) for calculating volume. Subsamples were oven-dried at 80 °C for 24 hours and a digital analytical balance (± 0.0001 g) was used to measure initial (wet) and final (dry) weights of subsamples. Dry bulk density was quantified by dividing the dry weight by wet volume. Subsampling was conducted in a cold-room at -5 °C to prevent thaw. Subsamples taken for density calculation were not used in Hg analyses.

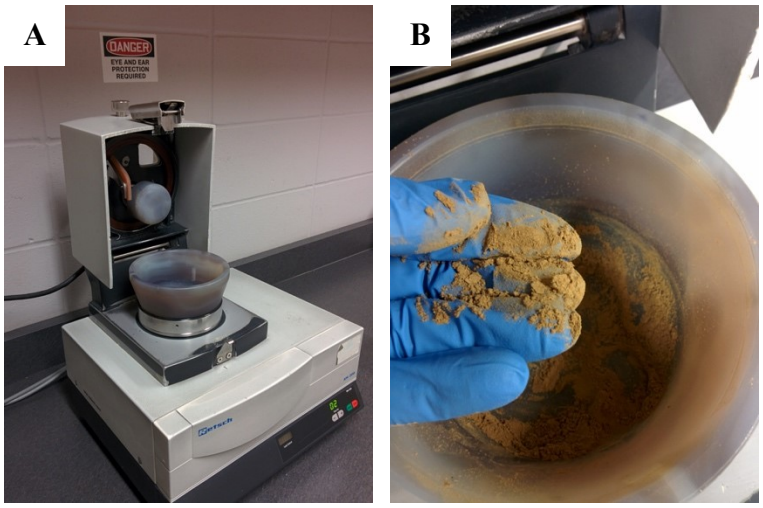

Figure A2.3 Peat homogenization method. (A) A Retsch RM 200 automated agate mortar and pestle was used for homogenizing samples. (B) Freeze-dried samples were individually ground for 2-3 minutes and subsequently brushed into 50 mL centrifuge tubes using a clean nitrile glove. All components of the automated agate mortar and pestle were rinsed with water and thoroughly wiped with paper towels damped with acetone and/or HPLC grade water to prevent cross-contamination.

Table A2.1 Field notes and cryostratigraphic classification of core segments based on Murton and French (1994).[3]

Site (thaw depth; collection date)	Core segment ID	Depth range (cm)	Cryofacies	Cryostructures in order of decreasing abundance	Descriptions
DHP170 (31 cm; June 26, 2015)	**DHP170 (1)**	0-31	Ice-poor peat (monolith)	Structureless	Dark brown fibrous peat lacking visible ice. Light brown woody macrofossils and roots scattered throughout
	DHP170 (2)	31-68	Ice-rich peat	Lenticular (wavy, non-parallel) and structureless	Brown to dark brown ice-rich peat
	DHP170 (3)	68-102	Ice-rich peat	Lenticular (wavy, non-parallel) and structureless	Brown to dark brown ice-rich peat with some (~2 mm diameter) brown woody macrofossils scattered throughout
	DHP170 (4)	102-134	Ice-rich peat	Lenticular (wavy, non-parallel) and structureless	Brown to dark brown ice-rich peat with some (up to 5 mm long) brown woody macrofossils scattered throughout
	DHP170 (5)	134-163	Ice-rich peat	Structureless and lenticular (wavy, non-parallel)	Dark brown ice-rich peat with some (~2 mm diameter) woody macrofossils scattered throughout
DHP174 (16 cm; June 9, 2013)	**DHP174 (1)**	0-16	Ice-poor peat (monolith)	Structureless	Orange-brown fibrous peat lacking visible ice
	DHP174 (2)	16-39	Ice-rich peat	Lenticular (wavy, non-parallel)	Orange-brown ice-rich peat with few small (~2 mm diameter) light brown woody macrofossils at base
	DHP174 (3)	39-76	Ice-rich peat	Lenticular (wavy, non-parallel) and layered (wavy, parallel)	Orange-brown ice-rich peat with black-brown peat layers (cms thick). Light brown woody macrofossils (up to 5 mm long)
	DHP174 (4)	76-108	Ice-rich peat	Lenticular (wavy, non-parallel)	Orange-brown to brown ice-rich peat with a few woody macrofossils (~5 mm diameter) scattered throughout
	DHP174 (5)	108-144	Ice-rich peat	Lenticular (wavy, parallel and non-parallel)	Black-brown to orange-brown ice-rich peat with a few woody macrofossils (up to 1.5 cm long)
	DHP174 (6)	144-169	Ice-rich peat	Lenticular (wavy, non-parallel) and structureless	Black-brown to orange-brown ice-rich peat with a large (4 cm diameter) fractured wood at depth
	DHP174 (7)	169-206	Ice-rich peat	Lenticular (wavy, parallel and non-parallel)	Orange-brown ice-rich peat with a few small (~2 mm diameter) light brown woody macrofossils scattered throughout
	DHP174 (8)	206-228	Ice-rich peat	Lenticular (wavy, parallel and non-parallel)	Orange-brown ice-rich peat with some small (~2 mm diameter) light brown woody macrofossils scattered throughout
	DHP174 (9)	228-245	Ice-rich peat	Lenticular (wavy, non-parallel)	Orange-brown ice-rich peat with black-brown peat layers. Some small (~2 mm diameter) woody macrofossils throughout
	DHP174 (10)	245-266	Ice-rich peat	Lenticular (wavy, non-parallel)	Orange-brown ice-rich peat with large woody macrofossil (~5 mm thick) diagonally crossing core segment at depth
	DHP174 (11)	266-298	Ice-rich peat	Lenticular (wavy, non-parallel) and layered	Black-brown to orange-brown ice-rich peat with a few woody macrofossils (<5 mm diameter) throughout. Ice lens at depth
	DHP174 (12)	298-320	Ice-rich peat	Lenticular (wavy, non-parallel)	Black-brown to orange-brown ice-rich peat with a few woody macrofossils (<5 mm diameter) scattered throughout
	DHP174 (13)	320-348	Ice-rich peat	Lenticular (wavy, non-parallel)	Black-brown to orange-brown ice-rich peat with thin light brown woody macrofossils (up to 5 mm long) scattered throughout
	DHP174 (14)	348-385	Ice-rich peat	Lenticular (wavy, non-parallel)	Orange-brown ice-rich peat with thin light brown woody macrofossils (up to 5 mm long) scattered throughout
OCP9 (36 cm; July 4, 2015)	**OCP9 (1)**	0-36	Ice-poor peat (monolith)	Structureless and lenticular (wavy, non-parallel)	Dark brown to brown fibrous peat lacking visible ice. Light brown woody macrofossils and roots near top
	OCP9 (2)	36-66	Ice-rich peat	Structureless and lenticular (wavy, non-parallel)	Dark brown to brown ice-rich peat with some small (<2 mm long) light brown woody macrofossils scattered throughout
	OCP9 (3)	66-93	Ice-rich peat	Structureless and lenticular (wavy, non-parallel)	Dark brown to brown ice-rich peat with many brown woody macrofossils (up to 1 cm diameter) scattered throughout
	OCP9 (4)	93-119	Ice-rich peat	Lenticular (wavy, non-parallel) and structureless	Brown to dark brown ice-rich peat with a few woody macrofossils (up to 5 mm diameter) in top half of core segment
	OCP9 (5)	119-146	Ice-rich peat	Lenticular (wavy, non-parallel) and structureless	Brown to orange-brown ice-rich peat with a few small (<2 mm long) woody macrofossils scattered throughout
	OCP9 (6)	146-168	Ice-rich peat	lenticular (wavy, non-parallel) and structureless	Brown to dark brown ice-rich peat with some small (~2 mm diameter) woody macrofossils at depth
	OCP9 (7)	168-193	Ice-rich peat	Structureless and lenticular (wavy, non-parallel)	Dark brown ice-rich peat with many woody macrofossils (~5 mm diameter) scattered throughout
	OCP9 (8)	193-229	Ice-rich peat and ice-rich mud	Lenticular (wavy, non-parallel) and layered (planar, parallel)	Dark brown ice-rich peat transitioning to grey ice-rich silt near top of core segment. Primarily grey ice-rich silt throughout
	OCP9 (9)	229-240	Ice-rich mud	Lenticular (wavy, non-parallel) and suspended	Grey to dark-grey ice-rich silt

Table A2.1 Field notes and cryostratigraphic classification of core segments based on Murton and French (1994)[3] *(continued).*

Site (thaw depth; collection date)	Core Segment ID	Depth range (cm)	Cryofacies	Cryostructures in order of decreasing abundance	Descriptions
OCP11 (22 cm; July 5, 2015)	**OCP11 (1)**	0-22	Ice-poor peat (monolith)	Structureless	Brown fibrous peat lacking visible ice. Light brown woody macrofossils (~3 mm diameter) scattered throughout
	OCP11 (2)	22-57	Ice-rich peat	Structureless and lenticular (wavy, non-parallel)	Orange-brown to dark brown ice-rich peat with some small (~2 mm diameter) woody macrofossils scattered throughout
	OCP11 (3)	57-91	Ice-rich peat	Lenticular (wavy, non-parallel)	Orange-brown to brown ice-rich peat with some small (~2 mm diameter) woody macrofossils scattered throughout
	OCP11 (4)	91-122	Ice-rich peat	lenticular (wavy, non-parallel)	Brown ice-rich peat with some large (up to 2 cm long) woody macrofossils in bottom half of core segment
	OCP11 (5)	122-152	Ice-rich peat	Lenticular (wavy, non-parallel) and structureless	Brown to dark-brown ice-rich peat with some woody macrofossils throughout. Thin layer of grey silt at base of core segment
	OCP11 (6)	152-189	Ice-rich mud	Lenticular (wavy, non-parallel) and suspended	Grey to dark grey ice-rich silt
OCP14 (40 cm; July 5, 2015)	**OCP14 (1)**	0-40	Ice-poor peat (monolith)	Structureless	Dark brown peat lacking visible ice. Some light brown woody macrofossils and roots near top of core segment
	OCP14 (2)	40-71	Ice-rich peat	Lenticular (wavy, non-parallel)	Orange-brown to dark brown ice-rich peat with some (~4 mm diameter) woody macrofossils in top half of core segment
	OCP14 (3)	71-107	Ice-rich peat	Lenticular (wavy, non-parallel)	Brown to dark brown ice-rich peat with large (~6 cm diameter) light-brown fractured wood at middle of core segment
	OCP14 (4)	107-139	Ice-rich peat	Lenticular (wavy, non-parallel)	Brown ice-rich peat with small (~4 mm long) woody macrofossils scattered throughout bottom half of core segment
	OCP14 (5)	139-175	Ice-rich peat and ice-rich mud	Structureless, lenticular (wavy, non-parallel), and layered (wavy, parallel)	Dark brown ice-rich peat with large (>2 cm long) woody macrofossils in top half of core segment and grey ice-rich silt at depth
	OCP14 (6)	175-208	Muddy ice-rich peat and ice-rich mud	Lenticular (wavy, non-parallel) and layered (wavy, parallel)	Primarily grey ice-rich silt with some dark brown muddy ice-rich peat spanning mid-section of core segment
	OCP14 (7)	208-235	Ice-rich mud	Layered (wavy, parallel) and suspended	Grey to dark grey ice-rich silt
BFP16 (44 cm; July 6, 2015)	**BFP16 (1)**	0-44	Ice-poor peat (monolith)	Structureless	Dark brown peat lacking visible ice. Some light brown woody macrofossils and roots near top of core segment
	BFP16 (2)	44-80	Ice-rich peat	Structureless and lenticular (wavy, non-parallel)	Orange-brown ice-rich peat with black-brown (~5 mm diameter) mottles scattered throughout
	BFP16 (3)	80-115	Ice-rich peat	Structureless and lenticular (wavy, non-parallel)	Brown ice-rich peat with a few light brown woody macrofossils (up to 2 cm long) scattered throughout
	BFP16 (4)	115-151	Ice-rich peat	Lenticular (wavy, non-parallel)	Orange-brown ice-rich peat with some thin brown (~1 cm long) woody macrofossils scattered throughout
	BFP16 (5)	151-181	Ice-rich peat and ice-rich mud	Lenticular (wavy, non-parallel) and suspended	Brown ice-rich peat in top half of core segment and brown-grey ice-rich silt at depth with some (~5 mm long) woody macrofossils
	BFP16 (6)	181-218	Ice-rich mud	Layered (wavy, parallel) and suspended	Brown-grey ice-rich silt with some (~5 mm long) woody macrofossils in top half of core segment
	BFP16 (7)	218-254	Ice-rich mud	Layered and lenticular (wavy, parallel)	Brown-grey ice-rich silt with a (~5 mm long) woody macrofossil near top of core segment
BFP19 (34 cm; July 6, 2015)	**BFP19 (1)**	0-34	Ice-poor peat (monolith)	Structureless	Brown peat lacking visible ice. Some light brown woody macrofossils (up to 1 cm long) near top of core segment
	BFP19 (2)	34-68	Ice-rich peat	Lenticular (wavy, non-parallel)	Orange-brown ice-rich peat with a few small (~2 mm diameter) light brown woody macrofossils in mid-section of core
	BFP19 (3)	68-94	Ice-rich peat	Lenticular (wavy, non-parallel) and structureless	Orange-brown ice-rich peat transitioning to dark brown ice-rich peat near the base of the core segment
	BFP19 (4)	94-131	Ice-rich peat	Structureless	Dark brown ice-rich peat with many small (~2 mm diameter) woody macrofossils scattered throughout
	BFP19 (5)	131-166	Muddy ice-rich peat	Structureless	Grey-brown muddy ice-rich peat with some woody macrofossils (up to 1 cm long) scattered throughout
	BFP19 (6)	166-189	Muddy ice-rich peat	Structureless	Grey-brown muddy ice-rich peat with some small (~2 mm diameter) woody macrofossils scattered throughout
	BFP19 (7)	189-209	Muddy ice-rich peat	Structureless	Grey-brown muddy ice-rich peat with some woody macrofossils (up to 5 mm long) scattered throughout
	BFP19 (8)	209-234	Muddy ice-rich peat and mud-rich ice	Structureless and suspended	Primarily grey silt-rich ice with some grey-brown muddy ice-rich peat near the top of the core segment

Table A2.2 AMS 14C data from acid-base-acid pretreated terrestrial plant macrofossils.

Site	Sample ID	Depth (cm)	^{14}C Age (years BP)	1 SD ^{14}C Error (years)	F^{14}C	1 SD F^{14}C Error	Lab ID
DHP170	DHP170 70	70	5900	15	0.4798	0.0009	UCIAMS-167494
	DHP170 136	136	8215	15	0.3595	0.0007	UCIAMS-163405
DHP174	DHP174 22	22	1165	45	0.8650	0.0046	UCIAMS-142067
	DHP174 260	260	6445	25	0.4484	0.0012	UCIAMS-131060
	DHP174 368	368	8610	30	0.3424	0.0011	UCIAMS-142072
	DHP174 385	385	8670	120	0.3399	0.0051	UCIAMS-131061
OCP9	OCP9 70	70	3700	25	0.6308	0.0016	UCIAMS-167491
	OCP9 194	194	6435	15	0.4489	0.0008	UCIAMS-163407
OCP11	OCP11 50	50	2565	15	0.7268	0.0012	UCIAMS-167492
	OCP11 145	145	4785	15	0.5512	0.0009	UCIAMS-163410
OCP14	OCP14 70	70	5025	15	0.5351	0.0010	UCIAMS-167498
	OCP14 100	100	5310	15	0.5163	0.0010	UCIAMS-167497
	OCP14 160	160	7675	20	0.3846	0.0008	UCIAMS-167496
	OCP14 175	175	9565	20	0.3040	0.0007	UCIAMS-163412
BFP16	BFP16 100	100	3590	15	0.6397	0.0011	UCIAMS-167485
	BFP16 1227	227	8920	20	0.3295	0.0007	UCIAMS-163413
BFP19	BFP19 100	100	8145	20	0.3627	0.0008	UCIAMS-167493
	BFP19 212	212	8715	20	0.3379	0.0008	UCIAMS-163414

Table A2.3 Accuracy and precision of instrument blanks, boat blanks, duplicates, quality controls, and the standard reference material for Hg measurements from DMA-80. MESS-3 (marine sediment, certified value: 91 ± 9 $ng \cdot g^{-1}$).

	Hg Concentration ($ng \cdot g^{-1}$)				Relative standard deviation (%)
	Min	Max	Mean	Standard deviation	
Instrument blank (n=6)	0.0324	0.0623	0.0475	0.0124	26.11
Boat blank total (n=6)	0.0357	0.0656	0.0461	0.0110	23.86
QCSB-DH15 (n=12)	13.1074	14.1946	13.7100	0.3203	2.336
MESS-3 (n=12)	81.8014	89.3468	85.7717	2.0427	2.382

***Duplicate average % difference (*n=11*): 1.54%**

Table A2.4 Modelled age, modelled accumulation rate (AR), bulk density (BD), Hg concentration, and Hg flux results organized by site and sample ID.

Site	Sample ID	Upper Depth (cm)	Modelled Age (cal BP)	Modelled Acc. Rate ($cm \cdot y^{-1}$)	Bulk Density ($g \cdot cm^{-3}$)	Hg Concentration ($ng \cdot g^{-1}$)	Hg Flux ($\mu g \cdot m^{-2} \cdot y^{-1}$)
DHP170	DHP170 30	30	2970	0.01	0.22	55.16	1.28
	DHP170 39	39	3770	0.01	0.18	16.89	0.35
	DHP170 49	49	4650	0.01	0.09	20.10	0.20
	DHP170 59	59	5530	0.01	0.09	49.04	0.42
	DHP170 69	69	6710	0.01	0.05	21.64	0.14
	DHP170 79	79	7165	0.03	0.12	20.68	0.63
	DHP170 89	89	7510	0.03	0.11	28.18	0.89
	DHP170 99	99	7850	0.03	0.09	18.47	0.50
	DHP170 109	109	8190	0.03	0.08	15.40	0.35
	DHP170 119	119	8530	0.03	0.14	26.94	1.08
	DHP170 129	129	8880	0.02	0.08	40.57	0.69
	DHP170 139	139	9460	0.02	0.12	41.61	0.80
	DHP170 149	149	10140	0.01	0.08	38.67	0.46
	DHP170 159	159	10820	0.01	0.08	16.06	0.19
DHP174	DHP174 26	26	1185	0.03	0.07	28.80	0.54
	DHP174 46	46	1710	0.04	0.07	14.40	0.38
	DHP174 66	66	2240	0.04	0.10	24.00	0.91
	DHP174 86	86	2770	0.04	0.07	7.50	0.20
	DHP174 106	106	3300	0.04	0.07	15.00	0.40
	DHP174 126	126	3825	0.04	0.07	22.50	0.60
	DHP174 146	146	4355	0.04	0.07	42.40	1.12
	DHP174 166	166	4885	0.04	0.07	18.10	0.48
	DHP174 186	186	5410	0.04	0.07	8.00	0.21
	DHP174 206	206	5940	0.04	0.07	20.80	0.55
	DHP174 226	226	6470	0.04	0.07	14.90	0.40
	DHP174 246	246	6995	0.04	0.07	32.40	0.89
	DHP174 266	266	7490	0.04	0.07	28.00	0.87
	DHP174 286	286	7895	0.05	0.07	39.00	1.34
	DHP174 306	306	8300	0.05	0.04	19.50	0.38
	DHP174 326	326	8705	0.05	0.07	20.40	0.70
	DHP174 346	346	9115	0.05	0.07	11.50	0.40
	DHP174 366	366	9520	0.06	0.06	14.50	0.52
	DHP174 382	382	9710	0.04	0.07	22.20	0.60
OCP9	OCP9 29	29	1730	0.02	0.15	28.16	0.84
	OCP9 39	39	2240	0.02	0.21	40.07	1.64
	OCP9 49	49	2750	0.02	0.18	42.80	1.49
	OCP9 59	59	3280	0.02	0.09	20.81	0.29
	OCP9 69	69	4040	0.02	0.10	21.31	0.38
	OCP9 79	79	4400	0.03	0.09	18.29	0.54
	OCP9 89	89	4650	0.04	0.10	21.52	0.84
	OCP9 99	99	4900	0.04	0.10	17.72	0.75
	OCP9 109	109	5150	0.04	0.14	23.61	1.34
	OCP9 119	119	5400	**---**	0.15	**---**	**---**
	OCP9 129	129	5650	---	0.09	---	---
	OCP9 139	139	5905	**---**	0.09	**---**	**---**
	OCP9 149	149	6160	0.04	0.07	12.54	0.35
	OCP9 159	159	6410	0.04	0.10	22.89	0.90
	OCP9 169	169	6655	0.04	0.11	28.44	1.31
	OCP9 179	179	6905	0.04	0.14	29.99	1.57
	OCP9 189	189	7180	0.03	0.12	28.71	1.00
	OCP9 199	199	7590	0.02	0.51	79.00	10.08
	OCP9 209	209	7980	0.03	0.62	78.61	12.66
	OCP9 219	219	8365	0.03	0.37	85.36	8.34
	OCP9 229	229	8750	---	0.39	---	---
	OCP9 239	239	9130	0.03	0.50	92.85	12.08
OCP11	OCP11 22	22	1240	0.02	0.15	53.75	1.50
	OCP11 29	29	1570	0.02	0.15	32.04	1.01
	OCP11 39	39	2065	0.02	0.21	38.67	1.39
	OCP11 49	49	2730	0.02	0.15	29.67	0.87
	OCP11 59	59	3095	0.03	0.09	12.16	0.36
	OCP11 69	69	3370	0.04	0.06	8.52	0.17
	OCP11 79	79	3640	0.04	0.06	9.06	0.20
	OCP11 89	89	3920	0.04	0.05	8.59	0.17
	OCP11 99	99	4195	0.04	0.07	7.63	0.19
	OCP11 109	109	4470	0.04	0.07	16.92	0.40
	OCP11 119	119	4745	0.04	0.05	11.09	0.22
	OCP11 129	129	5020	0.04	0.09	10.46	0.32
	OCP11 139	139	5300	0.03	0.09	11.50	0.30
	OCP11 149	149	5710	0.03	0.12	16.52	0.50
	OCP11 159	159	6095	0.03	0.38	76.79	7.54
	OCP11 169	169	6480	0.03	0.34	60.17	5.31
	OCP11 179	179	6865	0.03	0.43	69.57	7.78

Table A2.4 Modelled age, modelled accumulation rate (AR), bulk density (BD), Hg concentration, and Hg flux results organized by site and sample ID *(continued).*

Site	Sample ID	Upper Depth (cm)	Modelled Age (cal BP)	Modelled Acc. Rate ($cm \cdot y^{-1}$)	Bulk Density ($g \cdot cm^{-3}$)	Hg Concentration ($ng \cdot g^{-1}$)	Hg Flux ($\mu g \cdot m^{-2} \cdot y^{-1}$)
OCP14	OCP14 39	39	3280	0.01	0.10	18.62	0.23
	OCP14 49	49	4090	0.01	0.15	26.49	0.49
	OCP14 59	59	4880	0.01	0.04	11.85	0.05
	OCP14 69	69	5800	0.02	0.06	15.63	0.20
	OCP14 79	79	5900	0.11	0.04	12.22	0.47
	OCP14 89	89	5990	0.11	0.13	14.93	2.07
	OCP14 99	99	6090	0.04	0.08	22.76	0.69
	OCP14 109	109	6520	0.02	0.07	17.32	0.30
	OCP14 119	119	6890	0.03	0.06	22.72	0.37
	OCP14 129	129	7275	0.03	0.06	19.62	0.30
	OCP14 139	139	7655	0.03	0.12	28.35	0.90
	OCP14 149	149	8030	0.02	0.13	38.53	1.20
	OCP14 159	159	8460	0.01	0.58	78.45	4.55
	OCP14 169	169	10030	0.01	0.57	72.81	3.02
	OCP14 179	179	11230	0.01	0.27	39.07	1.15
	OCP14 189	189	11855	0.02	0.19	55.34	1.68
	OCP14 199	199	12480	0.02	0.39	98.68	6.17
	OCP14 209	209	13110	0.02	0.39	103.44	6.48
	OCP14 219	219	13740	0.02	0.45	67.00	4.81
	OCP14 229	229	14365	0.02	0.96	52.40	8.05
BFP16	BFP16 44	44	1730	0.03	0.08	28.81	0.62
	BFP16 49	49	1915	0.03	0.07	14.59	0.27
	BFP16 59	59	2285	0.03	0.02	8.77	0.05
	BFP16 69	69	2660	0.03	0.04	9.47	0.10
	BFP16 79	79	3035	0.03	0.03	11.75	0.10
	BFP16 79	79	3035	0.03	0.05	9.21	0.11
	BFP16 89	89	3415	0.02	0.04	17.11	0.17
	BFP16 99	99	3895	0.02	0.06	20.45	0.22
	BFP16 109	109	4480	0.02	0.06	30.04	0.33
	BFP16 119	119	4955	0.02	0.05	34.17	0.33
	BFP16 129	129	5420	0.02	0.05	19.30	0.19
	BFP16 139	139	5880	0.02	0.04	12.68	0.10
	BFP16 149	149	6340	0.02	0.04	11.05	0.10
	BFP16 159	159	6805	0.02	0.07	35.01	0.51
	BFP16 169	169	7265	0.02	0.35	67.68	5.17
	BFP16 179	179	7730\	0.02	0.36	70.07	5.36
	BFP16 179	179	7730	0.02	0.31	68.88	4.62
	BFP16 189	189	8190	0.02	0.28	70.54	4.25
	BFP16 199	199	8655	0.02	0.38	68.06	5.50
	BFP16 209	209	9120	0.02	0.33	67.96	4.74
	BFP16 219	219	9600	0.02	0.46	76.63	6.70
	BFP16 229	229	10175	0.02	0.58	68.64	7.86
	BFP16 239	239	10620	0.02	0.49	80.00	8.72
	BFP16 249	249	11065	0.02	0.53	81.99	9.76
BFP19	BFP19 33	33	3105	0.01	0.19	33.79	0.70
	BFP19 39	39	3625	0.01	0.14	16.98	0.26
	BFP19 49	49	4500	0.01	0.09	13.19	0.13
	BFP19 59	59	5370	0.01	0.06	10.51	0.07
	BFP19 69	69	6240	0.01	0.09	8.96	0.09
	BFP19 79	79	7115	0.01	0.08	8.46	0.08
	BFP19 89	89	8010	0.01	0.16	25.90	0.42
	BFP19 99	99	9070	0.02	0.20	37.77	1.33
	BFP19 109	109	9130	0.18	0.16	29.95	8.63
	BFP19 119	119	9180	0.20	0.11	25.56	5.77
	BFP19 129	129	9230	0.20	0.12	26.25	6.29
	BFP19 139	139	9280	0.20	0.14	37.05	10.38
	BFP19 149	149	9330	0.20	0.05	36.27	3.92
	BFP19 159	159	9380	0.20	0.05	22.25	2.23
	BFP19 169	169	9430	0.20	0.04	29.79	2.44
	BFP19 179	179	9480	0.20	0.06	40.90	4.85
	BFP19 189	189	9530	0.20	0.02	35.31	1.64
	BFP19 199	199	9580	0.22	0.02	31.29	1.49
	BFP19 209	209	9620	0.05	0.06	48.87	1.37
	BFP19 219	219	10020	0.02	0.12	61.58	1.79
	BFP19 229	229	10480	0.02	0.45	58.63	5.83

Example Hg stock calculation for a Holocene DTLB peat deposit. Total Hg inventory (g) was estimated using the following equation:

$$\text{THg inventory} = dC \cdot dT \cdot BD \cdot [Hg] \cdot 10^{-3}$$

where dC is deposit coverage in m^2, dT is deposit thickness in m, BD is average peat bulk density in $g \cdot cm^{-3}$, and [Hg] is average peat Hg concentration in $ng \cdot g^{-1}$.

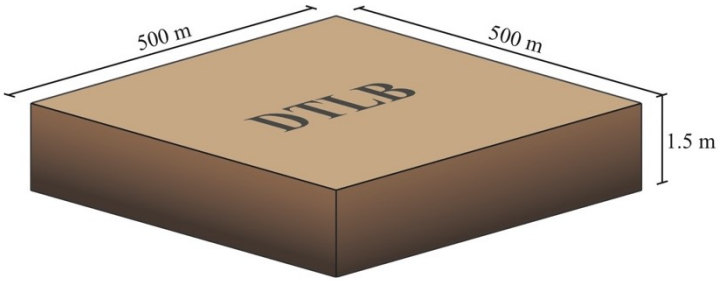

For a relatively small (500 m x 500 m x 1.5 m) DTLB peat deposit, like schematized above, with an average BD of 0.1 $g \cdot cm^{-3}$ and average [Hg] of 20.7 ± 9.8 $ng \cdot g^{-1}$, the total Hg inventory can be estimated as follows:

$$\text{Total Hg inventory} = (500 \text{ m x } 500 \text{ m}) \cdot (1.5 \text{ m}) \cdot (0.1 \text{ g} \cdot \text{cm}^{-3}) \cdot (20.7 \pm 9.8 \text{ ng} \cdot \text{g}^{-1}) \cdot (10^{-3})$$

$$\text{Total Hg inventory} = \mathbf{776.25 \pm 367.50 \text{ g}}$$

References

(1) Bronk Ramsey, C. Bayesian Analysis of Radiocarbon Dates. *Radiocarbon* **2009**, *51* (1), 337–360.

(2) Reimer, P. J.; Bard, E.; Bayliss, A.; Beck, J. W.; Blackwell, P. G.; Bronk, M.; Grootes, P. M.; Guilderson, T. P.; Haflidason, H.; Hajdas; et al. IntCal 13 and Marine 13 radiocarbon age calibration curves 0–50,000 years cal BP. *Radiocarbon* **2013**, *55*, 1869–1887.

(3) Murton, J. B.; French, H. M. Cryostructures in permafrost, Tuktoyaktuk coastlands, western arctic Canada. *Can. J. Earth Sci.* **1994**, *31* (4), 737–747.